JOURNAL OF APPLIED PHYSICS

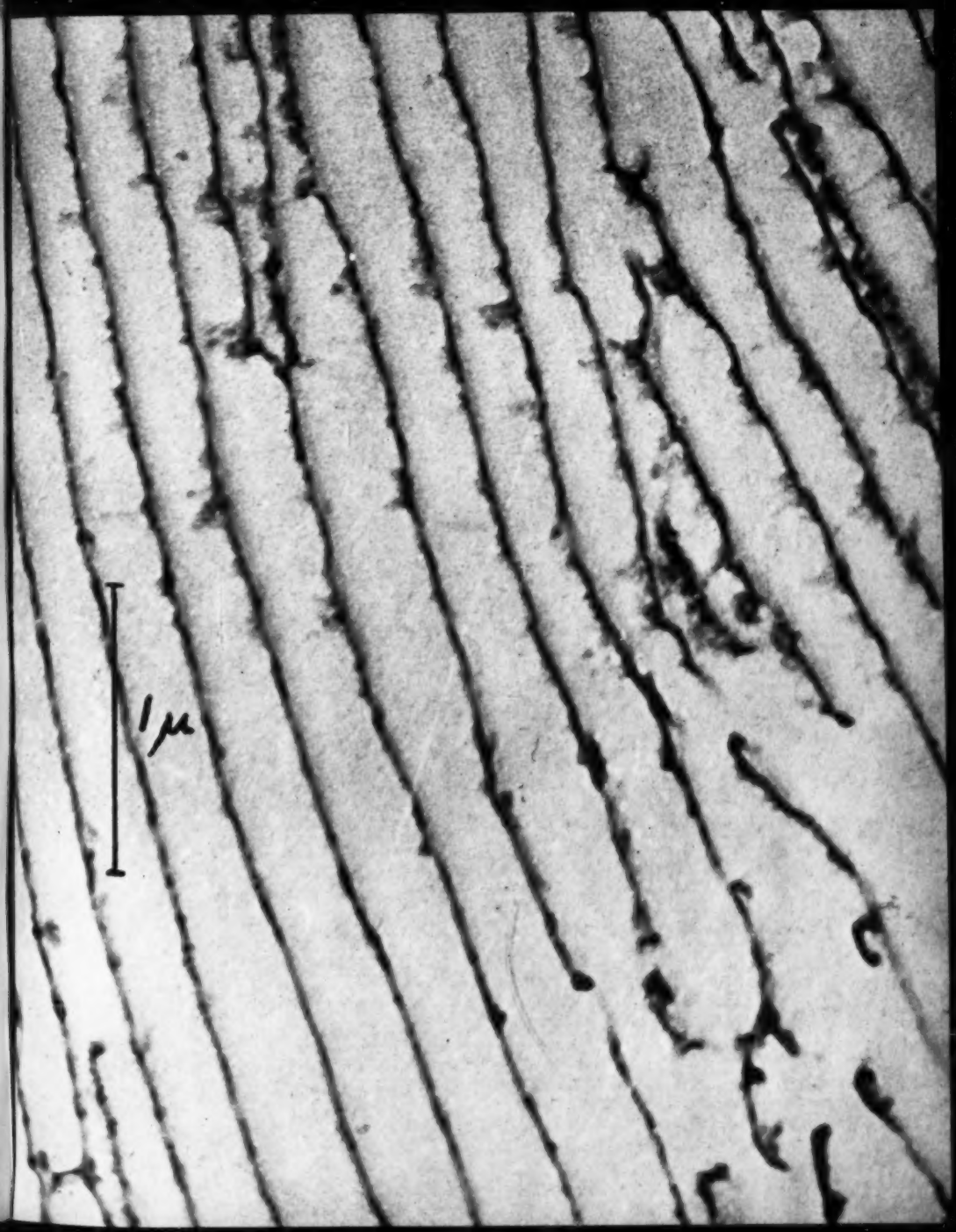

JOURNAL
OF
APPLIED PHYSICS

SEPTEMBER, 1941 Vol. 12, No. 9

In This Issue

Page

The "Supply" of Physicists 655

Résumés of Recent Research 658

Ignitor Characteristics E. G. F. Arnott 660

Structure and Dynamics of Liquids
W. E. Roseveare, R. E. Powell, and Henry Eyring 669

Correlation Between Elastic Moduli and Viscosity of Liquids and Plastics Andrew Gemant 680

Solution of A. C. Circuit Problems Louis A. Pipes 685

Surface Studies with the Electron Microscope
V. K. Zworykin and E. G. Ramberg 692

Silver-Magnesium Alloy as a Secondary Electron Emitting Material
V. K. Zworykin, J. E. Ruedy, and E. W. Pike 696

Glass-to-Metal Seals. II.
A. W. Hull, E. E. Burger, and L. Navias 698

Diffusion Calculations. Interrelation Between Two Solutions of the Fourier Equation Herman A. Liebhafsky 707

In Every Issue

Here and There 659

Index to Advertisers viii

BOARD OF EDITORS

Elmer Hutchisson,
Editor

Associate Editors

Francis Bitter
W. F. Busse
Robley D. Evans
Morris Muskat
B. E. Warren
J. B. Whitehead

Publication of the American Institute of Physics

ADMINISTRATIVE STAFF

Henry A. Barton,
Director

Madeline M. Mitchell,
Publications Manager

John T. Tate,
Adviser on Publications

GOVERNING BOARD

Paul E. Klopsteg,
Chairman
George B. Pegram,
Secretary
Karl T. Compton
Wheeler P. Davey
Floyd A. Firestone
Harvey Fletcher
R. C. Gibbs
Arthur C. Hardy
George R. Harrison
A. Stuart Hunter
H. R. Lillie
A. G. Worthing
W. B. Rayton
John T. Tate
Wallace Waterfall

The Journal of Applied Physics, published monthly at Prince and Lemon Sts., Lancaster, Pa., is devoted to physics in its role as the science basic to other natural sciences and to the arts and industries. Previous to 1937 this publication was known as Physics. It aims to be of service not only in physical laboratories, but also in the laboratories of industrial, chemical, geological, geophysical, meteorological, radio, and similar concerns. The Journal of Applied Physics publishes editorials, news of physicists and reviews, as well as technical papers of applied physics.

Manuscripts should be submitted to Elmer Hutchisson, Editor, American Institute of Physics, 175 Fifth Avenue, New York, New York.

Subscriptions and orders for back numbers should be addressed to Prince and Lemon Streets, Lancaster, Pa. or to the American Institute of Physics, 175 Fifth Avenue, New York, N. Y.

SUBSCRIPTION PRICE

	U. S. AND CANADA	ELSEWHERE
To members of scientific societies	$5.00	$5.70
To all others	7.00	7.70

Single copies are $.70 each.

Changes of address and proofs should be addressed to the Publications Manager.

Advertising rates supplied on request. Orders, advertising copy and cuts should be sent to the American Institute of Physics.

Entered as second class matter at the Post Office at Lancaster, Pennsylvania, under the Act of March 3, 1897.
Accepted for mailing at the special rate of postage provided for in the Act of February 28, 1925, authorized May 2, 1932.

Copyright 1941, by the American Institute of Physics.

Journal
of
Applied Physics

Volume 12 September, 1941 Number 9

The "Supply" of Physicists

THROUGH the National Roster of Specialized Personnel we have for the first time a detailed breakdown of the professional interests of practically all of the physicists in the United States. Each person, in filling out a questionnaire, was asked to indicate in the order of his interest or competence five rather narrow fields of physics. The sub-divisions from which his selections were made were chosen in consultation with a considerable number of able physicists. The charts printed on this and the next two pages represent a summary of data supplied by the Office of the Roster from all of the questionnaires in the field of physics. Since it is impossible to evaluate the relative interest in the various fields chosen by a given person, the charts were drawn merely indicating the number of people who have given each field as their first interest, second interest and third interest. Together, the charts indicate the "supply" of physicists skilled in each field. Another analysis which is now being made by the American Institute of Physics will indicate the number of people now being employed in each field on defense projects, and thus will provide an indication of the "demand" for physicists in the national defense effort.

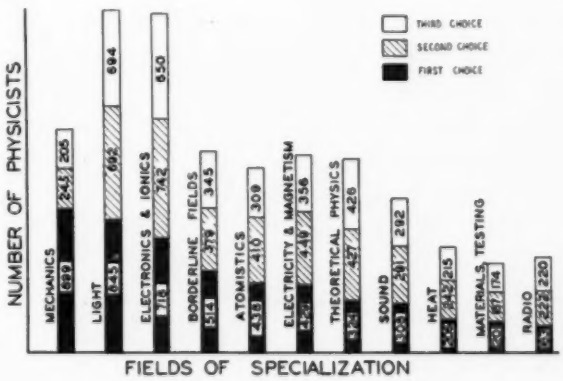

A few words regarding the origin of the National Roster of Specialized Personnel and its operation are in order. The National Roster is a program jointly administered by the National Resources Planning Board and the United States Civil Service Commission and was formally brought into existence one year ago. Dr. Leonard Carmichael is director of the program and Mr. James C. O'Brien is its executive officer. It was formed with two basic principles in mind; first, to have a roster listing the qualifications of the specialized individual and his availability for appointment to the Federal service, and second, to conserve the brain power of the nation.

The National Roster has been left on a purely voluntary basis; there has been no attempt to conscript or draft any individual. When there are openings in the Federal service where an individual registered with the National Roster can be of service to the nation, he is offered the opportunity of rendering this service, either as a consultant or full-time official. Whether he wishes to accept the offer or not is entirely his own choice; no pressure of any type is brought to bear on any individual.

As an example of this, the following will illustrate the methods used by the Roster in selecting personnel:

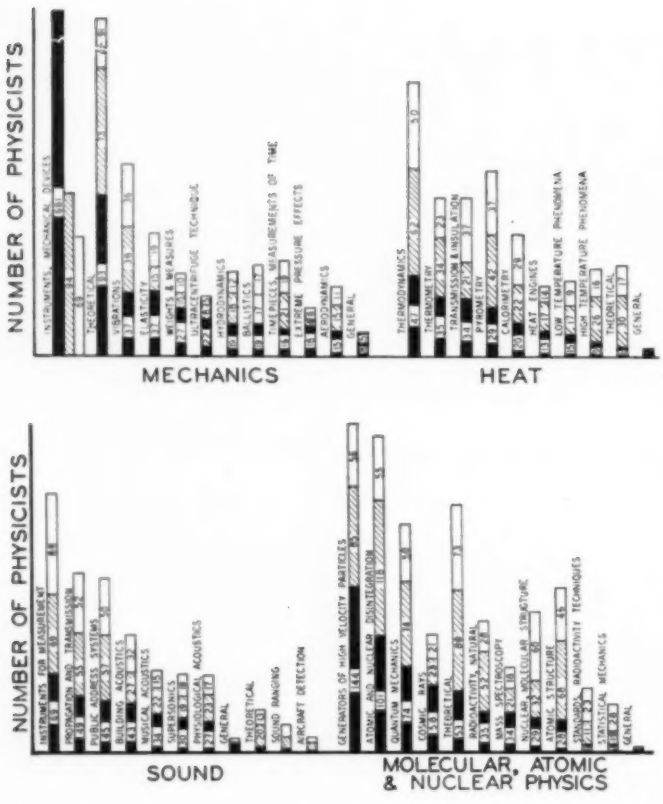

(Because of the confidential nature of numerous appointments, it is necessary to use a hypothetical case.)

The Navy Department requests the National Roster to submit the names of four physicists skilled in geometrical and wave optics for instrument design. The request is forwarded by the National Roster to its Machine Unit for a preliminary selection. The skills of all individuals registered with the National Roster have been coded and punched on tabulating cards, in order to speed up the selection process by the use of machines to the point where a qualitative analysis is necessary. The machines then select all cards coded 33.3.20, which is the code for physicists skilled in geometrical and wave optics. The names of these persons are sent to the File Unit, where the questionnaires submitted by the individuals are removed from the file and sent to the Certification Unit for qualitative review. On the supposition that the Machine Unit has selected a group of two hundred names, the Certification Unit, after an analytical review, may select the questionnaires of thirty-five individuals who meet the requirements of the Navy Department's request. There may be numerous reasons why the remaining one hundred and sixty-five names were rejected for this particular selection. One of the major reasons may be that the individual is employed either by private industry or another Federal agency, where he would be of more value to the defense effort than in the vacant position in the Navy Department.

The thirty-five remaining names are certified to the Navy Department, in order that it may contact these persons concerning their availability for appointment to one of the four positions open. The foregoing procedures require, generally, less than twenty-four hours, from the time the request is received by the National Roster until the time the names are certified to the requesting agency.

In the science field the procedure of certifying names has been improved by the formation under a contract with N.D.R.C. of an Office of Scientific Personnel by the National Research Council. Dr. Henry A. Barton, Director of the American Institute of Physics, is chairman of the governing committee of this organization, while Dr. Joseph C. Morris is its director. The Office of Scientific Personnel is finding that the majority

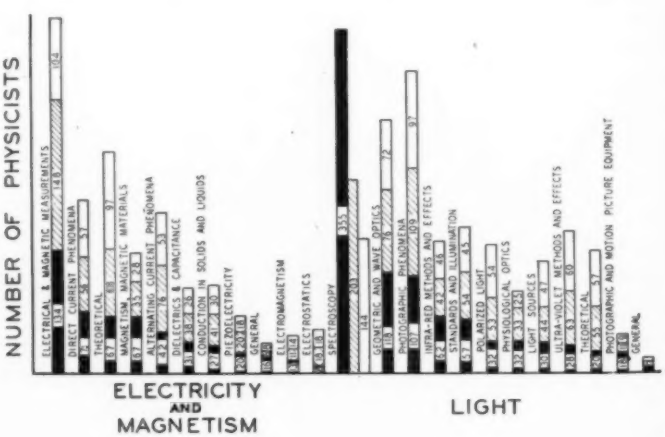

of the calls it receives are for physicists and those in related fields in which there is such a great shortage of trained men.

As a sidelight, it is interesting to note that the first request for personnel received by the National Roster was for physicists and the last request received as the fiscal year closed June 30, 1941, was also from this field. Up until June 30, 1941, the National Roster had submitted the names of more than six hundred physicists to various Federal and affiliated agencies for consideration for appointment. The same demand is being made on the Roster for individuals in other fields of specialization. It is urged that not only physicists but all individuals with scientific or professional skills write to the National Roster of Scientific and Specialized Personnel, Washington, D. C. for questionnaires, in order that they may be registered in this census of the "brains of the Nation." When writing, state what your field of specialization is, that is, physicist, chemist, radio engineer, etc., so that the appropriate "check list" may be sent with the questionnaire. If you have scientific training and are interested in doing defense work, write to the Office of Scientific Personnel, National Research Council, 2101 Constitution Avenue, Washington, D. C. so that you may be placed on the list of available personnel. An individual registered in the Roster may never be called upon to serve, but his own particular skill may be the one necessary to strengthen our defense program and thus protect the Nation.

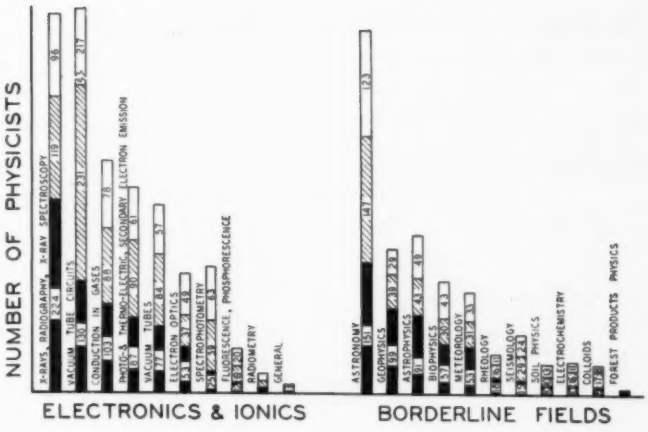

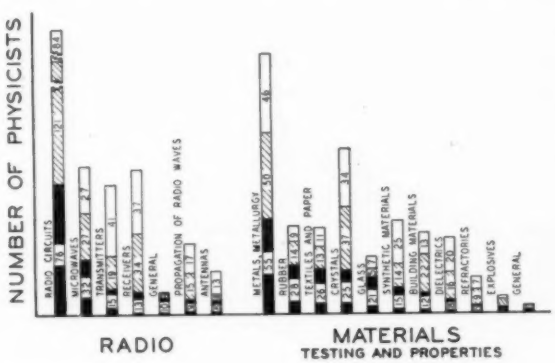

Résumés of Recent Research

A Theory of the Melting Process The most obvious properties which distinguish a crystalline solid from a liquid are its ability to support a shearing stress and the ordered arrangement of its molecules, demonstrated by x-ray diffraction. In the fusion process these properties are destroyed. In 1939 Born[1] suggested the vanishing of the rigidity modulus as the criterion of fusion. In the same year Lennard-Jones and Devonshire[2] proposed a theory of fusion based upon the idea of an order-disorder transformation between normal and interstitial sites of a crystal lattice. Recently, John G. Kirkwood and Elizabeth Monroe at Cornell University have presented a theory of fusion, based upon the order-disorder criterion, in which the molecular configuration is not artificially restricted to the sites of a basic lattice.

Using classical statistical mechanics, Kirkwood and Monroe formulate an integral equation for the distribution function of average molecular density in a region occupied by a system of molecules. They investigate periodic solutions of the integral equation subject to the restraint of macroscopic homogeneity. When the distribution function with the period of a specified space lattice is expanded in a Fourier series, the authors find that outside a certain temperature-volume domain the series reduces to its constant term in which all characteristics of the lattice have disappeared. The corresponding thermodynamic system no longer possesses long range crystalline order and is, therefore, identified with the liquid phase.

With the aid of certain approximations the authors obtain explicit solutions of their equation for the face-centered cubic lattice. They find that there should be no critical temperature for the liquid-solid transition for this lattice. With the Lennard-Jones potential of interatomic force, they make numerical calculations of the molar fusion parameters of argon. The calculated entropy of fusion and volume increment of fusion at 83.9°K and one atmosphere are 3.48 E.U. and 3.25 cc. Their values compare favorably with the observed fusion parameters, 3.36 E.U. and 3.53 cc.

[1] M. Born, J. Chem. Phys. **7**, 591 (1939).
[2] Lennard-Jones and Devonshire, Proc. Roy. Soc. **A170**, 464 (1939).
[3] J. G. Kirkwood and E. Monroe, J. Chem. Phys. **9**, 514 (1941).

Reflection of Light from Ceramic Tiles In the design of lighting systems for rooms, the illuminating engineer should have data on the light reflection properties of the materials to be used for floor, walls, ceiling, and furniture. The reflection factors and colors of these materials have a marked effect on the amount and spectral quality of the light reaching the work. What is even more important, they play a dominant role in fixing the brightness distribution throughout the visual field, which recent research has shown to have an important bearing on visual fatigue.

Hitherto, no comprehensive data have been available on the amount and color of light reflected from commercially available materials, and it is generally impracticable for the engineer to make tests on all the materials to be used in a given room or building. To meet this need, a large number of representative materials have been tested at the Massachusetts Institute of Technology, and data from these tests have been computed and tabulated. The results consist of curves of reflection factor *vs.* wave-length, obtained automatically on the Hardy recording spectrophotometer, and tables of total reflection factors and trichromatic coefficients for the samples when illuminated with light from incandescent lamps and with daylight (C.I.E. Standard Illuminants *A* and *C*).

A recent paper[1] gives such results for 91 samples of ceramic tiles, while forthcoming papers will give data on other materials. The tables and graphs should be of value to lighting experts and interior decorators. Also, since ceramic tiles are very permanent in reflecting properties, and are carefully controlled for uniformity, the tabulation allows tile samples to be used as rough comparison standards for judging the color and reflection factors of other materials.

[1] Parry Moon, "Colors of ceramic tiles," J. Opt. Soc. Am. **31**, 482 (1941).

Here and There

Tri-University Operation of McDonald Observatory

On July 12 the University of Indiana joined the Universities of Chicago and Texas in their operation of the McDonald Observatory, located on Mt. Locke in West Texas. This observatory is the second largest in the world, its 82-inch mirror being surpassed only by the 100-inch reflector at Mt. Wilson.

★

Summer Program at Brown University

A program entitled "Advanced Instruction and Research in Mechanics" has been in progress during the summer at Brown University, Providence, Rhode Island. Among those giving special lectures were the following:

PROFESSOR NORBERT WIENER, *Massachusetts Institute of Technology.*
DR. A. NADAI, *Westinghouse Electric and Manufacturing Company.*
DR. HILLEL PORITSKY, *General Electric Company.*
PROFESSOR S. TIMOSHENKO, *Stanford University.*
PROFESSOR J. N. GOODIER, *Cornell University,* **Buckling and Vibration of Bars Involving Simultaneous Bending and Torsion.**
MR. R. M. FOSTER, *Bell Telephone Laboratories,* **Electrical Networks and their Analog in the General Dynamical Problem.**
PROFESSOR R. D. COURANT, *New York University,* **The Rayleigh-Ritz Method.**
DR. THEODORE THEODORSEN, *Chief, Physical Research Division, National Advisory Committee for Aeronautics, Langley Field,* **Introduction to the Theory of Wing Flutters.**
DR. THORNTON C. FRY, *Mathematical Research Director, Bell Telephone Laboratories,* **Mathematical Research in the Industries.**
PROFESSOR R. B. LINDSAY, *Brown University,* **Filtration of Elastic Waves in Fluids and Solids.**

★

Additions to Staff at Armour Research Foundation

The appointment of Dr. Raymond G. Spencer and Dr. Carl C. Gamertsfelder to the staff of the Light and Optics division of the Armour Research Foundation has been announced.

Dr. Spencer, who is conducting x-ray diffraction research, is on leave of absence from Albion College, Albion, Michigan, where he is Professor of Physics and head of the Physics Department. Dr. Gamertsfelder has completed his doctorate at the University of Missouri and is working in spectroscopy and x-ray investigations.

★

Meeting of Scientific Photographers

The Biological Photographic Association, an international group of photographers in the natural sciences, will hold its eleventh annual meeting in the Hotel Buffalo, Buffalo, New York, September 11–13, 1941.

The program emphasizes the latest methods and processes which are likely to contribute to the national defense. The annual salon will again be a prominent feature of the meeting. Visitors are welcome. For further information write the Secretary of the Biological Photographic Association, University Office, Magee Hospital, Pittsburgh, Pennsylvania.

★

Defense Courses in Physics

The nation-wide plan for emergency defense courses in engineering at the college level, supported by government funds and administered by the U. S. Office of Education, has been expanded in scope for the fiscal year which began July 1. It now provides for courses in physics, chemistry, and production management, as well as the several branches of engineering included in the program last year. The Advisory Committee of the Office which is composed of prominent educators has likewise been enlarged. Dean Homer L. Dodge of the University of Oklahoma has been appointed to the Committee to represent the field of physics in its deliberations. Another member of the Committee whose interest lies largely in the field of physics is Professor F. L. Bishop of the University of Pittsburgh. The Chairman of the Committee is Dean A. A. Potter of Purdue University. Inquiries concerning the program should be addressed to Commissioner John W. Studebaker of the Office of Education, Federal Security Agency, Washington, D. C.

★

Conference on Visual Problems

A conference on visual problems was held at Ohio State University, June 18–20. The following took part in the conference:

SELIG HECHT, *Columbia University,* **Energy and Vision.**
H. K. HARTLINE, *University of Pennsylvania,* **The Discharge of Nerve Impulses by the Visual Sense Cells under Conditions of Light and Dark Adaptation.**
CLARENCE H. GRAHAM, *Brown University,* **The Influence of Adapting Intensity on the Excitability Cycle of the Photoreceptor Unit.**
S. HOWARD BARTLEY, *Washington University,* **The Optic Nerve Discharge and Its Relation to Other Neurophysiological Records in the Study of Vision.**
WALTER R. MILES, *Yale University,* **The Steady Potential of the Human Eye.**
EARL M. LOWRY AND DAVID MACADAM, *Eastman Kodak Company,* **Visual Sensitometry.**
WOLFGANG KOHLER, *Swarthmore College,* **Fatigue After-Effects in Vision.**
J. P. NAFE, *Washington University,* **Adaptation.**
FRANK A. GELDARD, *University of Virginia,* **Persistence of Vision.**
SIDNEY M. NEWHALL, *Johns Hopkins University,* **Simultaneous Contrast.**
HARRY HELSON, *Bryn Mawr College,* **Interrelations of Hue, Lightness and Saturation as a Function of Conditions and Modes of Viewing with Implications for Measurement and Specifications of Colors.**
DEANE B. JUDD, *National Bureau of Standards,* **Current Research Bearing on Choice of a Standard Color System.**
F. L. DIMMICK, *Hobart College,* **A Test of Color Aptitude.**
W. B. LANCASTER, *Dartmouth Eye Institute,* **Anomalous Spatial Localization Associated with Phorias.**
MATTHEW LUCKIESH AND FRANK K. MOSS, *Nela Research Laboratories,* **A New Method of Subjective Refraction Involving Identical Techniques in Static and Dynamic Tests.**
FRANK K. MOSS AND MATTHEW LUCKIESH, *Nela Research Laboratories,* **The Rate of Involuntary Blinking as a Criterion of Relative Ease of Seeing.**
FRANCES ILG, *Yale University,* **Directions and Eye Movements in Young Children.**
A. M. SKEFFINGTON, **Round Table on Problems of Refraction.**

Contributed Original Research

Ignitor Characteristics

E. G. F. Arnott
Research Department, Westinghouse Lamp Division, Bloomfield, New Jersey
(Received December 5, 1940)

This article reports an investigation of the current and voltage characteristics of "ignitor" electrodes in a mercury pool rectifier (ignitron). Experiments were made on square rods of smooth homogeneous materials of various sizes and resistivities with the following results: (1) A frequency distribution curve is found for the voltage required by the ignitor which is approximately a Normal or Gaussian distribution. (2) The total current required for the ignition of an arc, divided by the perimeter is a constant, for a given material. (3) The total current required per unit length of perimeter times the square root of the resistivity is a constant. (4) For identical ignitors operated in parallel, the total current required is equal to the square root of the number of ignitors times the current required for one ignitor. (5) An expression is derived for the fraction of the total current which is useful in starting the arc and this is found to be inversely proportional to the square root of the width. This derivation is verified by the behavior of ignitors operated in parallel.

Introduction

FOR a good many years, the problem of the initiation of an arc has been of considerable interest to the electrical industry. Various methods have been used, such as the thermionic cathode, separating contacts, high frequency discharge, etc. All of these methods were unsatisfactory for the recurrent rapid production of high current arcs, where only low voltage was available.

About ten years ago, Slepian and Ludwig[1] discovered that an arc could be initiated by passing a current through a rod of high resistance material dipping into a mercury pool.

The current and voltage required for the initiation of the arc were not excessive, being of the order of 10 amperes and 100 volts. This arc starter was developed to a point where it could be used commercially and is at present in use in various types of tubes manufactured for welding and power rectifier applications. Tubes using this method for initiating the arc are called ignitrons and the starting electrode itself is called an ignitor.

Figure 1 shows a section of a typical sealed-off metal ignitron capable of delivering 140 amperes average current and several thousand amperes maximum R.M.S. current. The ignitor is shown dipping about $\frac{1}{4}''$ into the mercury pool cathode.

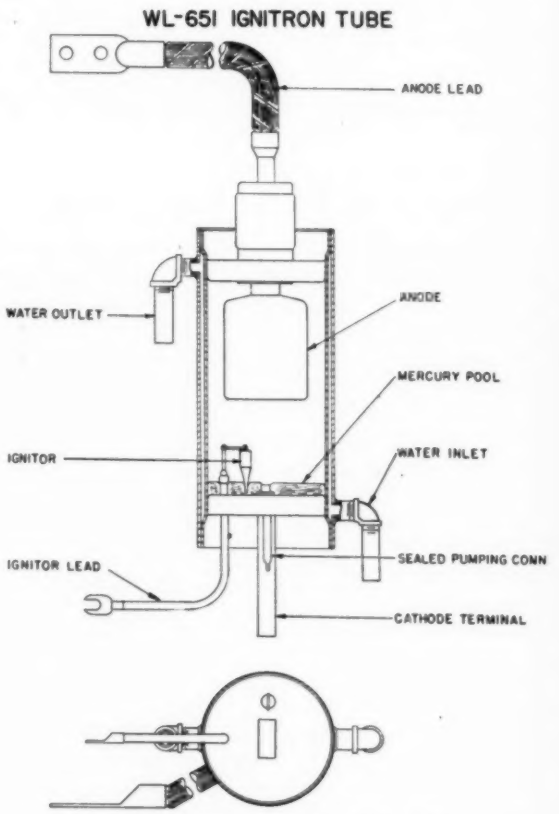

FIG. 1. Section of an ignitron tube.

[1] A. I. E. E. Winter Convention, January 23–27, 1932.

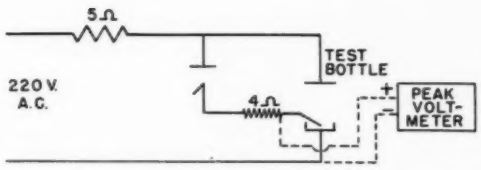

FIG. 2. Test circuit.

Due to the agitation of the surface of the mercury pool, there is considerable variation in the current and voltage required by the ignitor. It is the purpose of the present paper to discuss these current and voltage characteristics and to show what relations exist between the characteristics and the size and resistivity of the ignitor material.

METHOD OF TEST

The test circuit is given in Fig. 2 which shows schematically the ignitor mounted in a test bottle which has a mercury pool and a graphite anode. The ignitor is connected to the anode supply through a 4-ohm resistance and a hot cathode rectifier tube, or a thyratron, so that current flows through the ignitor to the mercury pool only when the ignitor and anode are both positive with respect to the pool. The peak voltmeter shown can be connected either across the ignitor itself, to measure the ignitor peak voltage, or across the 4-ohm resistance to measure the ignitor peak current. Figure 3 shows an oscillogram taken which records the ignitor voltage and current, and the tube voltage drop for about seventy consecutive cycles. This figure indicates the variable nature of the quantities which are to be measured.

Since the temperature of the mercury pool and also of the tube walls plays an important part in determining the voltage and current required by the ignitor, the test tube was operated at an average anode current of about 20 amperes for at least five minutes before each test reading was made. Two methods of measuring the characteristics have been used; the first is to take oscillograms of the ignitor voltage and current, and then to measure the values from the films. This method has been extremely useful, though somewhat tedious, in determining the voltage and current distribution for a single ignitor.

The second method, however, is one which is more practical, though less definite, where a large number of ignitors are to be tested. This consists of using the peak voltmeter and adjusting it so that it records a voltage or current above the setting, less than once in 30 seconds. For example, if the peak voltmeter is set at 100 volts and the ignitor does not require more than this value in a period of 30 seconds, then the probability of this ignitor requiring more than the 100 volts to fire is less than 1 in 1800. This method is used in testing ignitors to determine

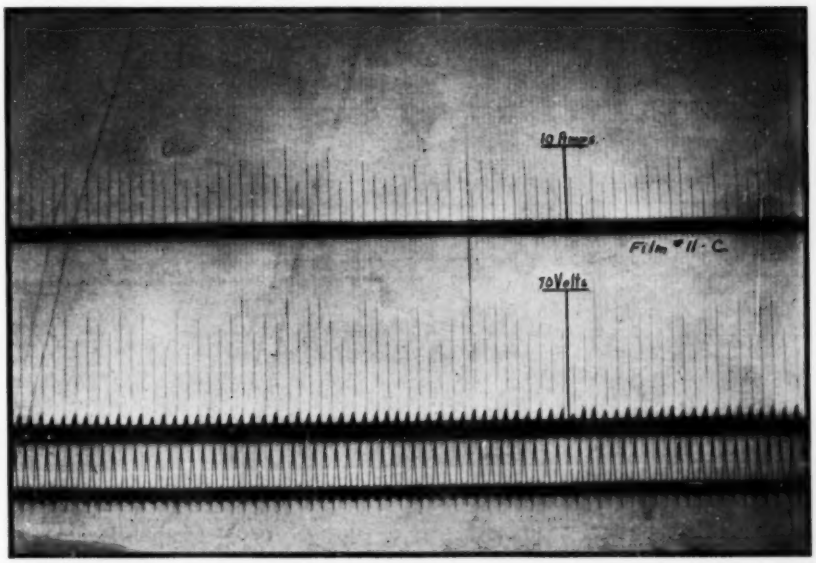

FIG. 3. Oscillograms showing peak currents (top trace) and peak voltages (middle trace) of an ignitor and starting voltage (bottom trace) of the ignitron.

whether the characteristics are suitable for use in tubes. It has been used in the following work where the characteristics are determined for various ignitors of different sizes and materials.

Individual Characteristics

Returning to the ignitor current and voltage traces shown in Fig. 2, it can be seen that, in general, on the cycles where a high current is required to fire, a high voltage is also necessary, and for a low current only a low voltage is required. This suggests that the resistance of the ignitor remains essentially constant from one cycle to the next. This is indeed found to be the case where the agitation of the pool is not too violent.

A large number of oscillograms were taken under various conditions. About 8000 cycles were measured visually. The results from several films, which were taken as nearly as possible under equilibrium conditions, after operating for more than an hour, were combined, and a voltage distribution curve was plotted. 656 cycles were used and the data were handled statistically to determine the type of theoretical curve which would give the best fit to the experimental points.

Figure 4 shows the theoretical curves and the

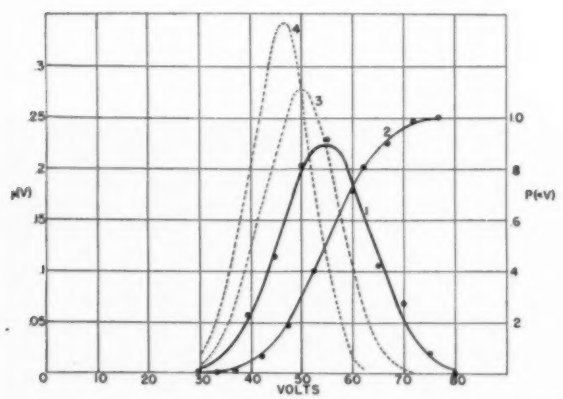

Fig. 4. (1) Voltage distribution curve for an ignitor. (2) Area under (1) from $-\infty$ to V. (3) Calculated distribution curve for 2 ignitors in parallel. (4) Calculated distribution curve for 4 ignitors in parallel.

experimental points. Curve 1 is the voltage distribution curve and shows the fraction of the total number of times the ignitor fired in each voltage interval of 5 volts. It is a plot of the equation

$$p(V)=\frac{1}{\sigma(2\pi)^{\frac{1}{2}}}\times\exp\left[-(V-54.91)^2/2\times8.72^2\right]\Delta V, \quad (1)$$

where $P(V)$ is the probability of firing in the interval ΔV.

Table I.

V	Obs. f	Vf	V^2f	V^3f	V^4f
25	0	0	0	0	0
30	1	30	900	27,000	810,000
35	12	420	14,700	514,500	18,007,500
40	38	1,520	60,800	2,432,000	97,280,000
45	76	3,420	153,900	6,925,500	311,647,500
50	133	6,650	332,500	16,625,000	831,250,000
55	152	8,360	459,800	25,289,000	1,390,895,000
60	118	7,080	424,800	25,488,000	1,529,280,000
65	69	4,485	291,525	18,949,125	1,231,693,125
70	44	3,080	215,600	15,092,000	1,056,440,000
75	13	975	73,125	5,484,376	411,328,125
80	0	0	0	0	0
	656	36,020	2,027,650	116,826,500	6,878,631,250

$\bar{V}=54.91\pm0.34$, $(\beta_1)^{\frac{1}{2}}=0.040\pm0.096$, $J_{\min}=0.9$,
$\sigma=8.72\pm0.24$, $\beta_2=2.68\pm0.19$, $J_{\max}=2.1$.

Curve 2 is the area under Curve 1 and shows the fraction of the total number of times the ignitor fired below a voltage V. It is given by

$$P(<V)=\frac{1}{\sigma(2\pi)^{\frac{1}{2}}}\int_{-\infty}^{V}\exp\left[\frac{-(V-54.91)^2}{2\times8.72^2}\right]dV. \quad (2)$$

The other curves, 3 and 4, will be discussed later.

Table I shows the frequency of occurrence in the different voltage intervals and how these frequencies are used in determining the average ($\bar{V}$), the standard deviation (σ) and the other quantities necessary for determining the type of distribution represented by the experimental results.[2] For a true Gaussian distribution $(\beta_1)^{\frac{1}{2}}$ and J should both be zero. The values obtained show that a fit might be had with either a Poisson distribution or the binominal law. Since the experimental curve is very nearly symmetrical and the Gaussian distribution is at times a good approximation to either of these two distributions, it was tried first with the

[2] T. C. Fry, *Probability and its Engineering Uses* (1928), Chapter 9.

results shown in Table II. This gives the deviations of the experimental frequencies from those calculated from a Gaussian distribution determined from the value of $\bar{V}$ and σ. From these deviations, the goodness of fit can be determined, and is given by $P(>\chi^2)$ which gives the probability of a repetition of the experiment showing values further from the theoretical distribution than the experimental values already obtained. The value of $P(>\chi^2)$ was found to be .55 showing a much better fit than would normally be expected from such data. In plotting the data, it was found that the observer had a personal preference for numbers ending in 2, 3, 7 and 8. This was eliminated by selecting the voltage intervals between numbers ending in 2.5 and 7.5 volts.

A similar type of distribution curve was found for the ignitor current though sufficient data were not obtained to give a complete analysis.

The reason for the existence of the voltage and current distribution curves is not thoroughly understood. One suggested explanation is that it is due to a general change in mercury level due to the agitation of the pool. That this explanation is not correct can be seen from the oscillograms of current and voltage where it is shown that the high voltages occur with the high currents. If an ignitor, which has been tested at a given immersion, is immersed further into the pool, it is found that while the current is increased the voltage required is decreased. This clearly shows that the deviation from the average depends only slightly, if at all, on the general mercury level for low anode currents. At high anode currents, where the agitation is increased, there is some evidence of both factors occurring simultaneously.

The author's theory is that the agitation of the pool causes random fluctuations in the shape of the mercury meniscus, which affect the formation of the required voltage gradient or energy density. This theory is borne out by the results obtained by W. E. Berkey on an ignitor immersed in a solid tin cathode. In this case, both the current and voltage deviations from the average were extremely small. Fortunately, it seems probable that a recording counting circuit can

TABLE II.

$$p_{12}(V)=\frac{1}{(2\pi)^{\frac{1}{2}}}\left[\int_{-\infty}^{y_2}\exp(y^2/2)dy-\int_{-\infty}^{y_1}\exp(-y^2/2)dy\right],\quad \exp(-y^2/2)=\exp[-(V_1-54.91)^2/2\sigma^2]$$

V	(V_1)	$(V_1-54.91)$	$\left(\frac{V_1-54.91}{8.72}\right)=y$	$\frac{1}{(2\pi)^{\frac{1}{2}}}\int_{-\infty}^{y}\exp(-y^2/2)dy$	$\rho(V)$	Exp. f	Obs. f	Dev.	Div.
30					0.005	3.3	1	−2.3	1.600
	32.5	−22.41	−2.57	0.005					
35					.018	11.8	12	+0.2	.004
	37.5	−17.41	−2.00	.023					
40					.055	36.1	38	+1.9	.100
	42.5	−12.41	−1.42	.078					
45					.122	80.0	76	−4.0	.200
	47.5	− 7.41	−0.83	.200					
50					.197	129.2	133	+3.8	.115
	52.5	− 2.41	−0.28	.397					
55					.223	146.0	152	+6.0	.247
	57.5	+ 2.59	+0.30	.620					
60					.190	124.5	118	−6.5	.338
	62.5	+ 7.59	+0.87	.810					
65					.115	75.5	69	−6.5	.560
	67.5	+12.59	+1.44	.925					
70					.053	34.8	44	+9.2	2.430
	72.5	+17.59	+2.02	.978					
75					.017	11.2	13		
	77.5	+22.59	+2.59	.995				−1.5	.155
80					.005	3.3	0		
	∞	∞	∞	1.000	1.000				5.750

$S'=7$, $P(>\chi^2)=0.55$

be made which in the future, will give in a few minutes, the data which required many hours of measuring to obtain before.

General Characteristics

In the earlier work on ignitors, current and voltage readings were recorded for different materials. It was noticed that, while there was a great deal of variation in the results, most of the values obtained showed a definite tendency for the current to increase as the voltage decreased. When the voltage *versus* current was plotted, it was found to approach a rectangular hyperbola of the form $VI=K$. Figure 5 shows the approximate range of the experimental points and the curve which seems to represent the average. The values of current and voltage found in these measurements were all taken with a peak voltmeter in the manner already described.

Straight rods of square cross section accurately ground to within $\pm.001''$ were then obtained of different resistivities and having smooth surfaces.

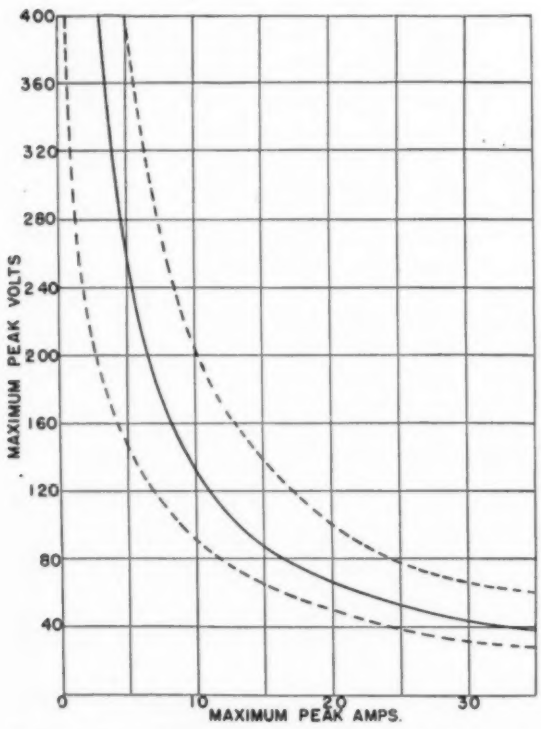

FIG. 5. Approximate range of voltage and current characteristics of a large number of ignitors showing the wide range of values.

TABLE III.

MATL. NO.	ρ $\Omega/In.^3$	d	V	I	I_0	$\rho^{\frac{1}{2}}$	$I_0\rho^{\frac{1}{2}}$	$V/\rho^{\frac{1}{2}}$	$V(4d)^{\frac{1}{2}}$
3	1.73	1/16″	198	8.3	33.2	1.32	43.7	150	
11	2.27	1/16″	204	7.2	28.8	1.51	43.5	135	
5	2.25	1/16″	206	8.0	32.0	1.5	48.0	137	
5	2.45	1/16″	207	7.4	29.5	1.56	46.0	132	
1		1/16″	*129	*15.4	61.5	0.82	50.5	157	64.5
1	0.64	5/64″	114	19.5	62.5	0.80	50.0	143	65.0
1	0.71	3/32″	107	22.7	60.5	0.84	50.8	124	65.5
1	0.69	7/64″	97	26.8	61.5	0.83	51.0	117	64.0
2	0.21	1/32″	74	14.0	112.0	0.46	51.5		
2	0.22	1/16″	70	27.8	111.0	0.47	52.2	149	

* Calculated.

All the samples used on these tests were $1\frac{1}{4}''$ long and were immersed $\frac{1}{4}''$ in the mercury with about $\frac{3}{4}''$ between the mercury and the ignitor holder. On testing samples of different sizes, it was found that a definite relation existed between the currents and the width of the side of the rod. This relation was that the current divided by the perimeter (or by the length of the side) was a constant for a given material as is shown in Table III.

$$I/4d = \text{constant} \doteq I_0. \qquad (3)$$

This suggests that for a given material, a definite linear current density or current per inch of perimeter is required to start the arc. Each of the values given are the average of those obtained for several ignitors of the same size and material.

Three different materials were used in these tests and when the voltage was plotted against the current per inch, the wide variation similar to that which existed in the older current-voltage curves, largely disappeared. Figure 6 shows the curve obtained. It will be noticed that the points for the material with $\rho=.68$ ohm/cm³ are spread vertically. For this set, it was found that the voltage times the square root of the width was approximately a constant. However, there is not sufficient variation in size to make this very conclusive except over a small range. The point at 129 volts and 61.5 amperes per inch was calculated for this constant for an ignitor with a $\frac{1}{16}''$ side. This allowed the heavy curve to be drawn through three points all for $\frac{1}{16}''$ ignitors.

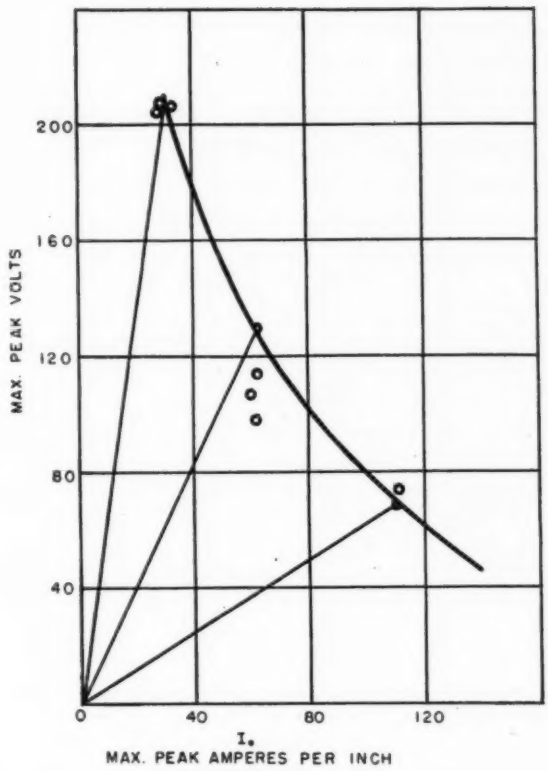

FIG. 6. Voltage plotted against current per inch for ignitors of different sizes and materials.

The light lines running from the origin to the maximum peak voltage and current points are drawn to show where the lower firing values due to the distribution curve will fall for each ignitor. This curve has a different shape from that of the earlier one, but when account is taken of the fact that the lower resistivity material operates at a considerably higher temperature, it is believed it will return to a curve represented by

$$(V-a)(I_0-b)=\text{constant}, \qquad (4)$$

where b is probably $=0$.

When it was found that the current per inch was constant for different materials, an attempt was made to find out what relation existed between this current and the resistivity. This is complicated by the fact that all the materials used have a large negative temperature coefficient of resistivity. When an ignitor is operating, its temperature may reach several hundred degrees centigrade, and is not uniform along its length. Thus it is very difficult to determine the hot resistivity near the surface of the mercury with any degree of accuracy. However, the fact that for different size ignitors of the same material $I/4d$ is a constant indicates that the temperature of the ignitor very close to the mercury surface is determined largely by the temperature of the pool itself. When the values of cold resistivity were compared with the current, it was found that approximately the current was inversely proportional to the square root of the cold resistivity. This suggests again, as the early current voltage curves had, that a definite amount of energy is required to form the arc.

Figure 7 shows $1/\rho^{\frac{1}{2}}$ plotted against I_0. The points are reasonably close to a straight line. Since this line should go through the origin, the two upper sets of points are progressively further from it. It is felt that this is due to the resistance *versus* temperature curves being slightly different for the three different materials used.

It should be emphasized that the current and

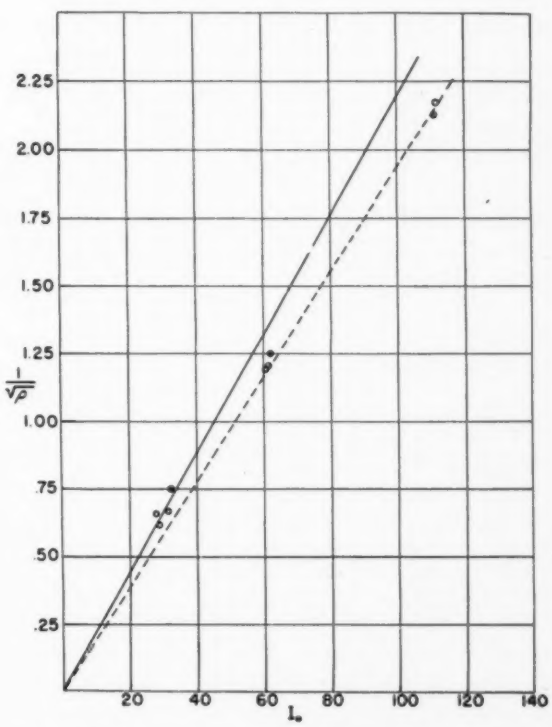

FIG. 7. $1/\rho^{\frac{1}{2}}$ *versus* the maximum peak current per inch. The dotted curve is the apparent straight line which fits the points. The solid curve is the straight line which is probably more correct if account is taken of the difference in the temperature coefficients of the materials.

voltage readings being discussed are the maximum peak values which are not exceeded in a time of 30 seconds. While the above results are of considerable practical value in designing ignitors, they must be regarded with caution in trying to determine the fundamental processes which are responsible for the starting of an arc by this method. For this purpose, it is felt that the average or most probable values are the ones which should be used in investigating the fundamental processes. This fact must be remembered, since it is not necessarily true that the same relations will hold for the most probable values given by the distribution curves as hold for the maximum peak values.

Ignitors Operated in Parallel

Since the firing of an ignitor is of a statistical nature and the measurement of voltage and current can be interpreted as giving the probability of firing, this combined with the relation $I/4d=K$ suggests that further information might be gained by operating two or more ignitors in parallel. This was done with the square ignitors, and it was found that the maximum peak current required for nearly identical ignitors was given approximately by

$$I_n=n^{\frac{1}{2}}I_1, \tag{5}$$

where n is the number of ignitors and I_1 is the current required for one ignitor operated alone.

From Eq. (3)

$$I/4d=K,$$

we would expect to get

$$I_n=nI_1 \tag{6}$$

for n ignitors in parallel and the voltage should remain about the same.

The following argument, however, shows that the observed results are to be expected, at least qualitatively.

Let P = the probability of one ignitor firing below V volts. Then $(1-P)$ = the probability of one ignitor firing above V volts. If two identical ignitors are operated in parallel, then $(1-P)(1-P)=(1-P)^2$ = the probability of both ignitors firing above V volts and $P_2=1-(1-P)^2$ = the probability of one or the other, or both ignitors firing below V volts, P will, in general, be given by

$$P_n=1-(1-P)^n, \tag{7}$$

where n is the number of identical ignitors operated in parallel. Returning to the case of just two ignitors in parallel

$$P_2=1-(1-P)^2, \tag{8}$$

$$dP_2=2(1-P)dP. \tag{9}$$

Now a plot of dP *versus* V is just the distribution curve shown previously and dP_2 *versus* V will be the distribution curve for two ignitors. This curve and one for $n=4$ are shown in Fig. 4, curves (3) and (4) and both of them are still reasonably symmetrical about the most probable value and resemble a Gaussian distribution.

It is seen from curves (1) and (3) that with two ignitors, the probability of firing is increased for values of V below the most probable value for one ignitor, and is decreased above this value of V. A similar relation is found between curves (3) and (4).

This analysis is, of course, only justified if each ignition is completely independent of the previous one. This in general seems to be the case since, on a rough test, the values of V are found to be distributed at random with respect to time.

Theory

The theories proposed for the starting of an arc by an ignitor depend on either the formation of a large voltage gradient or a high energy density at or very near the point where the surface of the mercury joins the ignitor. Slepian[1] has shown that the current density will be extremely high at the point of contact. However, the experimental results obtained suggest that not all of the current which passes from the ignitor into the mercury is useful in starting the arc.

It is possible to derive an expression for the ratio of useful to total ignitor current and this will be used with the experimental results to determine the effect of surface contact area on the total current required to start the arc. The experimental values of the total current referred to are the maximum peak values obtained as described above, with a peak voltmeter. As

shown by Fig. 2, a current distribution exists similar to that shown for voltage and it is for this reason, that the value of the firing current is affected less than would be expected by change in size of the ignitor and by the number of ignitors used together.

Expressions are given by Maxwell[3] for the equipotentials and lines of current flow in a thin sheet of a conductor of such shape that it represents a vertical cross section of an ignitor dipping into a mercury pool. It is assumed here that these expressions can be used as a sufficiently good approximation for the three-dimensional current flow to give the ratio of the current entering the mercury above any point to the total current flowing into the mercury.

In Fig. 8, x is the distance from the point of contact with the mercury $\pi b = d$ is the length of one side of a square ignitor, and l is the length of ignitor immersed in the mercury.

Then if φ is the potential function and ψ the current function, Maxwell gives

$$x = \frac{b}{2} \log \frac{1}{4}(\exp(2\varphi) + \exp(-2\varphi) + 2\cos 2\psi), \quad (10)$$

$$y = b \tan^{-1} \frac{(\exp(\varphi) - \exp(-\varphi)\tan\psi)}{\exp(\varphi) - \exp(-\varphi)}. \quad (11)$$

The equipotentials are given by setting $\varphi =$ constant and the lines of current flow by setting $\psi =$ constant.

To find the amount of current which enters the mercury close to the surface we set $\varphi = 0$ for the surface of the ignitor below the mercury. This gives

$$x = \frac{b}{2} \log \frac{1}{2}(1 + \cos 2\psi) \quad (12)$$

from which

$$\psi = \cos^{-1} \exp(x/b).$$

Since we are concerned only with the distance below the mercury contact, we can write

$$\psi = \cos^{-1} \exp(-x/b), \quad (13)$$

where x is now taken as the distance on the surface of the ignitor below the mercury.

[3] Maxwell, *Electricity and Magnetism*, third edition, article 93, p. 297.

From this equation, the amount of current passing into the mercury within a distance x of the surface is given by

$$\psi_x - \psi_0 = \cos^{-1} \exp(-x/b) - \cos^{-1} e^0$$
$$= \cos^{-1} \exp(-x/b)$$

and the proportion of the total current which passes into the mercury within a distance x of the surface is

$$\frac{\psi_x - \psi_0}{\psi_1 - \psi_0} = \frac{\cos^{-1} \exp(-x/b)}{\cos^{-1} \exp(-1/b)}$$
$$= \frac{\cos^{-1} \exp(-x/b)}{\pi/2} \quad \text{for } 1 \gg \pi b.$$

Thus if we call i the useful current and I the total ignitor current

$$\frac{i}{I} = \frac{2}{\pi} \cos^{-1} \exp(-x/b). \quad (14)$$

If x is taken as .001", $\pi b = d$ as .062", 1 as .25",

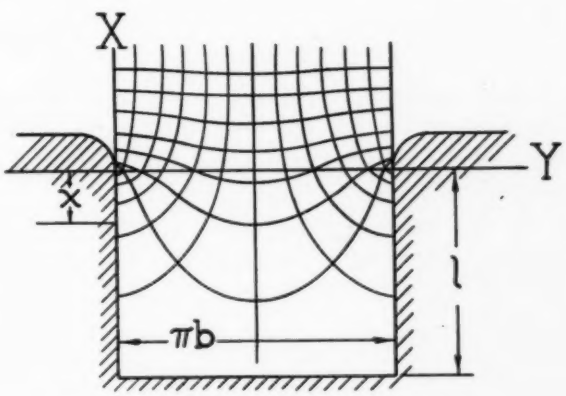

FIG. 8. Equipotentials and lines of current flow in an ignitor immersed in mercury.

then $i = 0.2I$. Since the value of x must be extremely small, probably much less than .001"

$$\exp(-x/b) = 1 - x/b \text{ approx.}$$

and

$$\therefore \quad \cos\frac{\pi i}{2I} = 1 - \frac{x}{b},$$

similarly for small values of i/I

$$\cos\frac{\pi i}{2I} = 1 - \frac{\pi^2 i^2}{8I^2} \text{ approx.}$$

and

$$\therefore \quad \frac{\pi^2 i^2}{8I} = \frac{x}{b}$$

or

$$i = I(8x/\pi^2 b)^{\frac{1}{2}} \tag{15}$$

or since d, the width of the ignitor is equal to πb

$$i = I(8x/\pi d)^{\frac{1}{2}}. \tag{16}$$

This equation shows that the proportion of useful current decreases as the width of the ignitor increases. Let x_0 be the distance below which current entering the mercury cannot aid in starting the arc. Then

$$i = I(8x_0/\pi d)^{\frac{1}{2}} = aI/d^{\frac{1}{2}} \tag{17}$$

where

$$a = (8x_0/\pi)^{\frac{1}{2}} = \text{constant}.$$

Since it was found that the current required to fire the ignitor

$$I = 4dI_0, \tag{3}$$

then the useful current will be given by

$$i = 4dI_0 a/d^{\frac{1}{2}} \tag{18}$$

or

$$i = 4aI_0 d^{\frac{1}{2}}. \tag{19}$$

This shows that the useful current required to start the arc is proportional to the square root of the perimeter of the ignitor for square ignitors of a given material.

In the case of n identical ignitors each of width d operating in parallel, it is seen from (17) that for each ignitor, the ratio of useful to total current will be

$$i_1/I_1 = a/(d_1)^{\frac{1}{2}} \tag{20}$$

and

$$\therefore \quad i_n/I_n = a/(d_1)^{\frac{1}{2}}, \tag{21}$$

since this ratio will remain constant regardless of the number of ignitors used because they are all of the same size.

But from (19)

$$i_n = 4aI_0(nd_1)^{\frac{1}{2}}, \tag{22}$$

since $4nd_1$ is now the total perimeter in contact with the mercury and

$$\therefore \quad I_n = \frac{i_n(d_1)^{\frac{1}{2}}}{a} = \frac{4aI_0(nd_1)^{\frac{1}{2}}(d_1)^{\frac{1}{2}}}{a}$$

or

$$I_n = 4I_0 d_1 n^{\frac{1}{2}}. \tag{23}$$

Since, in this case, d is a constant, then

$$I_n = n^{\frac{1}{2}} I_1. \tag{24}$$

That is, the total current required to fire a number of identical ignitors in parallel is proportional to the square root of the number of ignitors.

This result has been approximately verified experimentally, and thus justifies the approximations made in deriving the expression for the useful current. Dividing the useful current by $4d$, we get the value of useful current per inch around the ignitor which it requires to start an arc.

$$i_0 = i/4d = 4aI_0 d^{\frac{1}{2}}/4d = aI_0/d^{\frac{1}{2}}, \tag{25}$$

since I_0 is a constant, i_0 cannot be, and the reason for this is to be found in the statistical nature of the firing process.

That this result is to be expected qualitatively can be seen by considering the surface of the ignitor, at the junction with the mercury, as composed of a large number of small points, any one of which is ready to start an arc under the proper conditions. A certain number of these will be found ready to start an arc for some value of useful ignitor current per inch, i_0'. As the perimeter of the ignitor is increased, the number of points available for firing is increased so that the chance of there being at least one point ready to fire at a given value of current will also be increased. This means that the chance of firing at low values of i_0 is increased, and therefore, a new value i_0'' can be found which is less than i_0', for which the chance of firing is the same as it was for i_0' with the smaller ignitor.

Thus the total useful current $4di_0$ will not increase linearly with d but will increase more slowly than this.

Summary

It would be unwise at the present stage of this work to try to draw too definite conclusions from the results. It is felt, however, that the following general statements are justified for square rod ignitors of smooth homogeneous material.

1. A frequency distribution curve can be obtained for the current and voltage required to

fire an ignitor. This curve is approximately a Gaussian error distribution.

2. The total current required to fire, divided by the perimeter, is a constant for a given resistivity.

$$I/4d = I_0.$$

3. The total current per unit length of perimeter times the square root of the resistivity is a constant

$$I_0\rho^{\frac{1}{2}} = K.$$

4. The proportion of useful current required to fire the ignitor is inversely proportional to the square root of the width

$$i/I = a/d^{\frac{1}{2}}.$$

5. For identical ignitors in parallel, the current required to fire is equal to the square root of the number of ignitors times the current required for one ignitor.

$$I_n = n^{\frac{1}{2}} I_1.$$

6. The effect of the statistical distribution on the firing current is proportional to the square root of the perimeter.

Work is being continued in order to determine from the distribution curves how the most probable values depend on the size and resistivity of the ignitors.

The writer wishes to express his appreciation to Mr. D. E. Marshall for his continued help and criticism and to Dr. J. Slepian for his comments during the various stages of the work.

The Structure and Dynamics of Liquids*

W. E. Roseveare, R. E. Powell and Henry Eyring
Frick Chemical Laboratory, Princeton University, Princeton, New Jersey
(Received December 7, 1940)

By coordinating our information on viscosity, diffusion, melting, and other rate and thermodynamic properties, we arrive at a detailed picture of liquid structure. Thus we find that a liquid is best thought of as a solid to which a large number of empty equilibrium positions are added. In fact the expansion on melting, as well as the expansion with a rise in temperature, arises almost entirely from this introduction of new equilibrium positions, and only to a minor extent from lattice expansion. We shall obtain information as to the number, size and energy of formation of these empty lattice points.

I. Theory of Melting

SEVERAL mathematical treatments of phenomena in the liquid state have taken as a model liquid a binary mixture of holes and molecules. Thus Eyring was led to postulate the presence of holes in liquids in a theory of the law of rectilinear diameters of Cailletet and Mathias as well as to explain viscous flow.[1] Lennard-Jones and Devonshire[2] assume that in the process of melting a number of new lattice positions called β-sites equal in number to the original α-sites appear. The redistribution of the atoms between the old α-sites and the new β-sites involves an increase in entropy, energy, and volume, and with a suitable and reasonable choice of parameters excellent agreement with experiment has been obtained by these authors. Cernuschi and Eyring have considered liquids as being made up of a binary mixture of holes and molecules, the holes having the same size as the molecules.[3] A mathematically equivalent treatment has been given by Kirkwood who treated critical phenomena as order-disorder transformations.[4]

We will now make the assumption that a liquid is a random distribution of molecules over

* Presented at the 1940 annual meeting of the Society of Rheology.

[1] H. Eyring, J. Chem. Phys. **4**, 283 (1936).

[2] J. E. Lennard-Jones and A. F. Devonshire, Proc. Roy. Soc. London **A169**, 317 (1939); *ibid.* **A170**, 464 (1939).

[3] F. Cernuschi and H. Eyring, J. Chem. Phys. **7**, 547 (1939).

[4] J. G. Kirkwood, J. Phys. Chem. **43**, 97 (1939).

TABLE I.

SUBSTANCE	$\frac{V-V_s}{V_s}$	VOLUME OF ION / VOLUME OF ATOM	$\frac{n_h}{N}$	ΔS_m CALC.	ΔS_m OBS.
Mercury	0.0259	0.114	1.363	3.2 e.u.	2.37 e.u.
Lithium	.006	.097	0.37	1.58	1.83
Sodium	.0271	.170	0.955	2.68	1.70
Potassium	.0231	.206	0.672	2.24	1.75
Rubidium	.0284	.245	0.695	2.27	1.67
Cesium	.0256	.273	0.562	2.08	1.69
Benzene	.1338*	——	0.801	2.46	8.5
"	.0677	——	0.406	1.68	8.5
Carbon disulfide	.0673	——	0.404	1.67	—
Argon	.12	——	0.72	2.32	3.19
Nitrogen	.09	——	0.54	2.00	2.69

* From Bridgman's data on the change of melting point with pressure.

occupied and unoccupied equilibrium positions, and that the volume and energy associated with one of these equilibrium positions is characteristic of the material. The fusion of a mole of molecules, N, results in the introduction of n_h of these holes, to give an entropy increase of

$$\Delta S = -Nk \ln \frac{N}{N+n_h} - n_h k \ln \frac{n_h}{N+n_h}. \quad (1)$$

If the volume increase on melting is due to the introduction of such new equilibrium positions, we have:

$$n_h/N = n'(v-v_s)/v_s, \quad (2)$$

where v_s is the volume of the solid, v is the volume of the liquid at the melting point, and the volume of an empty equilibrium position is taken as $1/n'$ of the volume of a molecule. A numerical value of n' may be found as follows: Batschinski has shown that for a large number of liquids the fluidity is proportional to the increase in volume: or in our terminology, the fluidity is to a large extent determined by the number of empty equilibrium positions alone.[5,6] From a study of the pressure effect on fluidity, Frisch, Kincaid and Eyring have shown that the volume of one of these holes required for flow is about $\frac{1}{6}$ the volume of a molecule.[7]

Taking n' as 6, the observed expansion on melting permits us to compute by Eq. (2) the number of holes in the liquid at the melting point and thus permits a rough computation by Eq. (1) of that part of the entropy of melting due to the increase in lattice disorder. Table I presents the calculated and experimental results. Fluidity data has been interpreted as showing that in molten metals the ion is the flowing species, so for the metals, n' is taken as 6/(volume of ion/volume of atom).[8]

The calculated entropies of fusion are seen to cluster about 2 entropy units: this is just the observed entropy of fusion for a large number of monatomic substances.[9] Except for the simplest substances, melting will involve other entropy changes besides that arising from the increase in disorder.[10,11] The number of holes just equivalent to 2 e.u. is $n_h = 0.54N$. The results of Table I may be summarized by saying: The entropy of melting due to lattice disorder will be reproduced by the distribution of 1 mole of molecules at random upon 1.54 moles of lattice positions. Further, the volume change of melting will be reproduced if the volume of a hole is about $\frac{1}{6}$ the volume of a molecule. The thermodynamic equation $dp/dT = \Delta S_m/\Delta V_m$ insures that a theory which gives correctly the entropy of melting and expansion of melting will also give the proper dependence of the melting point on pressure.

II. THE PARTITION FUNCTION FOR A LIQUID

We can now formulate, in terms of holes, a simple partition function for a liquid. The partition function for the liquid is intermediate between that for the solid and that for the gas. In a solid the molecules vibrate in a field of the type shown in Fig. 1*a*, while in a liquid some of the degrees of freedom are of the type shown in

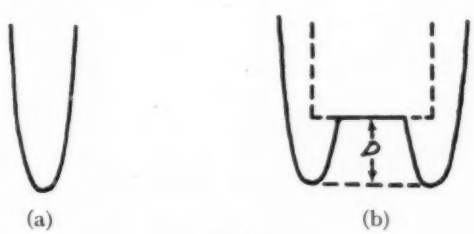

FIG. 1.

[5] A. J. Batschinski, Zeits. f. physik. Chemie **84**, 643 (1913).
[6] E. C. Bingham, *Fluidity and Plasticity* (McGraw-Hill, 1922).
[7] D. Frisch, H. Eyring and J. F. Kincaid, J. App. Phys. **11**, 75 (1940).
[8] R. Ewell and H. Eyring, J. Chem. Phys. **5**, 726 (1937).
[9] Cf. Taylor, editor, *Treatise on Physical Chemistry* (Van Nostrand, 1931) second edition.
[10] L. Pauling, Phys. Rev. **36**, 430 (1930).
[11] J. Hirschfelder, D. Stevenson and H. Eyring, J. Chem. Phys. **5**, 896 (1937).

Fig. 1*b*, where D is the activation energy for passage to an adjacent vacant equilibrium position. The partition function for one degree of freedom of a molecule in a potential field of the type shown in Fig. 1*a* is:

$$f_1=(1-\exp(-h\nu/kT))^{-1}\exp(-E_s/3RT), \quad (3)$$

where ν is the characteristic vibration frequency of the solid and E_s is the potential energy of the system when all the molecules are at their equilibrium positions. The number of degrees of freedom of this type will be three times the number of molecules multiplied by the mole fraction $N_1(v)$ of filled equilibrium positions. The total partition function for all degrees of freedom of this type will be:

$$F_1=[(1-\exp(-h\nu/kT))^{-1}\times\exp(-E_s/3RT)]^{3NN_1(v)}. \quad (4)$$

For a molecule in a potential field of the type shown in Fig. 1*b*, the partition function in that degree of freedom will be that for a simple harmonic oscillator up to the internal dissociation energy D. Above this we have half the partition function for the harmonic oscillator plus the partition function of a particle in a box of length $(v_s/n')^{\frac{1}{3}}$ as indicated by the adjacent dotted lines. The partition function for a single degree of freedom of this type is:

$$f_2=\left[\sum_{nh\nu=0}^{D}\exp(-nh\nu/kT)+\tfrac{1}{2}\sum_{nh\nu=D}^{\infty}\exp(-nh\nu/kT)+\frac{(2\pi mkT)^{\frac{1}{2}}}{h}\left(\frac{v_s}{n'}\right)^{\frac{1}{3}}\exp(-D/kT)\right]\times\exp(-E_s-3D/3RT) \quad (5)$$

or

$$f_2=\left[\frac{1-\frac{1}{2}\exp(-D/kT)}{1-\exp(-h\nu/kT)}+\exp(-D/kT)\frac{(2\pi mkT)^{\frac{1}{2}}}{h}\left(\frac{v_s}{n'}\right)^{\frac{1}{3}}\right]\times\exp(-E_s-3D/3RT). \quad (6)$$

The number of degrees of freedom of this type will be three times the number of molecules multiplied by the mole fraction $N_2(v)=1-N_1(v)$ of holes. The partition function for degrees of freedom of this type for N molecules will be:

$$F_2=\left[\left(\frac{1-\frac{1}{2}\exp(-D/kT)}{1-\exp(-h\nu/kT)}+\exp(-D/kT)\frac{(2\pi mkT)^{\frac{1}{2}}}{h}\left(\frac{v_s}{n'}\right)^{\frac{1}{3}}\right)\times\exp[-(E_s-3D)/3RT]\right]^{3NN_2(v)}. \quad (7)$$

In addition the partition function contains a term corresponding to the entropy of lattice disorder:

$$F_3=\frac{(N+n_h)!}{N!\,n_h!}. \quad (8)$$

The complete partition function for N molecules is then:

$$F=F_1F_2F_3. \quad (9)$$

This partition function becomes at the lower limit that for the solid, at the upper limit that for the gas. Since the energy of making a hole is given as $\frac{1}{3}$ the energy of vaporization, the partition function will give the critical point approximately correctly.[12]

From the well-known equation

$$A=-kT\ln f \quad (10)$$

and equations of the type

$$P=-(\partial A/\partial V)_T \quad (11)$$

the thermodynamics of liquids may be derived when an expression is found for $N_1(v)$. Applications of this type of a partition function to thermodynamic properties will be given elsewhere.[11a]

III. Fluidity at Constant Volume

Bridgman's data at high pressures shows that, for non-associated liquids, the temperature coefficient of fluidity at constant volume is insignificant compared to the temperature coefficient at constant pressure.[13] These results indicate that

[11a] J. Walter and H. Eyring, J. Chem. Phys. **9**, 393 (1941).
[12] J. G. Kirkwood, J. Chem. Phys. **7**, 909 (1939).
[13] P. W. Bridgman, *The Physics of High Pressures* (Macmillan, 1931).

the fluidity of normal liquids under ordinary conditions is to a large extent a function of the volume alone.

As we shall see later, diffusion can be best interpreted as the passage of a single molecule over a potential barrier into a hole. Thus the most likely mechanism of flow is the moving of single molecules into adjacent holes.

For a molecule located at a particular point, its average velocity of moving forward will be equal to the product of the number of equilibrium positions, or holes, to which it may flow times the average velocity of the molecule parallel to the direction of flow times an exponential term involving the free energy of activation for flowing from one equilibrium position to another. This latter activation free energy is generally small compared with the free energy of forming the hole F_h. The number of new equilibrium positions available may be set equal to the increase in volume over that of the solid, i.e., $v-v_s$ divided by v_h the volume increase required per new equilibrium position. The average velocity of the molecules parallel to the direction of flow is $(kT/2\pi m)^{\frac{1}{2}}$. The average distance between equilibrium positions in the direction of motion is taken as λ while the distance between neighboring molecules in the same direction is λ_2. The distance between molecules normal to the direction of flow and perpendicular to the velocity gradient is λ_3. The shearing force per square centimeter is f. The force acting on a single molecule is $f\lambda_2\lambda_3$, and it acts to lessen the work of passing over the potential barrier through a distance $\lambda/2$, so that in the forward direction the height of the barrier is in effect lowered by the amount of work $f\lambda_2\lambda_3\lambda/2$, while in the backward direction it is raised by the same amount. The number of times that a molecule moves in the forward direction in a second may then be written as the corresponding specific reaction rate:

$$k_f=\frac{v-v_s}{v_h}\frac{1}{\lambda}\left(\frac{kT}{2\pi m}\right)^{\frac{1}{2}} \times\exp\left[(-\Delta H_v+f\lambda_2\lambda_3\lambda/2)/kT\right]. \quad (12)$$

For the backward direction:

$$k_b=\frac{v-v_s}{v_h}\frac{1}{\lambda}\left(\frac{kT}{2\pi m}\right)^{\frac{1}{2}} \times\exp\left[(-\Delta H_v-f\lambda_2\lambda_3\lambda/2)/kT\right]. \quad (13)$$

For the fluidity we have:

$$\phi=\frac{\Delta v}{f\lambda_1}=\frac{\lambda(k_f-k_b)}{f\lambda_1}, \quad (14)$$

$$=\frac{\lambda}{f\lambda_1}\frac{v-v_s}{v_h}\frac{1}{\lambda}\left(\frac{kT}{2\pi m}\right)^{\frac{1}{2}}\exp\left(-\Delta H_v/kT\right) \times 2\sinh\left(f\lambda_2\lambda_3\lambda/2kT\right). \quad (15)$$

For ordinary viscous flow $f\lambda_2\lambda_3\lambda \ll kt$, so that expanding the exponential, retaining only the first power terms and letting $\lambda_2\lambda_3=V^{\frac{1}{3}}$ we have:

$$\phi=\frac{\lambda}{\lambda_1}v^{\frac{1}{3}}\left(\frac{v-v_s}{v_h}\right)(2\pi mkT)^{-\frac{1}{2}}\exp\left(-\Delta H_v/kT\right). \quad (16)$$

If we take λ/λ_1 equal to $(v_s/v)^{\frac{1}{3}}$ and $v_h=v_s/n'$, the fluidity is given as follows:

$$\phi=(v_sv)^{\frac{1}{3}}\left(\frac{v-v_s}{v_s}\right)n'(2\pi mkT)^{-\frac{1}{2}} \times\exp\left(-\Delta H_v/kT\right). \quad (17)$$

Taking n' as a constant, we have at constant volume for two different temperatures:

$$\Delta H_v=k(\Delta\ln\phi+\tfrac{1}{2}\Delta\ln T)\Big/\Delta\left(\frac{1}{T}\right). \quad (18)$$

Table II gives values of ΔH_v in calories per mole

TABLE II.

SUBSTANCE	ΔH_v	SUBSTANCE	ΔH_v
Mercury	700	Acetone	−110
Ether	700	*n*-octane	1180
Benzene	700	methyl alcohol	1340
Chlorobenzene	640	ethyl alcohol	3030
Brombenzene	740	*n*-propyl alcohol	3000
Iodobenzene	780	*i*-propyl alcohol	3640
Carbon tetrachloride	530	*n*-butyl alcohol	3000
Carbon disulfide	530	*i*-butyl alcohol	4120
n-pentane	750	*i*-amyl alcohol	4390
i-pentane	460	Glycerine	1820
Hexane	640		

TABLE III.

SUBSTANCE	MELTING POINT	$\phi/\exp\left(\frac{-\Delta H_v}{kT}\right)$ CALCULATED	ϕ CALCULATED	ϕ OBSERVED
Mercury	234°K	51.5	11	48.8
Cadmium	250	45		66
Lead	601	41		68
Tin	505	55		24
Bismuth	544	44		54
Nitrogen	63	484		339
Argon	84	633		357
Benzene	278	252	71	121
Carbon disulfide	160	242	46	59
Carbon tetrachloride	250	206	71	49.2
Chlorobenzene	228	378	92	44.4
Bromobenzene	243	227	49	37
Iodobenzene	242	175	30	22
n-pentane	142	410	31	24
n-hexane	178	356	58	50.8
n-heptane	283	302		37.2
n-octane	216	314	24	56.2
n-decane	243	350		47.6
o-xylene	244	328		56.4
Methyl acetate	175	354		31.4
Chlorine	170	178		110
Bromine	266	131		69.0
Iodine	386	101		44.8
Sodium chloride	1077			61.9
Potassium nitrate				35.7
Sodium nitrate				32.9
Ethyl alcohol	156	322	.050	.031
n-propyl alcohol	146	314	.068	.034
l-amyl alcohol	156	320	.00003	.00007
Glycerine	290	314	.087	.082

determined from this formula using fluidities at 30° and 75° at constant volume. These fluidities were obtained by graphical interpolation of Bridgman's data in the lower pressure range where the temperature coefficient of fluidity at constant volume increases with increase in density. The uncertainty in the determined values of ΔH_v is about 100 calories. The normal substances in the first column of Table II have values of ΔH_v constant within about the experimental error. Acetone like water has a negative value of ΔH_v which may be interpreted as due to a change in structure or coordination number with temperature at constant volume. Most of the alcohols have activation energies at constant volume corresponding in magnitude to the energy required to break a hydrogen bond.

At the melting point we may substitute Eq. (2) into Eq. (17), set $n_h = 0.54N$, and obtain:

$$\phi_m = 0.54(v_s v)^{\frac{1}{3}}(2\pi mkT)^{-\frac{1}{2}} \exp \frac{(-\Delta H_v)}{kT}. \quad (19)$$

Table III gives the observed values of the fluidities at the freezing point for various types of substances, and those calculated from Eq. (19). The calculated values agree with the experimental values within a factor of about two. The uncertainty in the values of ΔH_v is sufficient to account for all divergence between the calculated and experimental values except in the case of mercury, which is four times more fluid than calculated. This discrepancy is removed if in Eq. (19) we take n' as 6/(volume of ion/volume of atom) for metals as we should if the ions rather than the atoms are the units of flow. The value of the exponential factor for most substances varies from four to six, while for the hydrogen bonded substances the value is very much larger. It is 10^7 for isoamyl alcohol. The table also indicates that except for the substances melting below 100°K the fluidities at the freezing point tend toward a value of about fifty for normal substances.

If v_s, n' and ΔH_v are independent of volume, then $\phi T^{\frac{1}{3}}/[v^{\frac{1}{3}} \exp(-\Delta H_v/kT)]$ should be a linear function of the volume, according to Eq. (17). Figure 2 shows this to be true for benzene, carbon tetrachloride, carbon disulfide, chlorobenzene, isopentane and *n*-butyl alcohol. The range of data plotted for benzene is 10–185°C, for carbon tetrachloride 0–65°C, for carbon

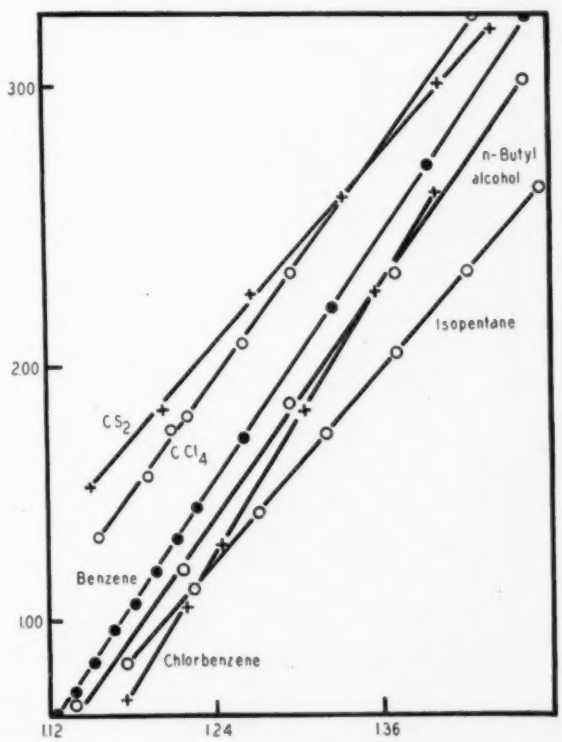

FIG. 2.

disulfide 0–46°C, for chlorobenzene 0–120°C, for isopentane 0–30°C and for *n*-butyl alcohol 0–38°C. In Fig. 3, mercury gives a straight line from −20 to 100°C while showing very marked curvature from 100 to 350°. In this latter range it is probable that the value of n' is decreasing toward the value for normal nonmetallic liquids. In Fig. 3, ether, ethyl alcohol and glycerine do not give straight lines, suggesting a change in the liquid structure. (In Figs. 2 and 3 the scales of coordinates are for benzene and mercury respectively, while the values for the other substances are in arbitrary units and with the axes displaced to fit the graph.)

IV. Fluidity at Constant Pressure

Since most of the available fluidity data are at constant pressure, instead of at constant volume, it will be useful to see what results the hole theory of liquid structure yields in this case.

The equation for fluidity at constant pressure may be written[8]

$$\frac{1}{\eta}=\phi=\frac{v}{Nh}\exp\left(-\Delta F^{\ddagger}/RT\right), \tag{20}$$

$$=\frac{v}{Nh}\exp\left(\Delta S^{\ddagger}/R\right)\left(\exp -\Delta H^{\ddagger}/RT\right), \tag{21}$$

where the term $\Delta H^{\ddagger}$ now contains both the heat of activation for forming the hole and the heat of activation at constant volume, and the term $\Delta S^{\ddagger}$ includes any other factors. This is, of course, only an alternative way of writing previous expressions.

The free energy of activation $\Delta F^{\ddagger}$ may be estimated as some fraction of the total free energy change ΔF of an analogous reaction. In order to make a hole, or new equilibrium position, the same kind of bonds must be broken as are broken in vaporization; however, the work RT per mole of expansion against the atmosphere is not needed, neither is the entropy of expansion into the vapor state available. Thus the thermodynamic quantity with which $\Delta F^{\ddagger}$ may be correlated is

$$\Delta F_{\text{vap}}+T\Delta S_{\text{vap}}-RT=\Delta H_{\text{vap}}-RT=\Delta E_{\text{vap}}.$$

Ewell and Eyring have pointed out that $\Delta H^{\ddagger}$ is about $\frac{1}{3}\Delta E_{\text{vap}}$ for a number of liquids. Fig. 4 gives an experimental test of this relation. For normal liquids, the experimental points fall well along a straight line: for associated liquids, more energy is required. As we have seen, for such liquids the heat of forming holes is no longer the determining factor, but rather the necessity of the flowing molecules breaking hydrogen bonds. An examination of the entropy of activation (Fig. 5) shows that these same associated liquids show a high positive $\Delta S^{\ddagger}$; in terms of our model, after the flowing molecule has broken its hydrogen bond it can rotate freely, and thus gains entropy. The entropy change tends to compensate the heat change,[14] so that when $\Delta F^{\ddagger}$ is plotted against ΔE_{vap} an excellent straight line is obtained (Fig. 6). The absolute value of the fluidity can be predicted, knowing only the

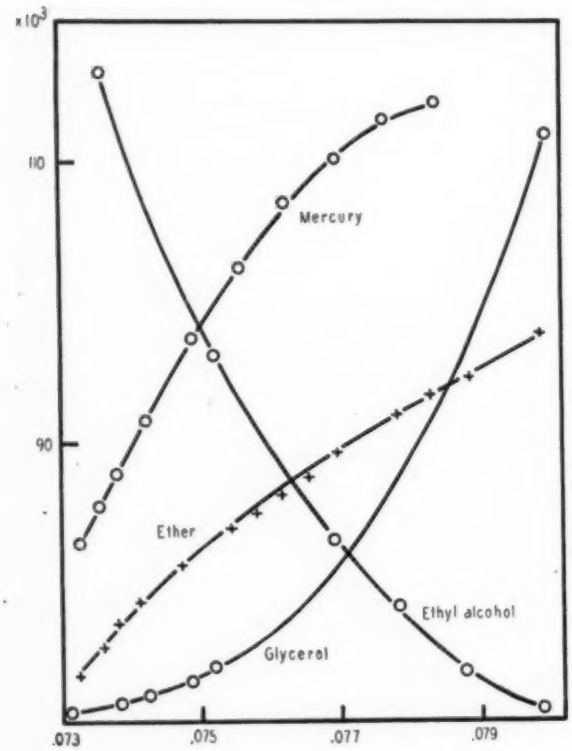

Fig. 3.

[14] A. E. Stearn and H. Eyring, J. Chem. Phys. **5**, 113 (1937).

molal volume and the heat of vaporization, from the equation:

$$\phi=\frac{v}{Nh}\exp\left(-\Delta E_{\text{vap}}/2.45RT\right). \qquad (22)$$

V. The Mixture Law for Fluidity

The viscosity of a mixture of liquids is not related to the viscosities of the pure components by any simple additive relation such as

$$\eta=N_1\eta_1+N_2\eta_2. \qquad (23a)$$

Several equations have been tested in the search for an additive function for fluidity, among them being[15]

$$\phi=N_1\phi_1+N_2\phi_2, \qquad (23b)$$

$$\phi^{\frac{1}{2}}=N_1\phi_1^{\frac{1}{2}}+N_2\phi_2^{\frac{1}{2}}, \qquad (23c)$$

$$\phi^{n}=N_1\phi_1^{n}+N_2\phi_2^{n}, \qquad (23d)$$

$$\log\phi=N_1\log\phi_1+N_2\log\phi_2, \qquad (23e)$$

the weighting being done according to weight fraction, volume fraction and mole fraction. There is also a wide variety of equations containing one or more adjustable constants. For example, an equation of the type of Eq. (23d) but with an adjustable exponent has been used by petroleum engineers to estimate the viscosity of mixtures of lubricating oils; for high-viscosity paraffin-base plus low-viscosity naphthene base, the exponent is 1/30; for the opposite case, the exponent is 1/3.1; for two oils of the same base, the exponent is 1/6.5.[16] Such equations are convenient for interpolation purposes, but that they fit the experimental data is more a matter of arithmetical inevitability than of merit. Of the equations not containing an adjustable constant, Eq. (23e) fits the experimental data rather better than the others.

If the flow process were strictly determined by the properties of one molecule flowing, Eq. (23b) would be expected to hold. If it were determined by the properties of two molecules flowing past each other, Eq. (23c) would be expected to hold. However, if the presence of holes is necessary

[15] Cf. J. Kendall and K. P. Monroe, J. Am. Chem. Soc. **43**, 115 (1921).

[16] G. Wilson, Nat. Petroleum News, May 22, 1929.

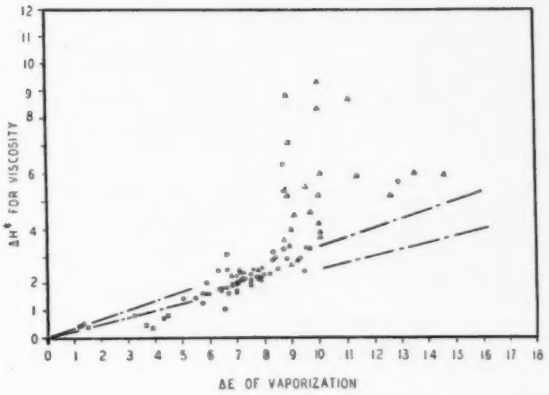

FIG. 4.

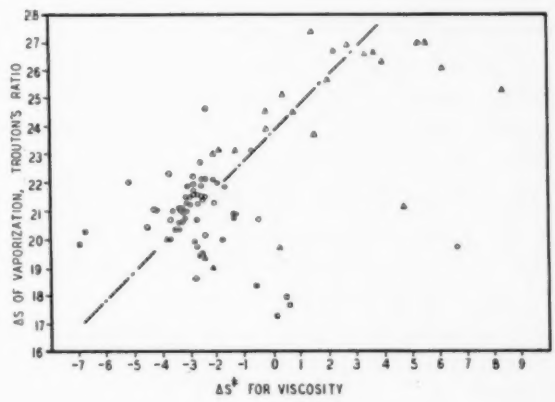

FIG. 5.

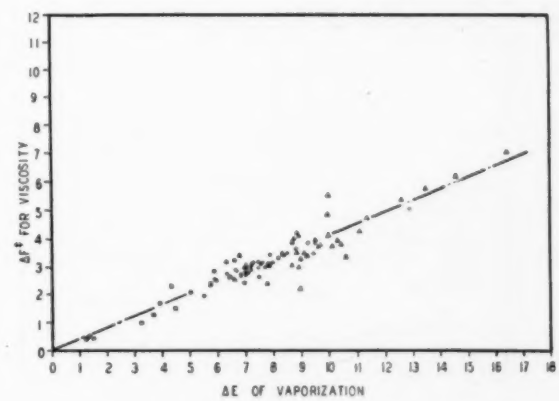

FIG. 6.

FIGS. 4 to 6.

Squares: N_2, CO, A, O_2, C_2H_4, HCl, HBr, HI, H_2S.
Circles: Typical organic liquids.
Triangles: Water, alcohols, organic acids, glycerol.

for flow, the ability of the solvent to provide holes is the determining factor. Thus the average thermodynamic properties of the entire liquid will be involved when any individual molecule flows.

As a simple approximation, Eq. (20) may be used for mixtures if for V is inserted the actual value of the average molal volume, and for $\Delta F^{\ddagger}$ is inserted the weighted arithmetic mean of the values for the pure components:

$$\phi=\frac{\bar{V}}{Nh}\exp\left[-(N_1\Delta F_1^{\ddagger}+N_2\Delta F_2^{\ddagger})/RT\right]. \quad (24)$$

When V_1 and V_2 are not too different, Eq. (24) reduces to Kendall's equation, Eq. (23c).

As a test of Eq. (24), $\Delta F^{\ddagger}$ has been plotted against mole-fraction for a number of pairs of liquids. Three types of curves are obtained, of which typical examples are shown in Fig. 7:

(a) Closely similar liquids, e.g., benzene and anisole, give a straight line.

(b) Liquids which definitely form a compound, e.g., chloroform and ether, give a convex curve.

(c) Liquids which are slightly dissimilar give a slightly concave curve; liquids which are markedly dissimilar, e.g., benzene and alcohol, give a markedly concave curve.

In order to give a quantitative explanation of this effect, we recall the model of flow. When liquids are mixed, there is a free energy change (in addition to the change of ideal mixing) due to new bonds being made. When bonds are broken to make a hole, an additional amount of free energy is required which is a fraction of the free energy of this "quasi-reaction." The deviations of $\Delta F^{\ddagger}$ from a linear law (calories, at 50 mole percent) have been plotted against the deviations from Raoult's law (calories, at 50 mole percent) in Fig. 8, for systems for which

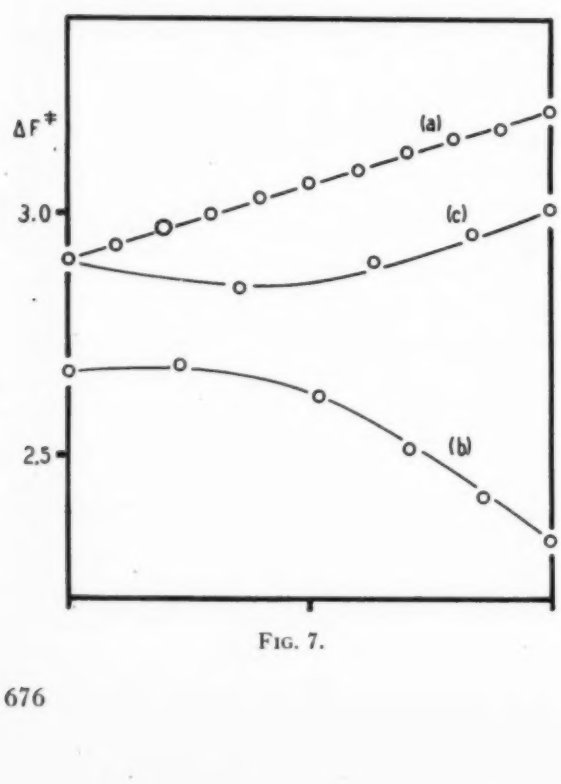

FIG. 7.

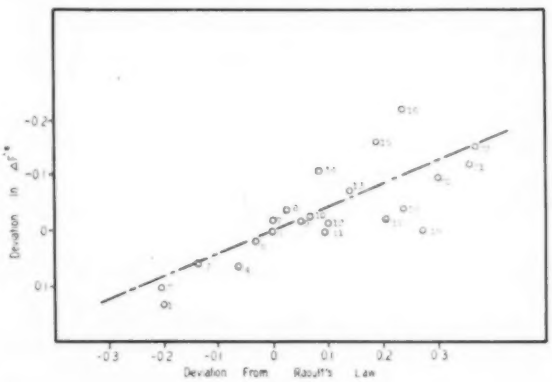

FIG. 8.

1. Chloroform—ether
2. Acetone—aniline
3. Chloroform—acetone
4. Acetone—nitrobenzene
5. Ethyl alcohol—methyl alcohol
6. Benzene—toluene
   Benzene—anisole
7. Benzene—ether
8. Benzene—carbon tetrachloride
9. Benzene—nitrobenzene
10. Benzene—carbon disulfide
11. Carbon disulfide—ether
12. Acetone—ether
13. Benzene—aniline
14. Benzene—cyclohexane
15. Ethyl alcohol—ether
16. Benzene—cyclohexanol
17. Benzene—ethyl acetate
18. Carbon disulfide—acetone
19. Ethyl alcohol—carbon tetrachloride
20. Benzene—phenol
21. Benzene—ethyl alcohol
22. Benzene—acetic acid

partial-pressure data are available or can be estimated. It is seen that the experimental points do show a definite trend, and moreover that they tend to fall along a line drawn through the zero point with a slope of 1/2.45, as was found in Fig. 4. In view of the fact that these experimental points represent small deviations in large experimental quantities, the correlation is quite satisfying. The mixture law of Eq. (24) is to be modified to read

$$\phi=\frac{\bar{v}}{Nh}\exp\left[-\left((N_1\Delta F_1^{\ddagger}+N_2\Delta F_2^{\ddagger}-\frac{\Delta F^E}{2.45}\right)\Big/RT\right], \quad (25)$$

where ΔF^E is the excess free energy of mixing.[17]

[17] G. Scatchard, J. Am. Chem. Soc. **53**, 3186 (1931); *ibid.* **56**, 995 (1934); *ibid.* **57**, 1805 (1935); Trans. Faraday Soc. **33**, 160 (1937).

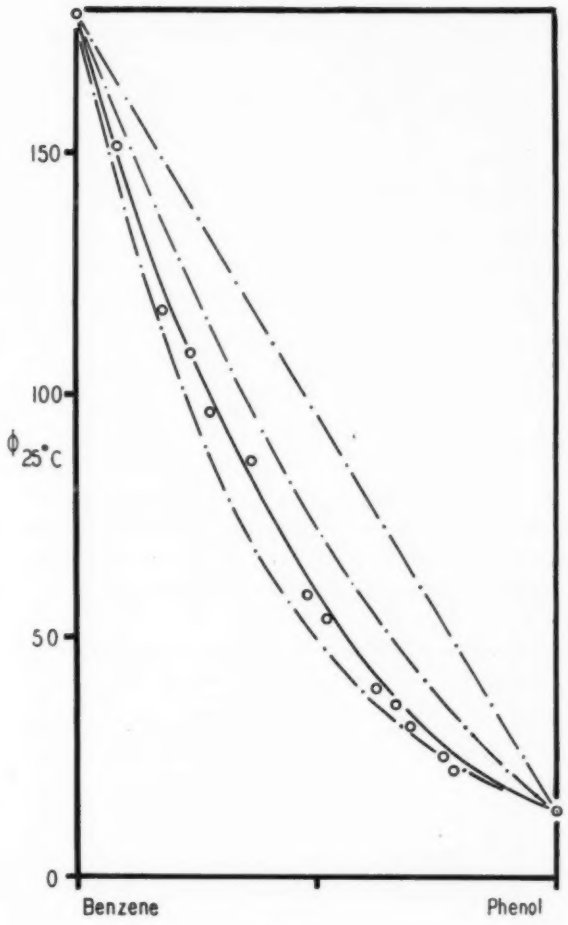

FIG. 9.

The application of this mixture law is illustrated in Fig. 9 where the experimental values for the fluidity of the system benzene-phenol are plotted, together with the curves calculated according to several different mixture laws.

VI. MIXTURE LAW FOR DIFFUSION

The absolute rate theory treatment of the self-diffusion of liquids has given the expression[1]

$$D=\lambda^2\frac{kT}{h}\exp\left(-\Delta F^{\ddagger}/RT\right) \tag{26}$$

or, upon combining with Eq. (20),

$$D\eta=\lambda_1 kT/\lambda_2\lambda_3. \tag{27}$$

If we picture a solute, partitioned at equilibrium between two different solvents, it is clear that there is no net diffusion across the interface. Hence it is the activity, and not the concentration, which is the driving force in diffusion. The appropriate variants of Eqs. (26) and (27), which will be found useful in the treatment of diffusion in imperfect solutions, may be derived as follows:[18]

Consider a diffusing molecule passing over the potential barrier of Fig. 10, with the concentra-

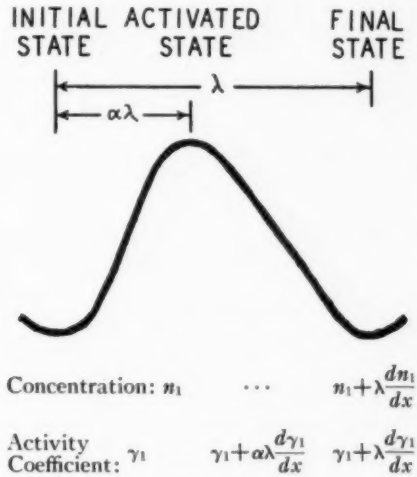

FIG. 10.

tions and activity coefficients as illustrated. The general rate expression will be used in the form

$$k'=\frac{kT}{h}\exp\left(-\Delta\overset{\circ}{F}^{\ddagger}/RT\right)\frac{\gamma_n}{\gamma^{\ddagger}}. \tag{28}$$

Then the forward and backward rates of transport are

$$\text{rate}_f=n_1\lambda\frac{kT}{h}\exp\left(-\Delta\overset{\circ}{F}^{\ddagger}/RT\right)\times\frac{\gamma_1}{\gamma_1\left[1+\frac{\alpha\lambda}{\gamma_1}\frac{d\gamma_1}{dx}\right]}, \tag{29}$$

$$\text{rate}_b=\left(n_1+\lambda\frac{dn_1}{dx}\right)\lambda\frac{kT}{h}\exp\left(-\Delta\overset{\circ}{F}^{\ddagger}/RT\right)\times\frac{\gamma_1\left[1+\frac{\lambda}{\gamma_1}\frac{d\gamma_1}{dx}\right]}{\gamma_1\left[1+\frac{\alpha\lambda}{\gamma_1}\frac{d\gamma_1}{dx}\right]} \tag{30}$$

[18] A. E. Stearn, E. M. Irish and H. Eyring, J. Phys. Chem. **44**, 981 (1940).

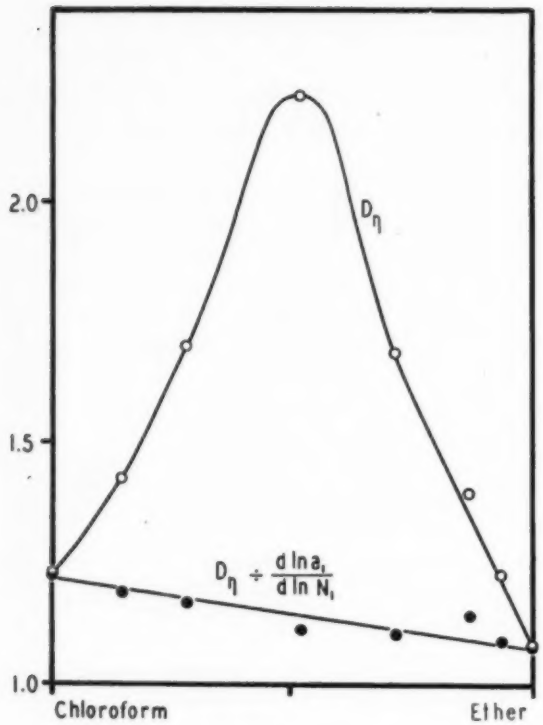

FIG. 11.

and the net rate is, upon simplifying,

$$\text{rate}_{\text{net}} = -\frac{dn_1}{dx}\lambda^2 \frac{kT}{h} \exp\left(-\Delta \overset{0}{F}^{\ddagger}/RT\right) \times \left[1+\frac{d \ln \gamma_1}{d \ln n_1}\right]. \quad (31)$$

The diffusion constant D is defined by the relation

$$\text{rate}_{\text{net}} = -D\frac{dn_1}{dx} \quad (32)$$

and upon combining (31) and (32),

$$D = \lambda^2 \frac{kT}{h} \exp\left(-\Delta \overset{0}{F}^{\ddagger}/RT\right)\left[1+\frac{d \ln \gamma_1}{d \ln n_1}\right]. \quad (33)$$

If V_1 and V_2 are not too different,* Eq. (33) may be put in the form

$$D = \lambda^2 \frac{kT}{h} \exp\left(-\Delta \overset{0}{F}^{\ddagger}/RT\right)\left[\frac{d \ln a_1}{d \ln N_1}\right]. \quad (34)$$

Or the equivalent form

$$D\eta = \frac{\lambda_1 kT}{\lambda_2 \lambda_3}\left[\frac{d \ln a_1}{d \ln N_1}\right]. \quad (35)$$

As a test of Eq. (35) $D\eta$ and

$$D\eta \div \left[\frac{d \ln a_1}{d \ln N_1}\right]$$

have been plotted against mole-fraction for the systems chloroform-acetone and chloroform-ether in Figs. 11 and 12.[19] The resulting curves provide excellent confirmation of the equation.

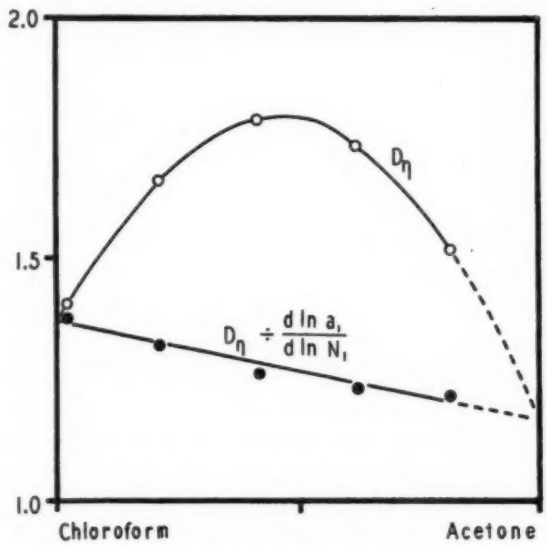

FIG. 12.

Even when the vapor-pressure data is inadequate for a quantitative check, Eq. (35) gives a good qualitative picture of the variation of diffusion with the composition. An example in the case of the system water-*n* propyl alcohol is shown in Fig. 13.

Equation (35) was derived on the assumption that a single molecule is the diffusing species; if diffusion were a bimolecular process, the diffusion equation would be given by Eq. (20) of

* Strictly speaking, when the units of concentration are changed to mole-fraction, the small correction factor $[1-N_1(1-V_1/V_2)]$ must be introduced; however, since this is a linear function of mole-fraction, it will simply be absorbed into the corresponding values of λ^2.

[19] H. Lemonde, Ann. de physique **9**, 539 (1938).

reference 18. Thus the experimental evidence is that the flow process involves a single molecule passing over a barrier into a hole.

VII. Flow Orientation

Absolute values of the diffusion coefficient predicted from Eq. (27) are consistently higher, by a factor of 2 to 5, than the values observed. This can be explained if the ratio $\lambda_2\lambda_3/\lambda_1$, is taken as greater than the average diameter, i.e., if the flowing molecule so orients itself that λ_1 is its smallest dimension, and $\lambda_2\lambda_3$ its largest area. Pure liquids in motion should then exhibit optical anisotropy, just as larger colloidal particles do. This effect in pure liquids was discovered by Maxwell in 1873.

We shall assume the following simple model for the Maxwell effect: If a molecule takes a particular orientation so that its area exposed to shear is $\lambda_2'\lambda_3'$, its index of refraction is n'; the average molecule, with area $\lambda^0{}_2\lambda^0{}_3$ exposed to shear, has an index of refraction n^0. Then the two kinds of molecules will have different energies, and the fraction of oriented molecules

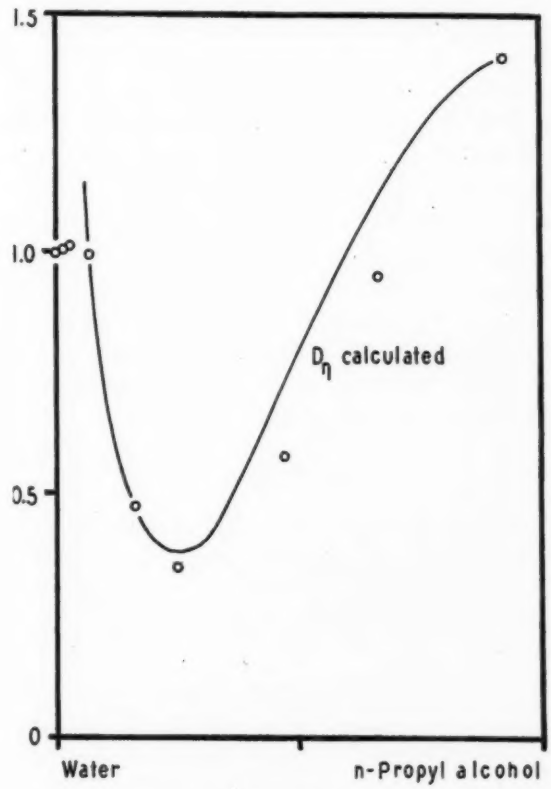

Fig. 13.

Table IV.

Substance	M 10^{10}
o-dichlorbenzene	1.85
p-xylene	1.84
mesitylene	1.31
m-xylene	1.29
chlorbenzene	1.22
o-xylene	1.21
toluene	1.04
phenyl ethanol	0.67
benzene	0.64
heptanol-1	0.41
carbon tetrachloride	0.06
cyclohexane	0.03

will be given by the Boltzmann factor

$$\frac{n'}{n^0}=\exp\left[-f(\lambda_2'\lambda_3'-\lambda_2{}^0\lambda_3{}^0)x/kT\right]$$
$$=1-f(\lambda_2'\lambda_3'-\lambda_2{}^0\lambda_3{}^0)x/kT, \quad (36)$$

which must be averaged over all x from zero to the top of the potential barrier. The quantity measured in the experiments, $\Delta n/n$, is given by

$$\frac{\Delta n}{n}=\frac{n^0-n'}{n^0}=1-\frac{n'}{n^0}=f(\lambda_2'\lambda_3'-\lambda_2{}^0\lambda_3{}^0)/$$
$$kT\left\{\frac{\int_0^{\lambda/2} x\exp(-E/RT)dx}{\int_0^{\lambda/2}\exp(-E/RT)dx}\right\}. \quad (37)$$

Maxwell's experimental formula is

$$\frac{\Delta n}{n}=fM, \quad (38)$$

where M is constant for a given substance. As an example, we may calculate M for benzene at 300°K: $\lambda_2'\lambda_3'$ is about 16×10^{-16} cm², $\lambda^0{}_2\lambda^0{}_3$ 11×10^{-16} cm²; the integration, carried out numerically for a 3-kcal. sinusoidal barrier, gives for the quantity in brackets $(\lambda/2)(0.145)$. The calculated Maxwell constant is 0.52×10^{-10}. For comparison, Table IV lists experimental values of the Maxwell constant for several liquids.[20]

It is seen that Eq. (37) not only gives a functional dependence agreeing with experiment, but also predicts correct values for the constant.

[20] W. Buchheim, H. A. Stuart and H. Menz, Zeits. f. Physik **112**, 407 (1939).

Correlation Between Elastic Moduli and Viscosity of Liquids and Plastics

ANDREW GEMANT
The Detroit Edison Company, Detroit, Michigan
(Received May 21, 1941)

The purpose of the paper is to indicate a method by means of which elastic constants (bulk and Young's moduli) and viscosity can be computed, one from the other, under conditions in which the direct determination of one of the data required is difficult or not feasible, and the other of the two quantities in question is known.

1. INTRODUCTION

THIS paper is concerned with a functional correlation between the elasticity moduli, including compressibility, of a liquid or plastic material and its constant of viscosity.

The chief purpose of this presentation is a practical one. The correlation mentioned appears to be valid also for plastic materials or for a series of materials ranging from the liquid to the plastic state. It is often required to know viscosity values of plastics where direct measurements are difficult or even impossible, yet the measurement of an elastic modulus is easy. On the other hand, it is often required to know the velocity of propagation of acoustical waves (i.e., compressibility) of liquids for which viscosity measurements can be carried out much more easily and quickly. These requirements can be met by means of the above-mentioned correlation in the following way.

The equation representing this correlation contains generally two parameters, their values depending upon the material in question and the temperature. Applied to a given substance, the equation connects compressibility and viscosity over the whole temperature or pressure range of the material. It further appears that for a given temperature the value of these parameters can be considered as constant, at least for practical purposes, even for a whole series of chemically related materials, by using a suitable average value of the parameter. If, now, for such a material or series of materials the two constants of the equation are known from a few available data, then the unknown data can be estimated from the value of their counterpart in a range where direct measurements are impractical.

It should be added that the experimental result of two papers,[1,2] to be discussed below, have led the author to the conclusion that a correlation of the above type must exist. By means of quantitative data contained in one of the papers it was possible for the author to set up an equation on an empirical basis, connecting compressibility and viscosity. As a further step, theoretical equations referring to compressibility on the one hand and viscosity on the other were consulted, with the result that an approximately correct theoretical equation, relating the two data and having exactly the form of the above-mentioned empirically obtained formula, could be set up. The value of the parameters occurring in the equation could now be estimated theoretically, and the agreement in the order of magnitude between computed and experimentally obtained values was quite satisfactory. Thus the significance of the empirical relation was considerably strengthened.

In the following pages a brief theoretical deduction of the relation in question will be given and, in a number of cases for which numerical data are available, the relation will then be verified. The possibilities of practical applications previously referred to will be discussed along with the numerical cases.

2. THEORY

In seeking a relation between bulk modulus (reciprocal of compressibility κ) and viscosity η, the internal energy u_0 of 1 g of the material, as determined by intermolecular forces, will be

[1] R. Matteson and C. J. Vogt, J. App. Phys. **11**, 658 (1940).
[2] J. M. Davies and W. F. Busse, "Dielectric properties of plasticized polyvinyl chloride," Am. Chem. Soc. Meeting, Cincinnati, April, 1940; also Davies, Miller and Busse, J. Am. Chem. Soc. **63**, 361 (1941).

considered. It is possible to establish a relation between κ and u_0 on the one hand, η and u_0 on the other. Eliminating u_0, the required relation $\kappa(\eta)$ is obtained. Again it should be stressed here that the following deduction is only approximate. However, it is felt that a more rigorous derivation will be worthwhile only if the suggested relation should really prove to be of practical value in the future.

The relation $\kappa(u_0)$ is based upon the existence of attractive and repulsive forces, as treated by M. Born, F. London, J. E. Lennard-Jones and others, and used for the explanation of the physical characteristics of liquids. The specific energy u_0 is here considered as a sum of two terms, the repulsive and the attractive, both being certain inverse powers of the molecular distance. Let us denote this inverse power as $3n$ for the attractive and $3m$ for the repulsive forces. The value of m is around 3 to 4, that of n 1 to 2. It is then possible to show[3] the following relation to hold:

$$\kappa = -1/mn\rho u_0 \tag{1}$$

with ρ = density of the material. This is the required relation $\kappa(u_0)$; it is an approximation, strictly valid only at absolute zero temperature.

The next relation required is $\eta(u_0)$. There are several theories of viscosity,[4] but all agree in an equation of the form

$$\eta = \eta_0 \exp(-lMu_0/RT). \tag{2}$$

Here η_0 is the product of certain molecular constants, l is a numerical factor, M = molecular weight, R = gas constant, T = absolute temperature; and the work against external pressure is neglected. By dividing by the density ρ, the same equation can be written down for the kinetic viscosity μ:

$$\mu = \mu_0 \exp(-lMu_0/RT). \tag{3}$$

By eliminating u_0 from Eqs. (1) and (2), and writing

$$A = 0.43Ml/mnRT \tag{4}$$

and

$$B = -\log_{10} \mu_0, \tag{5}$$

one obtains

$$A/\kappa = \rho(\log_{10} \mu + B), \tag{6}$$

the desired equation correlating κ and μ, and containing two parameters, A and B.

It should be added that B itself is a function of the temperature and the density. The nature of this function depends upon the deduction of the theoretical equation (2) of which there are several in the literature. We do not wish to follow up this point here; it should be mentioned, however, that for practical purposes it suffices for B to be considered either as a constant or as a quantity simply proportional to ρ, in which case one has, instead of (6):

$$A/\kappa = \rho(\log_{10} \mu + C\rho). \tag{7}$$

Equation (6) and, in one particular case, (7) will be used in the next sections.

The possible practical applications of Eq. (6), as pointed out above, are twofold. First, it can be used for one given substance, in order to correlate κ and η for varying temperature or pressure. The energy u_0 changes with both of these variables in an unknown manner; there is, however, no need to know this, since u_0 does not explicitly enter the equation. Second, the formula can be used for a series of related materials. Theoretically, both A and B do change from one member to another of such a series, but for practical purposes an average value assumed for A and B appears to give sufficiently accurate values in calculating η from κ, or vice versa, as the case may be.

3. Applications

(a) Hydrocarbons

As a first example, heptane in a temperature range from 10° to 60°C should be considered. Equation (6) will be used. The constant A will be defined as referring to room temperature (T_0 in deg. K), and thus the equation for other temperatures T has to be written:

$$A \cdot \frac{T_0}{T} \cdot \frac{1}{\kappa} = \rho(\log_{10} \mu + B). \tag{8}$$

Used in this sense, the equation takes the form of the well-known viscosity-temperature relation with the important difference that the factor of $1/T$ now varies with the temperature, as does $1/\kappa$.

[3] R. H. Fowler, *Statistical Mechanics* (Macmillan, New York, 1936), p. 140.

[4] J. M. Burgers, *Second Report on Viscosity and Plasticity* (Nordemann, New York, 1938), Chapter I.

In other words, the slope of the log $\mu(1/T)$ plot is not a constant, but decreases with increasing temperature, since the bulk modulus also decreases with increasing temperature. Such a deviation from the straight line is frequently observed. Whereas, as said above, Eq. (6), and thus (8), are by no means theoretically accurate, they are so for practical purposes, and so the deviation from the straight line of the log $\mu(1/T)$ plot is also sufficiently explained on this basis. We shall come back to this point when discussing oils.

The data for heptane are shown in Table I. Column 1 gives the temperature in degrees centigrade, column 2 the density and column 3 the viscosity. The next two columns give values of the bulk modulus, column 4 those determined by means of measurements[5] of sound propagation velocity, and column 5 those calculated from Eq. (8) with the following two constants:

$$A=0.031\times10^{-9};\quad B=2.63.$$

As can be seen, the agreement is satisfactory.

Next a series of various hydrocarbons is considered. Since the constants in this case are just average values, the formula is limited to related substances, as will be seen from Table II in which column 1 gives the name of the material, column 2 the density, column 3 the viscosity at room temperature, columns 4 and 5 the bulk modulus at room temperature as measured[5] and as calculated from Eq. (6) with

$$A=0.091\times10^{-9};\quad B=3.43.$$

Whereas the agreement is good for the saturated members, it is less satisfactory for tetralin, containing double bonds. This indicates that if (6) is to be used for a series of materials, A and B are constants only as long as related substances are considered.

Let us now check the empirical values of A and B in the light of Eqs. (4) and (5), deduced theoretically. It will be seen that the order of magnitude agrees very well. In order to get a plausible value for the hydrocarbon series, let us take hexane as representative of the series. For evaluating B, one of the existing viscosity

TABLE I. *Computations on heptane by means of Eq. (8).*

Temperature, °C	ρ	η, Centipoises	$1/\kappa$, abs. units Measured	Calculated
10	0.692	0.465	9.92×10^{9}	9.9×10^{9}
20	0.684	0.416	9.14	9.1
30	0.675	0.375	8.37	8.3
40	0.667	0.341	7.65	7.8
50	0.658	0.311	6.94	7.0
60	0.649	0.284	6.34	6.4

TABLE II. *Computations on various hydrocarbons (20–25°C) by means of Eq. (6).*

Substance	ρ	η, Centipoises	$1/\kappa$, abs. units Measured	Calculated
Pentane	0.626	0.235	6.90×10^{9}	6.9×10^{9}
Hexane	0.660	0.304	8.15	7.9
Heptane	0.684	0.403	9.07	9.0
Octane	0.704	0.520	10.0	10.0
Cyclohexane	0.779	0.93	12.4	12.8
Tetralin	0.971	2.00	20.7	18.4

theories has to be consulted, and accordingly the most recent one, that by Eyring[6] should be selected, according to which

$$\eta_0=1.1\times10^{-3}M^{\frac{1}{2}}T^{\frac{1}{2}}/V^{\frac{1}{3}}E$$

(M = molecular weight, V = molar volume, E = heat of evaporation per mole). For hexane $M=86$, $V=130$ cc, $E=6220$ cal. Thus $\mu_0=0.49\times10^{-3}$ and $B=3.3$, which agrees with the value assumed to satisfy the experimental data. In (4) we have the factor l which, according to Eyring, is about $\frac{1}{4}$. For n the value 2 is most likely; that for m is uncertain, but is quite probably 3. Thus $A=0.06\times10^{-9}$, again in satisfactory agreement with the assumed value.

(b) Petroleum oils

One of the papers, mentioned in the Introduction, is by Matteson and Vogt[1] on the velocity of acoustical waves in petroleum fractions. They found that the velocity was a function of the density and viscosity of the oil. This finding gave the author the idea that a functional correlation between κ and η must exist.

The experimental data are best reproduced by Eq. (7) in this case with

$$A=0.45\times10^{-9};\quad C=10.5.$$

[5] S. Parthasarathy, Proc. Ind. Acad. Sci. **2A**, 497 (1935).

[6] R. H. Ewell, J. App. Phys. **9**, 252 (1938).

The result over a number of oils of a fairly extensive series is shown in Fig. 1.

The figure shows the sound propagation velocity ($[1/\rho\kappa]^{\frac{1}{2}}$) as a function of the kinematic viscosity, the density of the oils being the parameter of the set. The agreement between individual curves seems only moderate, particularly for the highest viscosities. From what was said before, this cannot be expected to be otherwise. Besides, one has to consider that it is not one curve, but a whole set of curves that is here reproduced by an equation containing two constants only.

The usefulness of the equation in this case is evident, and follows from the paper of Matteson and Vogt. For any given petroleum fraction, to be used in Diesel engines, only density and viscosity have to be determined (both easy, routine operations), and the velocity of compressional waves, the knowledge of which is important for their operation, can be computed with fair accuracy.

For a given oil the relation can be used to estimate viscosity or compressibility for any temperature or pressure if one of the two data is known.

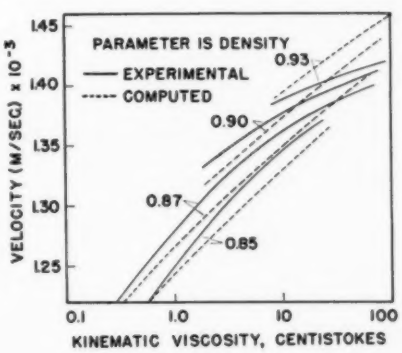

FIG. 1. Sound propagation velocity in petroleum fractions as function of viscosity and density. (Experimental curves after Matteson and Vogt.)

Let us check the validity of the relation in this respect. As to the variation with temperature, Eq. (8) has to be used as pointed out before. In other words the log $\eta(1/T)$ plot should not have a constant slope, as generally assumed in a first approximation, but should vary as $1/\kappa$—in a second approximation. Looking at a typical transformer oil between $-20°$ and $+80°$C,[7] the slope at $-20°$ to that at $+80°$ is in a ratio of about 2 : 1. As to κ, data from the *International Critical Tables*[8] for kerosene between $+20°$ and $+80°$C, and extrapolated to $-20°$C, can be taken. The extreme values for $1/\kappa$ are: 16.4 and 9.6×10^9, and their ratio is 1.7. Thus a large part of the variation of the log $\eta(1/T)$ slope can be accounted for by the corresponding change of κ, indicating the usefulness of the relation.

As to the pressure effect, it is known that both the bulk modulus and the viscosity increase with pressure. Moreover, the increase of the viscosity is exponential, that of the modulus linear, in agreement with Eq. (6). But we can go a step further, and see how far the numerical agreement goes. The viscosities of a mineral oil for 1100 and 2200 atmos. (and 40°C) are given by R. B. Dow and co-workers[9] as 1.5 and 9.0 poises. Writing

$$1/\kappa = 1/\kappa_0 + bP, \tag{9}$$

where b = a constant and P pressure (in atmos.), and substituting into Eq. (7), b can be computed to 1.3×10^6. In the *Critical Tables*,[8] b for kerosene and some lubricating oils is given as around 4×10^6, which agrees, as to its order of magnitude, with the value computed from viscosities and using Eq. (6) or (7). This choice makes no difference here since ρ is practically independent of the pressure.

(c) Polyvinyl chlorides

The second paper referred to in the Introduction is one by Davies and Busse[2] on the dielectric properties of plasticized polyvinyl chlorides. The authors quoted found pronounced power factor maxima with varying temperature, the curves shifting towards lower temperatures with increasing tricresyl phosphate content. Such curves show that the opposing forces of dipolar rotation are of a viscous nature, in contradistinction to other solids in which it is the solid friction that has to be overcome by the dipoles.

Now the maximum of power factor curves occur when the time constant of the dipoles coincides with the reciprocal of the a.c. frequency. Since the time constant according to Debye is proportional to the viscosity, it follows that the differently plasticized polymers at the respective

[7] Andrew Gemant, *Liquid Dielectrics* (Wiley, New York, 1933), p. 26.

[8] Int. Crit. Tab. **2**, 146 (1927).

[9] R. M. Dibert, R. B. Dow and C. E. Fink, J. App. Phys. **10**, 113 (1939).

temperatures of maximum power factor must possess the same viscosity. The viscosity of such polymers is not easy to measure and, instead, hardness figures were obtained by Davies and Busse by means of the Shore Durometer, with the surprising result that these figures at the temperatures in question were very nearly the same.

The Durometer figure is chiefly a somewhat involved function of Young's modulus of the material; in other words, the elastic modulus was the same at the temperatures of power factor maxima. This result is understandable only if it is assumed that there is a definite relationship between the viscosity of the polymers and their elastic moduli. This conclusion is in complete agreement with the theory developed in these pages. The data presented by Davies and Busse are not of a nature to allow a check of the equation, as was possible for the simple hydrocarbons and the petroleum fractions.

(d) Glasses

Glasses are among the objects believed to be particularly suited for being applied in connection with Eq. (6). The reason is that the elastic modulus of glass (Young's modulus E in this case) is easily measured at lower temperatures; its viscosity, however, only at higher temperatures. The missing data, often quite important, can then be computed if the constants are known.

A check of Eq. (6) in this case is not easy and can be only approximate. The reason for this is that there are no corresponding data for both η and E obtained on one particular glass by any one author. The data had to be compiled from work of different authors on similar, but certainly not identical, glasses. First we replace $1/\kappa$ by E, using the relation

$$\frac{1}{\kappa}=\frac{pE}{(1+p)(1-2p)}, \qquad (10)$$

where p = Poisson's ratio, in the average 0.25 for glass. Thus, $1/\kappa=E/2.5$. Further, ρ can be replaced by its average value 2.5, and its variation neglected. One then has for Eq. (8):

$$110AE/T=2.5\log\eta+(2.5B-1). \qquad (11)$$

TABLE III. *Glass at different temperatures.*

TEMPERATURE, °C	E IN ABS. UNITS	$\log_{10}\eta$ EXPERIMENTAL	$\log_{10}\eta$ COMPUTED
400	0.57×10^{12}	17	17.6
450	0.55	15.8	15.4
500	0.53	13.7	13.4
550	0.51	11.4	11.6
600	0.48	9.8	9.8

TABLE IV. *Glass of different sodium content at 600°C.*

PERCENT Na_2O	$\log_{10}\eta$	E_{20} EXPERIMENTAL	E_{20} COMPUTED
25	8.7	0.57×10^{12}	0.57×10^{12}
23	9.3	0.61	0.60
21	10.0	0.63	0.63
19	10.4	0.66	0.65
17	10.7	0.67	0.66
16	11.0	0.68	0.68
15	11.4	0.69	0.69
14	11.8	0.71	0.71

All data for the computations given in the following tables were taken from the monograph on glass by G. W. Morey.[10]

In Table III data are given for glass of about the following composition: SiO_2: 68 percent, Na_2O+K_2O: 20 percent, $CaO+MgO$: 8 percent, Al_2O_3: 4 percent. Young's modulus E was measured by Badger and Silverman from room temperature to 450°C, and the data up to 600°C are extrapolated values. Viscosity data were obtained by Scott, Irvine and Turner. The constants in Eq. (11) for this case are

$$A=0.60\times10^{-9}, \quad B=5.2.$$

The agreement between calculated and determined η values is satisfactory, and the order of magnitude of the constants is the same as in the previous cases, their absolute values necessarily being different.

Table IV summarizes data for glasses of different composition, all at the same temperature of 600°C. The SiO_2 content was around 74 percent, and the Na_2O content is shown in the table. Viscosity values are taken from measurements after English. Corresponding data of E are available only for room temperature (after Clarke and Turner), and these are shown in column 3. From the previous series at different tempera-

[10] G. W. Morey, *The Properties of Glass* (Reinhold, New York, 1938).

tures it could be concluded that the ratio E_{600}/E_{20} is about 0.74. Consequently the E data obtained from Eq. (11) were divided by 0.74 in order to bring them to room temperature level. The constants of the equation used for this case were

$$A=0.58\times10^{-9};\quad B=4.1$$

and the calculated E data are shown in the last column, showing good agreement with the experimental values. Hence, the usefulness of the formula for glass too is shown.

Summary

By means of a simple theory an equation, establishing a connection between elastic moduli of liquids and plastics and their viscosity, is derived. The equation, which contains two constants only, can be used either for a given substance in a range of varying temperature and pressure, or for a series of chemically related materials. The usefulness of the equation is shown on simple hydrocarbons, petroleum fractions, plasticized polyvinyl chlorides, and glasses.

The Solution of A.C. Circuit Problems

Louis A. Pipes

Graduate School of Engineering, Harvard University, Cambridge, Massachusetts

(Received May 31, 1941)

Starting with the set of linear equations that determine the complex currents of a general n-mesh circuit, a method is presented for the numerical solution of the equations to determine the various mesh currents of the system.

The method presented has computational advantages over the conventional methods usually used in that only real numbers are involved in the various numerical operations and only the evaluation of second-order determinants is involved. The operations required are those of matrix multiplication and are most conveniently performed with a calculating machine. The paper is concluded by the solution of a general Y–Y circuit with a neutral return as an example of the method presented.

Introduction

MANY articles have appeared in the literature during the past few years on the application of matrix algebra to electrical problems. In all these papers, the concept of the inverse of a square matrix is involved. Since in the solution of alternating current problems, the elements of the various matrices are complex numbers, it is seen that the amount of computational labor involved in the inversion of these matrices is enormous.

For example, consider a general four-mesh network. To determine the four-mesh currents from the impressed complex voltages and the complex impedances of the system we must invert a square matrix of the fourth order whose elements are complex numbers. This involves the evaluation of the determinant of the matrix itself which, in this case, is one of the fourth order and also the evaluation of sixteen determinants of the third order if the original matrix is not symmetric or ten third-order determinants if it is symmetric. Since in general all these determinants have complex elements, it is seen that the labor involved is very great.

In this paper a method is presented that attacks the problem in an entirely different manner. By the use of this method, the computational labor is greatly reduced since only real quantities are involved and the procedure is one of matrix multiplication which is so easily performed by means of a calculating machine. The elements of matrix algebra presented in (1) will be assumed in this discussion.

1. The General Equations

Let us consider a general n-mesh circuit in the steady state. Let the various complex mesh currents have the values $(I_1, I_2, \cdots I_n)$ and let the complex voltages impressed on the contours

of the meshes be $(E_1, E_2, \cdots E_n)$. The voltages and currents are related by the equations:

$$\begin{aligned} Z_{11}I_1+Z_{12}I_2+\cdots+Z_{1n}I_n&=E_1 \\ \cdots\cdots\cdots\cdots\cdots\cdots\cdots\cdots\cdots\cdots&, \\ Z_{n1}I_1+Z_{n2}I_2+\cdots+Z_{nn}I_n&=E_n \end{aligned} \tag{1}$$

where the complex numbers Z_{rr} are the various self-impedances of the meshes and Z_{rs} where $r \neq s$ are complex numbers that are the mutual impedances of the system. In static networks, the condition:

$$Z_{rs}=Z_{sr} \tag{2}$$

holds.

The set of linear Eqs. (1), may be written in the compact matrix form:

$$[Z](I)=(E), \tag{3}$$

where $[Z]$ is a square matrix of the nth order whose elements are the complex numbers Z_{rs}, (I) is a column matrix whose elements are the various complex mesh currents and (E) is a column matrix whose elements are the complex mesh voltages.

In the usual problem of circuit analysis, the mesh voltages and the complex impedances are given and it is required to determine the complex mesh currents. The fundamental problem is therefore to solve the set of Eqs. (1) for the complex currents, I_r.

2. The Admittance Matrix

If the circuit under consideration is a static one, then the condition (2) holds and the matrix $[Z]$ is a symmetric matrix so that we have:

$$[Z]'=[Z], \tag{4}$$

where $[Z]'$ is the transposed matrix of the matrix $[Z]$ obtained by interchanging the rows and the columns of $[Z]$. In the general case, the matrix $[Z]$ may be written in the form:

$$[Z]=[R]+j[X], \tag{5}$$

where $j=\sqrt{-1}$, $[R]$ is a square matrix of the nth order whose elements are the various self- and mutual resistance coefficients of the circuit, and may be termed the resistance matrix. $[X]$ is a square matrix of the nth order whose elements are the various self- and mutual reactance coefficients of the system.

Let us now define a matrix, $[Y]$, by the equation:

$$[Y]=[Z]^{-1}, \tag{6}$$

where $[Z]^{-1}$ is the inverse of the impedance matrix $[Z]$. This matrix, $[Y]$, is called the admittance matrix of the system. The elements of $[Y]$ are given explicitly by:

$$Y_{rs}=\text{Cofactor of } Z_{sr}/|Z|, \tag{7}$$

where $|Z|$ is the determinant of the matrix, $[Z]$. Since $[Y]$ is the inverse of $[Z]$, it has the property that:

$$[Z][Y]=[Y][Z]=U, \tag{8}$$

where U is the unit matrix of the nth order. From (7), it is seen that if $[Z]$ is a symmetric matrix, then $[Y]$ is also a symmetric matrix and satisfies the relation:

$$[Y]'=[Y], \tag{8a}$$

where $[Y]'$ is the transposed matrix of $[Y]$. In view of (6), if we premultiply both sides of (3) by $[Y]$, we obtain explicitly:

$$(I)=[Z]^{-1}(E)=[Y](E). \tag{9}$$

In (9) we thus have an explicit expression of the various mesh currents in terms of $[Z]^{-1}$ and the mesh voltages. In most articles on the application of matrix algebra to circuit theory, the Eq. (9) is given as the solution of the problem under consideration. However, when one comes to the actual numerical solution of a problem of this type, it is seen that the amount of computational effort required is enormous.

We now turn to the development of a procedure which materially reduces this computational labor and allows us to work with real numbers entirely.

Let us write:

$$[Y]=[G]+j[B]=[Z]^{-1}, \tag{10}$$

that is, we separate the complex matrix $[Y]$ into its real and imaginary parts. The square matrix of the nth order, $[G]$ will be called the conductance matrix and the square matrix of the nth order, $[B]$ will be called the susceptance matrix. From (7), it is seen that if $[Z]$ is a symmetric matrix, then both $[G]$ and $[B]$ are symmetric matrices. We may now perform the

multiplication:

$$[Z][Y]=[Z][Z]^{-1}=U$$
$$=([R]+j[X])([G]+j[B]) \quad (11)$$
$$=([R][G]-[X][B])$$
$$+j([R][B]+[X][G]).$$

Equating the real and imaginary coefficients of this expression, we obtain:

$$U=[R][G]-[X][B], \quad (12)$$

$$[0]=[X][G]+[R][B], \quad (13)$$

where U is the unit matrix of the nth order and $[0]$ is the zero matrix of the nth order. These two equations may be solved for the matrices $[G]$ and $[B]$ and we obtain:

$$[G]=([R]+[X][R]^{-1}[X])^{-1}, \quad (14)$$

$$[B]=-[R]^{-1}[X][G] \quad (15)$$

or

$$[B]=-([X]+[R][X]^{-1}[R])^{-1}, \quad (16)$$

$$[G]=-[X]^{-1}[R][B]. \quad (17)$$

Either the first or the second set of equations may be used to compute $[G]$ and $[B]$. Which set is used depends on the complexity of the matrices $[X]$ and $[R]$.

The computation of $[G]$ and $[B]$ by either of the two sets of equations is greatly facilitated by the use of a powerful iterative method of determining the inverse of a non-singular matrix whose elements are real numbers. This method will be described in a later section.

3. Determination of the Mesh Currents

To determine the mesh currents having obtained the conductance and susceptance matrices, let us decompose the voltage and current matrices into their real and imaginary parts as follows:

$$(E)=(c)+j(d) \quad (18)$$

and

$$(I)=(a)+j(b). \quad (19)$$

We then have:

$$(I)=[Y][E]=([G]+j[B])[(c)+j(d)]. \quad (20)$$

Equating real and imaginary coefficients, we obtain:

$$(a)=[G](c)-[B](d), \quad (21)$$

$$(b)=[B](c)+[G](d). \quad (22)$$

The elements of the column matrices (a) and (b) give the real and imaginary parts respectively of the various mesh currents.

4. Partitioned Matrices

Before proceeding to the discussion of a powerful iterative method for the inversion of real non-singular matrices that enables the operations indicated by the set of Eqs. (14) and (15) or (16) and (17) to be performed, it is necessary to digress briefly to discuss the subject of partitioned matrices since the method to be presented makes use of this concept.

(a) The order of a matrix

A matrix is said to be of the (m, n) order if it has m rows and n columns. The first quantity, m, refers to the rows, and the second quantity, n, refers to the columns.

(b) Multiplication of matrices of different orders

Two matrices of different orders can be multiplied together only if a certain condition is satisfied. If the number of *columns* of a matrix, $[B]$ is equal to the number of *rows* of a matrix, $[A]$, then these two matrices are described as *conformable*. They can then be multiplied in the order $[B][A]$. If $[B]$ is a matrix of the order (q, n) and $[A]$ is a matrix of the order (n, p), then the product $[B][A]$ is a matrix of the order (q, p). This rule may be expressed symbolically in the form:

$$(q, n)\times(n, p)=(q, p). \quad (23)$$

For example,

$$\begin{bmatrix} 4 & 2 & -1 & 2 \\ 3 & -7 & 1 & -8 \\ 2 & 4 & -3 & 1 \end{bmatrix}\begin{bmatrix} 2 & 3 \\ -3 & 0 \\ 1 & 5 \\ 3 & 1 \end{bmatrix}$$
$$=\begin{bmatrix} 7 & 9 \\ 4 & 6 \\ -8 & -8 \end{bmatrix}. \quad (24)$$

(c) Partitioning a matrix

It is possible to divide the array of a given matrix into smaller arrays by horizontal and vertical lines. The matrix is then said to be

partitioned into submatrices. As an example, consider

$$[a]=\left[\begin{array}{ccc|c}1 & 9 & 3 & \\ 2 & 8 & 4 & \\ \hline 6 & 2 & 7 & \end{array}\right]. \tag{25}$$

It is possible to represent each of the submatrices of a partitioned matrix by a single symbol and then the original matrix becomes a matrix of matrices. Partitioned matrices may be multiplied as if the submatrices were ordinary matrix elements provided they are conformable. An examination of this criterion leads to the rule that in general for the multiplication of two partitioned matrices it is necessary and sufficient that for every partitioning line between columns of the matrix on the left there shall be a partitioning line between the corresponding rows of the matrix on the right and no further horizontal partitioning. For example:

$$\left[\begin{array}{c|c|c}a_{11} & a_{12} & a_{13} \\ a_{21} & a_{22} & a_{23} \\ \hline a_{31} & a_{32} & a_{33}\end{array}\right]\left[\begin{array}{ccc}b_{11} & b_{12} & b_{13} \\ \hline b_{21} & b_{22} & b_{23} \\ \hline b_{31} & b_{32} & b_{33}\end{array}\right]$$

$$=\left[\begin{array}{ccc|c}a_{11} & a_{12} & a_{13} & \\ a_{21} & a_{22} & a_{23} & \\ \hline a_{31} & a_{32} & a_{33} & \end{array}\right]\left[\begin{array}{ccc}b_{11} & b_{12} & b_{13} \\ b_{21} & b_{22} & b_{23} \\ \hline b_{31} & b_{32} & b_{33}\end{array}\right]. \tag{26}$$

5. The Inversion of Matrices by the Use of Submatrices

Many methods for the inversion of nonsingular matrices may be devised. (See reference 2.) Of these methods, the one making use of submatrices appears to lend itself most readily to numerical computation. This method will now be described.

Let us suppose that we have given a nonsingular matrix, $[A]$, of the mth order, and we wish to determine its inverse, $[B]$. We then must have:

$$[B][A]=U_m, \tag{27}$$

where U_m is the unit matrix of the mth order. Now let the matrices $[A]$ and $[B]$ be partitioned in the following manner:

$$[A]=\begin{bmatrix}A_{11}(r,r) & A_{12}(r,s) \\ A_{21}(s,r) & A_{22}(s,s)\end{bmatrix}, \tag{28}$$

$$[B]=\begin{bmatrix}B_{11}(r,r) & B_{12}(r,s) \\ B_{21}(s,r) & B_{22}(s,s)\end{bmatrix}. \tag{29}$$

The orders of the submatrices are indicated by the notation of Section 4, and we have $r+s=m$. Performing the indicated operation (27), we obtain the relations:

$$B_{11}A_{11}+B_{12}A_{21}=U_r, \tag{30}$$

$$B_{11}A_{12}+B_{12}A_{22}=[0], \tag{31}$$

$$B_{21}A_{11}+B_{22}A_{21}=[0], \tag{32}$$

$$B_{21}A_{12}+B_{22}A_{22}=U_s, \tag{33}$$

where U_r and U_s are unit matrices of the rth and sth orders, respectively. These four equations may now be solved to give the four submatrices of $[B]$. If we use the notation:

$$M=A_{11}^{-1}A_{12}, \tag{34}$$

$$V=A_{21}A_{11}^{-1}, \tag{35}$$

$$W=A_{22}-VA_{12}=A_{22}-A_{21}M, \tag{36}$$

we then have:

$$B_{11}=A_{11}^{-1}+MW^{-1}V, \tag{37}$$

$$B_{12}=-MW^{-1}, \tag{38}$$

$$B_{21}=-W^{-1}V, \tag{39}$$

$$B_{22}=W^{-1}. \tag{40}$$

These equations determine the required matrix $[B]$ provided that the inverses A_{11}^{-1} and W^{-1} exist. When A_{11}^{-1} is found, the quantities M, V, W can be calculated and $[B]$ determined. The numerical work may be arranged in the following convenient tabular form:

	A_{21}	A_{22}
$M=A^{-1}A_{12}$	A_{11}^{-1}	A_{12}
W^{-1}	$V=A_{21}A_{11}^{-1}$	$W=A_{22}-VA_{12}$

then:

$$[A]^{-1}=\left[\begin{array}{c|c}A_{11}^{-1}+MW^{-1}V & -MW^{-1} \\ \hline -W^{-1}V & W^{-1}\end{array}\right]. \tag{41}$$

If we choose $r=m-1$, $s=1$, then A_{21} is a single row, A_{12} is a single column, A_{22} is a single element, and W is a scalar. This suggests the

following procedure for dealing with a given numerical matrix: Suppose that the matrix under consideration is:

$$[A]=\begin{bmatrix} A_{11} & A_{12} & \cdots & A_{1n} \\ A_{21} & A_{22} & \cdots & A_{2n} \\ \hline A_{n1} & A_{n2} & \cdots & A_{nn} \end{bmatrix}. \qquad (42)$$

We may then set up the following sequence of matrices, S_1, S_2, S_3, etc. which progressively include more and more of the principal diagonal elements of $[A]$ formed in the following manner:

$$S_1=[A_{11}], \qquad (43)$$

$$S_2=\begin{bmatrix} A_{11} & A_{12} \\ A_{21} & A_{22} \end{bmatrix}, \qquad (44)$$

$$S_3=\begin{bmatrix} A_{11} & A_{12} & A_{13} \\ A_{21} & A_{22} & A_{23} \\ A_{31} & A_{32} & A_{33} \end{bmatrix}=\left[\begin{array}{cc|c} & S_2 & A_{13} \\ & & A_{23} \\ \hline A_{31} & A_{32} & A_{33} \end{array}\right], \qquad (45)$$

$$S_4=\begin{bmatrix} A_{11} & A_{12} & A_{13} & A_{14} \\ A_{21} & A_{22} & A_{23} & A_{24} \\ A_{31} & A_{32} & A_{33} & A_{34} \\ A_{41} & A_{42} & A_{43} & A_{44} \end{bmatrix}$$

$$=\left[\begin{array}{ccc|c} & & & A_{14} \\ & S_3 & & A_{24} \\ & & & A_{34} \\ \hline A_{41} & A_{42} & A_{43} & A_{44} \end{array}\right]. \qquad (46)$$

Since S_2 is a second-order matrix, its inverse is easily computed and is given by:

$$S_2^{-1}=\frac{1}{(A_{11}A_{22}-A_{12}A_{21})}\begin{bmatrix} A_{22} & -A_{12} \\ -A_{21} & A_{11} \end{bmatrix}. \qquad (47)$$

Now using this value of S_2^{-1}, we can now apply to S_3 the scheme of computation described above and thus obtain S_3^{-1}. In the same manner, we use S_3^{-1} and apply the process to S_4. In this way we finally obtained S_n^{-1} or $[A]^{-1}$.

In exceptional cases it is possible that one may encounter a singular matrix, say the S_j matrix during the iterative process. This is indicated by obtaining $W=0$ for that particular matrix. In such cases, the simplest procedure is to transfer the ith row of $[A]$ to the last place and to continue in the normal manner. This rearrangement of the rows is equivalent to a premultiplication of $[A]$ by a matrix N, where N is the unit matrix of the nth order with its ith row transferred to the last place.

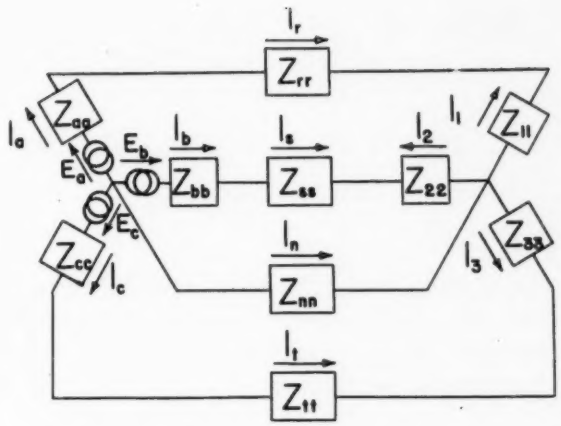

FIG. 1. General $Y-Y$ circuit.

The final reciprocal matrix will then have to be post-multiplied by N to give $[A]^{-1}$. The above iterative process for the computation of the reciprocal of a non-singular matrix is very easily carried out with a computing machine since the principal process required is that of matrix multiplication.

6. NUMERICAL EXAMPLE

To illustrate the above theory, let us apply it to the calculation of the performance of the general $Y-Y$ circuit of Fig. 1. For generality, we shall consider mutual impedances between the three sending-end impedances, the four line impedances, and the three receiving-end impedances. The sending-end potentials assumed are quite unbalanced. The problem is to compute the three line currents I_a, I_b and I_c and the current in the neutral.

Assumed numerical values

The following numerical values are assumed:

$$Z_{aa}=10+j4 \quad Z_{ab}=Z_{ba}=j2 \quad Z_{11}=2-j5$$
$$Z_{bb}=3-j7 \quad Z_{bc}=Z_{cb}=j3 \quad Z_{22}=3+j8$$
$$Z_{cc}=4+j9 \quad Z_{ca}=Z_{ac}=j1 \quad Z_{33}=1+j6$$
$$Z_{12}=Z_{21}=j4 \quad Z_{rr}=2+j6 \quad Z_{rs}=Z_{sr}=j3$$
$$Z_{13}=Z_{31}=j2 \quad Z_{ss}=8+j3 \quad Z_{rn}=Z_{nr}=j_2$$

$$Z_{32}=Z_{23}=j3 \quad Z_{tt}=6+j2 \quad Z_{rt}=Z_{tr}=j4$$
$$Z_{nn}=9+j3 \quad Z_{sn}=Z_{ns}=j1$$
$$Z_{st}=Z_{ts}=j3$$
$$E_a=110+j0 \quad Z_{nt}=Z_{tn}=j2$$
$$E_b=-58-j49$$
$$E_c=-5+j115.$$

By writing the Kirchhoff second law and taking the potential drops around the three independent meshes including the neutral return of the system, we obtain:

$$\begin{bmatrix} a_{11} & a_{12} & a_{13} \\ a_{21} & a_{22} & a_{23} \\ a_{31} & a_{32} & a_{33} \end{bmatrix} \begin{bmatrix} I_a \\ I_b \\ I_c \end{bmatrix} = \begin{bmatrix} E_a \\ E_b \\ E_c \end{bmatrix} = [Z](I). \quad (48)$$

The a_{ij} quantities have the values:

$$a_{11}=Z_{aa}+Z_{rr}-2Z_{nr}+Z_{nn}+Z_{11}=23+j4,$$
$$a_{22}=Z_{bb}+Z_{ss}-2Z_{ns}+Z_{nn}+Z_{22}=23+j5,$$
$$a_{33}=Z_{cc}+Z_{tt}-2Z_{nt}+Z_{nn}+Z_{33}=20+j16,$$
$$a_{12}=Z_{ab}+Z_{rs}-Z_{rn}-Z_{ns}+Z_{nn}+Z_{12}=a_{21}=9+j7,$$
$$a_{13}=Z_{ac}+Z_{rt}-Z_{rn}-Z_{nt}+Z_{nn}+Z_{13}=a_{31}=9+j6,$$
$$a_{23}=Z_{bc}+Z_{st}-Z_{sn}-Z_{nt}+Z_{nn}+Z_{23}=a_{32}=9+j9.$$

Separating the matrix $[Z]$ into its real and imaginary parts, we obtain:

$$[R]=\begin{bmatrix} 23 & 9 & 9 \\ 9 & 23 & 9 \\ 9 & 9 & 20 \end{bmatrix}, \quad [X]=\begin{bmatrix} 4 & 7 & 6 \\ 7 & 5 & 9 \\ 6 & 9 & 16 \end{bmatrix}.$$

In this example, the resistance matrix is particularly simple and it is more expedient to calculate the conductance and susceptance matrices by using the Eqs. (14) and (15) rather than (16) and (17). Before computing the inverse of $[R]$ we may first divide out the factor 9 and write:

$$[R]=9\begin{bmatrix} 2.555 & 1 & 1 \\ 1 & 2.555 & 1 \\ 1 & 1 & 2.222 \end{bmatrix}=9[A]$$

and hence:

$$[R]^{-1}=\tfrac{1}{9}\left[\begin{array}{cc|c} 2.555 & 1 & 1 \\ 1 & 2.555 & 1 \\ \hline 1 & 1 & 2.222 \end{array}\right]^{-1}=\tfrac{1}{9}[A]^{-1}.$$

To find the inverse of the above square matrix, we may now use the procedure developed in Section 5. First we compute the inverse of S_2 as follows:

$$S_2=\begin{bmatrix} 2.555 & 1.000 \\ 1.000 & 2.555 \end{bmatrix},$$
$$S_2^{-1}=\begin{bmatrix} 0.46228 & -0.18089 \\ -0.18089 & 0.46228 \end{bmatrix}.$$

From this, we now set up a table as in Section 5 as follows:

		1.00000	1.00000	2.222
M	0.28139	0.46228	−0.18089	1.000
	0.28139	−0.18089	0.46228	1.000
	0.60261	0.28139	0.28139	1.659
		W^{-1}	V	W

$$MW^{-1}V=\begin{bmatrix} 0.047714 & 0.047714 \\ 0.047714 & 0.047714 \end{bmatrix}.$$

Substituting into (42) of Section 5, we obtain:

$$[A]^{-1}=\begin{bmatrix} 0.50999 & -0.13318 & -0.16956 \\ -0.13318 & 0.50999 & -0.16956 \\ -0.16956 & -0.16956 & 0.60261 \end{bmatrix}$$

and hence:

$$[R]^{-1}=\tfrac{1}{9}[A]^{-1}$$
$$=\begin{bmatrix} 0.05666 & -0.01479 & -0.01884 \\ -0.01479 & 0.05666 & -0.01884 \\ -0.01884 & -0.01884 & 0.06695 \end{bmatrix}.$$

We now compute:

$$[R]^{-1}[X]=\begin{bmatrix} 0.01007 & 0.22442 & 0.19446 \\ 0.15311 & 0.01021 & 0.37647 \\ -0.09459 & 0.11976 & 0.78860 \end{bmatrix}$$

and

$$[X][R]^{-1}[X]$$
$$=\begin{bmatrix} 2.77798 & 2.94273 & 5.19156 \\ 2.94273 & 4.51105 & 7.03407 \\ 5.19156 & 7.03407 & 13.12790 \end{bmatrix},$$
$$[R]+[X][R]^{-1}[X]$$
$$=\left[\begin{array}{cc|c} 25.778 & 11.942 & 14.192 \\ 11.942 & 27.511 & 16.034 \\ \hline 14.192 & 16.034 & 33.128 \end{array}\right]=[A].$$

We now must compute the inverse of this new matrix $[A]$. We choose S_2 and compute its inverse as follows:

$$S_2=\begin{bmatrix}25.778 & 11.942\\ 11.942 & 27.511\end{bmatrix},$$

$$S_2^{-1}=\begin{bmatrix}0.04855 & -0.02107\\ -0.02107 & 0.04549\end{bmatrix}.$$

Again we compile the table:

		14.192	16.034	33.128
M	0.35119 0.43036	0.04855 −0.02107	−0.02107 0.04549	14.192 16.034
	0.04707	0.35119	0.43036	21.244
		W^{-1}	V	W

$$MW^{-1}V=\begin{bmatrix}0.00580 & 0.00711\\ 0.00711 & 0.00871\end{bmatrix}.$$

Hence substituting into (41) of Section 5, we obtain:

$$[[R]+[X][R]^{-1}[X]]^{-1}=[A]^{-1}$$

$$=\begin{bmatrix}0.05435 & -0.01396 & -0.01653\\ -0.01396 & 0.05420 & -0.02025\\ -0.01653 & -0.02025 & 0.04707\end{bmatrix}=[G].$$

We therefore have obtained the conductance matrix $[G]$, and note that it is symmetric. From (15), we now obtain the susceptance matrix, $[B]$ as follows:

$$[B]=-[R]^{-1}[X][G]$$

$$=\begin{bmatrix}0.00028 & -0.01007 & 0.00772\\ -0.01007 & 0.00500 & -0.00172\\ 0.00772 & -0.00172 & -0.03712\end{bmatrix}.$$

We note that both the matrices $[G]$ and $[B]$ are symmetric matrices as they should be. This is a check on the arithmetical work. To obtain the mesh currents, we use Eqs. (21) and (22) and obtain:

$$(a)=[G](c)-[B](d)=\begin{bmatrix}5.488\\ -4.135\\ 4.176\end{bmatrix},$$

$$(b)=[B](c)-[G](d)=\begin{bmatrix}1.342\\ -6.373\\ 7.539\end{bmatrix}$$

since in this case,

$$(c)=\begin{bmatrix}110\\ -58\\ -5\end{bmatrix},\quad (d)=\begin{bmatrix}0\\ -49\\ 115\end{bmatrix}.$$

The mesh currents are, accordingly:

$$I_a=5.488+j1.342,\quad I_b=-4.135-j6.373,$$
$$I_c=4.176+j7.539.$$

The current in the neutral is:

$$I_n=-(I_a+I_b+I_c)=-5.529-j2.508.$$

The problem is thus completely solved.

7. Conclusion

From the above example, it is seen that the amount of computational labor involved in the numerical solution of a.c. problems by the method presented in this paper is substantially less than that involved in the conventional procedure. The principal type of numerical operation involved is that of matrix multiplication. This operation is most simply performed by the use of a calculating machine. The procedure avoids operations with complex numbers entirely, and the work is extremely systematized. The saving in labor is more apparent in circuits having a large number of meshes. If the network under consideration has only resistance, or only reactance coefficients, then it is only necessary to find the inverse of $[R]$ or of $[X]$ respectively. This inversion may be carried out conveniently by the method of submatrices.

8. Bibliography

1. L. A. Pipes, "Matrices in engineering," Elec. Eng. pp. 1177–1190 (Sept. 1937).

2. R. A. Frazer, W. J. Duncan, and A. R. Collar, *Elementary Matrices* (University Press, Cambridge, 1938).

Surface Studies with the Electron Microscope

V. K. Zworykin and E. G. Ramberg
Research Laboratories, RCA Manufacturing Company, Inc., Camden, New Jersey
(Received May 23, 1941)

UP to the present time the electron microscope has achieved its greatest successes in the observation of objects thin enough to transmit readily electrons incident with 50 to 100 kv velocity—objects, like bacteria, viruses, smokes, thin films, which are materially less than 1 micron in thickness. The direct methods of observing surfaces of compact bodies have not, so far, led to comparable image quality at high magnifications. Among these methods may be mentioned:

(1) the observation of surfaces with the aid of thermionic electrons, photo-electrons, or secondary electrons emitted from the surface with very small velocities,[1–4] and

(2) surface observation with reflected electrons; here the surface may either be normal to the viewing direction,[5] the incident electrons striking it at a glancing angle, or it may be nearly parallel to both the direction of observation and the direction of illumination.[6] In the first case the wide velocity distribution of the reflected electrons makes high resolution impossible, while in the second case extreme foreshortening and unequal resolution in two mutually perpendicular directions are serious drawbacks.

Another method designed to accomplish the same purpose consists of scanning a small area of the surface with a very fine electron probe and reproducing the surface on the screen of a cathode-ray tube or some other type of recorder by the method of wired television.[7–9] It is impossible to gauge, at the present time, the full range of application of this last method. Results published so far, while very promising, have not materially exceeded the capabilities of the light microscope. However, active work which may lead to greatly improved performance is now in progress.

In view of the limitations of the direct methods of surface observation, it was decided to investigate the possibilities of adapting the standard transmission-type electron microscope[10,11] to surface studies by preparing suitable replicas of the original surface, these replicas being thin enough to readily transmit 50-kev electrons.

Such a procedure had already been suggested by H. Mahl, who prepared thin oxide films on aluminum surfaces[12–15] and floated them off after etching away the metal underneath with the aid of a saturated mercuric chloride solution.

Mahl[13] also mentioned the possibility of generalizing the method by using collodion films in place of oxide films, and prepared some replicas of aluminum surfaces using the aforementioned method for removing the film from the metal.[14] In addition to destroying the specimen, this method has the drawback of leaving large quantities of impurities on the replica unless great care is taken in washing it. It is, furthermore, restricted to materials which can be dissolved without affecting the replica film, i.e., primarily metals.

A large number of different methods of preparing replicas have been investigated by the authors. One method in particular has given excellent results, appears most general in its application, and does not destroy the specimen. Two alternative methods, which will be described later, share the advantage of not damaging the surface if properly applied.

A thick layer of metal, e.g., silver, is evaporated in a vacuum chamber onto the surface to be studied. This metal film is stripped mechanically

[1] E. Brüche and H. Johannson, Naturwiss. **20**, 353 (1932).
[2] M. Knoll, F. G. Houtermans, and W. Schulze, Zeits. f. Physik **78**, 340 (1932).
[3] E. Brüche, Zeits. f. Physik **86**, 448 (1933).
[4] V. K. Zworykin, J. Frank. Inst. **215**, 535 (1933).
[5] E. Ruska and H. O. Müller, Zeits. f. Physik **116**, 366 (1940).
[6] B. v. Borries, Zeits. f. Physik **116**, 370 (1940).
[7] M. Knoll, Zeits. f. tech. Physik **16**, 489 (1935).
[8] M. v. Ardenne, Zeits. f. Physik **109**, 553 (1938).
[9] F. R. Moulton, Sci. Monthly **49**, 189 (August, 1939).
[10] L. Marton, Phys. Rev. **58**, 57 (1940).
[11] J. Hillier and A. W. Vance, Proc. I. R. E. (in print).
[12] H. Mahl, Zeits. f. tech. Physik **21**, 17 (1940).
[13] H. Mahl, Jahrbuch d. AEG-Forschung **17**, 67 (1940).
[14] H. Mahl, Metallwirtschaft **19**, 488 (1940).
[15] H. Mahl, Metallwirtschaft **19**, 1082 (1940).

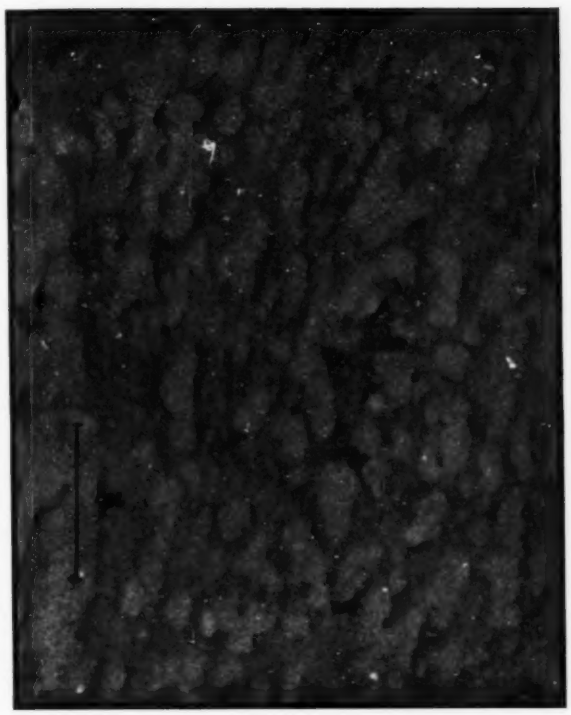

FIG. 1. Bainite (0.78 percent carbon steel). Positive replica obtained by silver-collodion process. Magnification: 20,000.

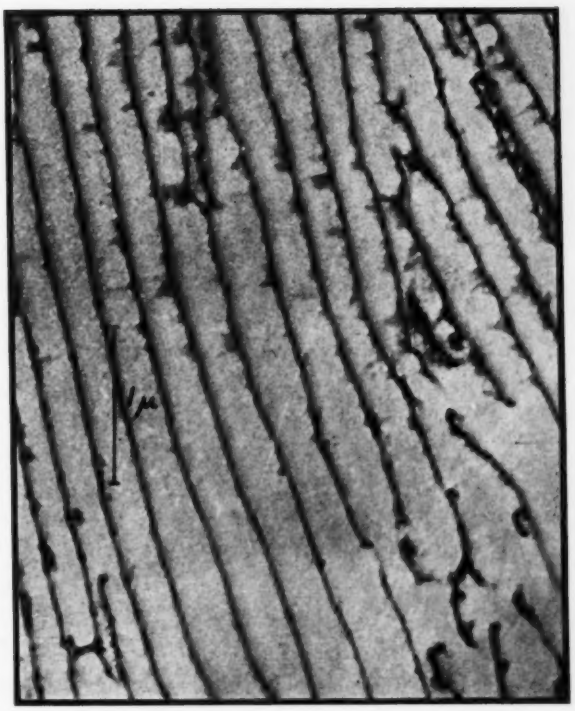

FIG. 2. Fine Pearlite (0.78 percent carbon steel). Positive replica obtained by silver collodion process. Magnification: 20,000.

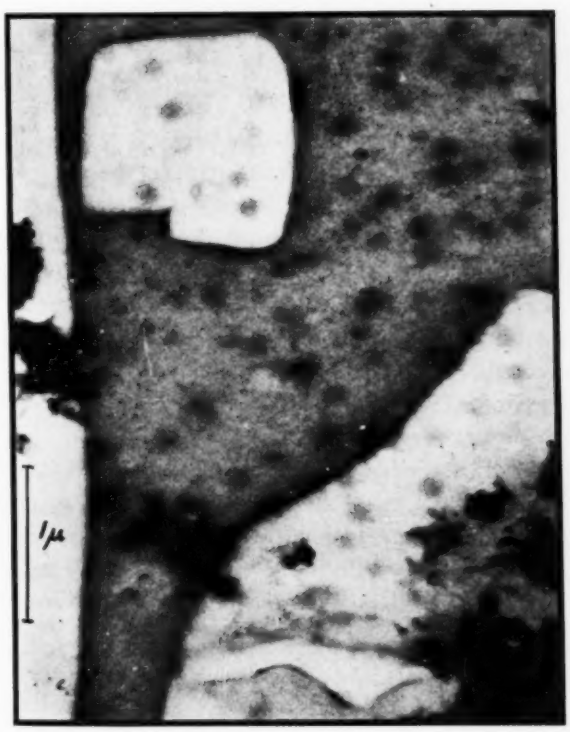

FIG. 3. Glazed porcelain surface. Positive replica obtained by silver-collodion process. Magnification: 20,000.

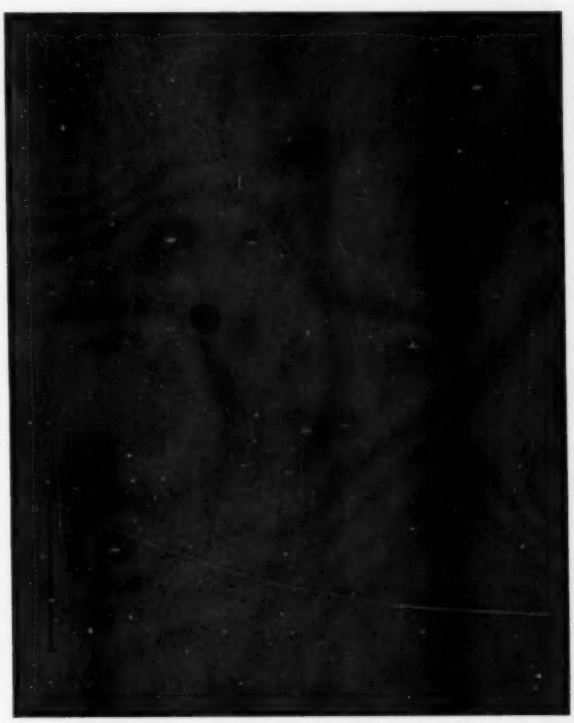

FIG. 4. Quartz cleavage surface. Positive replica obtained by silver-collodion process. Magnification: 20,000.

from the surface, yielding a negative metal replica of the surface. If too thin for the stripping process, the metal film may be reinforced by electroplating. Next, a dilute solution of the final replica material, e.g., a 1 percent solution of collodion in amyl acetate, is flowed over the negative replica surface and is permitted to dry. Then the metal replica with the adhering thin film is immersed for several hours in a suitable solvent for the metal—2 to 3 normal nitric acid in the case of silver. At the end of this period the metal is completely dissolved and, after washing in distilled water, the residual positive replica film may be placed on the fine-mesh screen (e.g., 250-mesh copper or stainless steel) which acts as the object support in the electron microscope.

The choice of metal to be used as transfer medium is dictated primarily by the adhesion properties of the evaporated metal with respect to the surface to be studied, and by the ease of evaporating and dissolving it. Silver has been found very satisfactory in the case of steels, brass, aluminum, various alloys, and non-metallic substances. On the other hand, for a silver surface some other material, such as aluminum, would be required.

FIG. 5. 15,000 line/inch diffraction grating with large periodic error. Positive replica obtained by gelatin-collodion process. Magnification: 8000.

As a first example of the application of the method just described, Fig. 1 shows an electron micrograph of Bainite (suitably heat-treated 0.78 percent carbon steel).* The same steel, with different heat treatment, has the fine pearlite structure seen in Fig. 2. Figures 3 and 4 show examples of the application of the method to non-metallic surfaces, i.e., a glazed porcelain surface and a cleavage surface of natural quartz, respectively. The heavy black particles visible in Figs. 3 and 4 are silver residues, which aid materially in the focusing of the image in the electron microscope.

Two other alternative methods which, though more limited in application, have given some interesting results, merit brief description. The first of these employs gelatin† in place of evaporated metal as the transfer medium. A concentrated aqueous solution of gelatin is spread on the surface of the specimen and is permitted to dry thoroughly. The gelatin will then either separate itself from the surface or can be split off from the surface with the aid of a razor blade. The solution of final replica material is flowed on the negative gelatin replica so obtained, dried, and the gelatin dissolved in a warm dilute solution of ammonium hydroxide. After washing with distilled water, the residual positive thin-film replica is transferred to the object-supporting mesh. This method is limited to objects which are not affected by the water in the gelatin solution, and thus cannot be used for the study of ordinary steels, for example. Furthermore, it was found that, with quartz and glass surfaces, the adhesion of the dried gelatin is often so strong that it cannot be removed without destroying part of the surface, limiting the usefulness of the method also in this case. As an example of the application of the gelatin-collodion method, Fig. 5 shows an electron micrograph obtained from a metallic copy of a 15,000 lines per inch grating with a very large periodic error.

The other alternative method to be discussed leads to a negative rather than a positive replica of the surface. It consists of direct mechanical stripping of the thin film to be observed from the surface of the specimen. The dilute solution of

* The metallographic specimens used in this study were prepared and supplied to us by Dr. R. F. Mehl, Director of the Metals Research Laboratory of the Carnegie Institute of Technology in Pittsburgh. Dr. Mehl's cooperation in this respect was an essential factor in obtaining the results here reported.

† Method suggested by Dr. L. Marton.

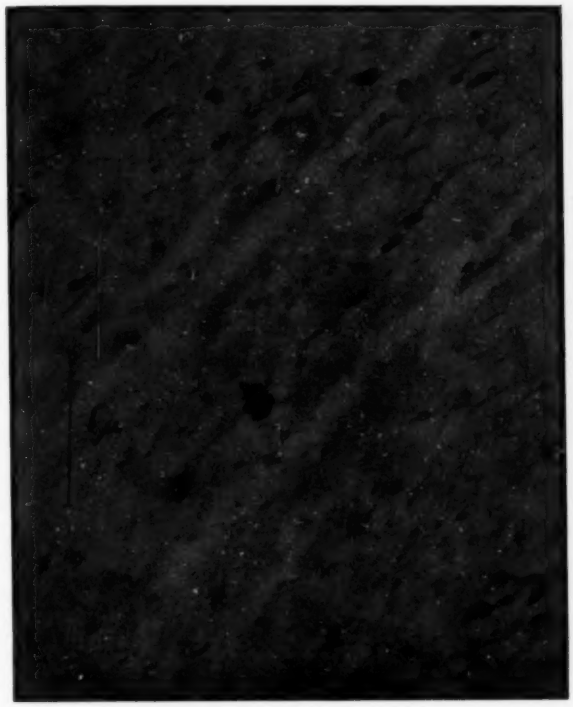

FIG. 6. Bainite (0.78 percent carbon steel). Negative collodion replica stripped from specimen. Magnification: 20,000.

FIG. 7. Fine Pearlite (0.78 percent carbon steel). Negative vinylite lacquer replica stripped from specimen. Magnification: 20,000.

replica material is flowed directly on the specimen surface and dried. A more concentrated solution is applied near one edge of the surface, forming a much thicker film at this point. This thick film, after drying, is raised with the aid of a razor blade. Using this raised portion as a handle, the film, or as much of it as will adhere to the thicker portion, is stripped off and placed on a clean water surface, from which it is finally transferred to the object-supporting mesh. Both collodion and vinylite lacquer* have proved to be suitable replica materials for this procedure. While extremely simple, it is relatively uncertain, and yields far poorer resolution than the first method discussed. Figures 6 and 7, obtained from the same Bainite and Pearlite specimens as Figs. 1 and 2, demonstrate its limitations. Finally, the possibility of greatly distorting the extremely thin film during stripping cannot be disregarded.

* Kindly furnished us by Dr. Mehl.

In conclusion, it is worth while to point out one basic advantage of the replica methods as compared to the direct methods of surface observation with the electron microscope. The density at any point of the picture of a positive replica is a direct measure of the height of that point with respect to a reference plane parallel to the surface. Ridges in the surface show as dark portions, depressions as bright portions of the image. Furthermore, if the exposure and the development procedure are standardized, image density can be correlated once and for all with replica thickness, so that the actual contour of any cross section of the surface imaged can be derived directly from the corresponding microphotometer record of the negative. The microscope is calibrated in advance by taking pictures either of superposed collodion films of known thickness or of evaporated films of known mass density.

Silver-Magnesium Alloy as a Secondary Electron Emitting Material

V. K. Zworykin, J. E. Ruedy, and E. W. Pike*
Research Laboratories, RCA Manufacturing Co., Inc., Camden, N. J.
(Received May 1, 1941)

THE wide use of secondary electron emission electrodes as a means of obtaining gain in thermionic vacuum tubes has been retarded by the lack of a sufficiently rugged emissive material. There are many such electrodes that can be built into tubes which will function satisfactorily for a few minutes, or a few hours, but the requirements are for thousands of hours of useful life. The failure with time of these initially satisfactory emitters is usually due to a combination of the effects of electron bombardment, residual gas, and temperature rise. The operating conditions are different for nearly every type of tube, but, roughly, the minimum requirements for a satisfactory secondary emission electrode are that it shall be able to operate at 300°C with a primary current density of 5 milliamperes per square centimeter in a reasonable vacuum for 1000 hours, with not more than 20 percent change in gain.

It had been known for a number of years that certain compounds of magnesium, when suitably combined with a conducting material, gave high secondary emission, but were not generally satisfactory in operating stability. On the basis of this information, some metal alloys containing magnesium were obtained and tested. The results were so promising that an investigation was undertaken to determine the most suitable alloy and the best technique for handling it. It was found that while alloys of a small percentage of magnesium with copper, silver, gold, and aluminum all had essentially the same secondary emission properties, the addition to some of these of a few percent of calcium, titanium, or beryllium did not produce any marked difference. Further work with alloys of different constituents was then discontinued in order to investigate the properties of the most promising of this group. The amount of magnesium in the alloy was found not critical between less than 1 percent and 15 percent, except in the matter of ductility. Various methods of making it, by both air and vacuum melting, gave satisfactory results. The simplest procedure was to melt a known weight of silver in a steel crucible in an electrically heated oven, quickly thrust a piece of magnesium beneath the surface of the melt by means of a steel wire, stir a little, and then allow the mixture to cool. The resulting ingots were sawed and rolled to a convenient thickness for the cutting out of electrodes.

After an electrode was formed, a final cleaning of the active surface was carried out in any one of a variety of ways, such as by washing with soap and water, alcohol, or acetone, or by scraping, sanding, buffing, or electrolytic etching. The electrode was then mounted in the desired structure and sealed into a glass tube, care being taken to avoid excessive heating of the alloy in the process.

When such a tube was simply pumped without baking or other special treatment, a gain of about 1.5 was observed. (Unless otherwise stated, all values of gain given are for the case of 200-volt primary electrons.) If, however, the tube was baked as in a normal outgassing routine, the gain was usually between 4 and 6. Induction heating of the alloy in the presence of oxygen would further raise the gain by several points. The gain as a function of bombarding voltage for a typical activation of this type is shown in Fig. 1. Accompanying the increase in gain, the alloy surface changed from a bright silver to a golden or yellow color. Examined by means of electron

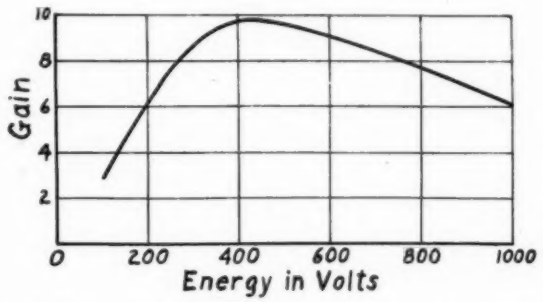

FIG. 1. Gain *vs.* primary electron energy for activated alloy.

* At present with Andrews and Petrillo, Inc.

diffraction, unactivated alloy showed only the pattern of silver, and, after activation, only the pattern of magnesium oxide. Since various preparations of magnesium oxide were known to have comparable gains, it was assumed that activation of the alloy was simply due to the formation of some of this compound, and that its superior life properties lay in the better binding of the oxide to the metal base.

The successful activation of alloy surfaces was a difficult process. Aside from those treatments which obviously affected the surface, and which might have been expected to influence the gain, there were some obscure causes of variability. A considerable amount of work was done in investigating these, and the conclusion was finally reached that minute traces of some gases or vapors given off from the inside of the tube during the initial bake were the principal factors in the uncontrolled variability. The alloy itself was found to be as potent a contamination carrier as any other part. The speed with which the contaminant was removed from the neighborhood of the active surfaces was also important, and for this reason different activation techniques were required for tubes of different geometries.

Satisfactory life characteristics are a matter of prime importance; hence life tests were undertaken as a routine procedure. A schematic cross section of the elements of the tube used for this purpose is shown in Fig. 2, together with its associated circuit. W is a ring of 0.005-inch tungsten wire used as cathode, mounted inside and connected to the nickel cylinder K in such a position that the alloy target A is not exposed in a direct line to any part of W. C is the nickel collector disk. The primary current I_p is adjustable by means of the rheostat R. The gain is the ratio I_s/I_p. The primary electrons strike the target over an area slightly greater than $\frac{1}{2}$ inch in diameter. Since the distribution over the bombarded area is not uniform, the observed life curves (gain *vs.* time) are composites, covering a range of current densities.

During early study of the alloy, the activation aim was always to obtain maximum initial gain, after which the tubes were sealed off, and placed on life test at an average primary current density of about 5 milliamperes per square centimeter. During the runs some of these became definitely gassy and exhibited rapid drops in gain, while the best ones showed a rather rapid decrease during the first fifty hours, and then a gradual flattening out to a slow linear decrease. The typical life curve of a high initial gain surface is shown in Fig. 3. Some surfaces which had been in operation for a few hundred hours and had decreased in gain were rejuvenated by the admission of a little oxygen, but after about thirty more hours of operation the gains were back on their original

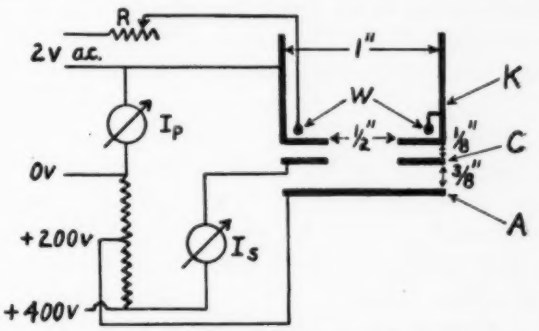

FIG. 2. Schematic section of life test tube elements and associated circuit.

curves as if there had been no reactivation at all.

The simplest procedure used for obtaining the type of activation described above was as follows: The tube was baked until outgassed. After it had cooled, the alloy and other metal parts were outgassed with high frequency. Oxygen was then introduced and the alloy heated by induction, after which the oxygen was pumped out, the alloy and metal parts again heated with high frequency, the Ba-Al getter exploded, and the tube sealed off.

The hope was held for some time that it would be possible, by proper pumping and activation, to produce surfaces that would maintain their high initial gains, but after building more than fifty tubes and always finding essentially the same life characteristics, it was decided that the decay effect was something fundamental.

Attention was then turned to the activation processes which gave lower initial gains, to see if some of them would yield surfaces of greater stability. The typical life curve of a surface activated by a modification of the procedure described above is shown in Fig. 4. The gain is here quite good, and the stability excellent after a preliminary aging. Another property of the alloy, which makes it valuable for use in high gain

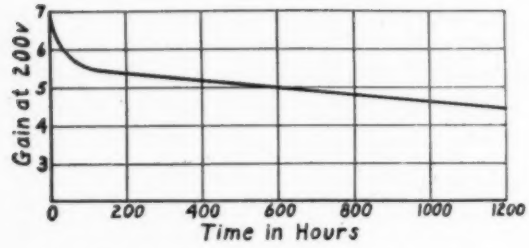

FIG. 3. Alloy activated for maximum initial gain.

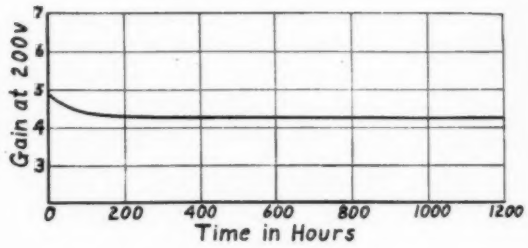

FIG. 4. Alloy activated for maximum stable gain.

multipliers, is its very low dark current,[1] as compared with the commonly used types of emitters employing alkali metals in their formation.

Although evidence upon which to base an explanation of the secondary emission behavior of the alloy is not conclusive, one reasonable hypothesis is that the stable gain of about 4 is due to the silver-magnesium oxide itself, while the higher gains are due to oxygen adsorbed or absorbed in the silver-magnesium surface. The initial rapid decrease in gain with time of operation is due primarily to the surface losing its absorbed oxygen. Thereafter the behavior is a function of ion bombardment, loss of oxygen by the surface, and rejuvenation by oxygen from other parts of the tube.

Another possible explanation is that the high gain is due to the Ag-MgO and that the decay under bombardment is caused by the decomposition of the MgO with the liberation of oxygen (which is taken up by the getter), and thus the gradual formation of a surface of silver magnesium. Curves of the type shown in Fig. 4 would be explained by the formation of a less decomposable silver-magnesium oxide structure.

Although there are many points of both theoretical and practical interest that still need clarifying, the use of the alloy as a secondary electron emitter in certain types of thermionic tubes is now feasible.

[1] Z. Bay, Rev. Sci. Inst. **12**, 127 (1941).

Glass-to-Metal Seals. II

A. W. HULL, E. E. BURGER, AND L. NAVIAS
Research Laboratory, General Electric Company, Schenectady, New York

(Received June 25, 1941)

This is a continuation of the work reported in 1934. The greater part of the paper is devoted to a discussion of the properties of iron-nickel-cobalt alloys, especially the composition Fe 54 percent, Ni 31 percent, Co 15 percent—called fernico—including sensitiveness to impurities and polymorphism. Three new glass-metal combinations are described, the metals being 42 percent nickel-iron, 26 percent chromium-iron, and pure iron, respectively. The strength of the glass-metal bond is discussed briefly.

1. INTRODUCTION

IN a previous article[1] we showed how the stress in wire seals can be calculated from the difference in expansion of wire and glass; and the calculated stresses in test seals were compared with photoelastically observed stresses for a number of common sealing materials. A new alloy of composition Fe 54 percent, Ni 28, Co 18 was described, whose thermal expansion matched very closely, over the whole range from room temperature to the sealing temperatures, the expansion of a special glass, 705-AO, developed by the Corning Glass Works for this purpose. It was shown that seals made with this alloy and 705-AO glass were practically free from strain.

The present article gives the results of a continuation of these studies. It includes the

[1] A. W. Hull and E. E. Burger, Physics **5**, 384 (1934).

properties of iron-nickel-cobalt alloys, especially an alloy of composition Fe 54 percent, Ni 31, Co 15; which will be referred to as fernico. Two new glasses that seal to 42 percent nickel-iron and pure iron, respectively, are described. Some data on the strength of seals are given.

2. Fernico

Iron-nickel-cobalt alloys have two properties which recommend them for sealing purposes: (1) Their thermal expansion in the neighborhood of room temperature is less than that of any other available metals or alloys, with the exception of tungsten and molybdenum. This is important for seals, because it allows the use of low coefficient glasses which are less likely to be broken by sudden changes of temperature than glasses of high expansion. (2) The thermal expansion of these alloys is non-linear like that of glasses, thus affording the possibility of a glass and metal with identical thermal expansion. The non-linear property of Fe-Ni-Co alloys appears to be associated with ferromagnetism; the expansion being low in the temperature range in which the alloy is ferromagnetic, and increasing by a factor of three at the temperature (Curie point) at which ferromagnetism is lost.

The expansion curves of the Fe-Ni-Co alloys which are of interest are shown in Fig. 1, compared to molybdenum, against which they were measured. It will be noted that the temperature of the transition from low to high expansion rises with increasing cobalt content, up to about 18 percent. However, as this percentage is approached, the alloy becomes less and less stable with respect to the $\gamma \rightarrow \alpha$ transformation (see next section). The composition 54 percent Fe, 28 Ni, 18 Co represents the highest transition temperature for stable low coefficient alloys.

The transition temperature of low expansion glasses, on the other hand, is in general high—higher than that of any of these alloys, or any known low expansion alloys; and the glasses become less stable, especially with respect to water solubility, the *lower* their transition temperature.

For strain-free seals the transitions of glass and metal should coincide, as well as their average expansions. This requirement could be satisfied only by choosing a metal alloy having the highest possible transition temperature, and a glass with the lowest possible transition temperature. The combination of 705-AO glass and 54 Fe, 28 Ni, 18 Co, given in our former paper, appeared to be the closest match obtainable.

Since that paper was published, we have succeeded in matching the expansion and transition of 705-AO glass with a still more stable alloy, *viz.*, 54 Fe, 31 Ni, 15 Co. This alloy is a correct match only when free from all impurities, including manganese and silicon, which are considered essential to the ductility of cast nickel alloys. We have found that pure Fe-Ni-Co alloys, without manganese or any other added element, made in hydrogen by the sintering process under proper conditions, are ductile and free from embrittlement under all the conditions of ordinary use. These conditions include heating and annealing in air, hydrogen, or gas; soldering; brazing; and welding. The following Table I gives some of the physical properties of pure 54 Fe, 31 Ni, 15 Co, made in this way. This alloy will be designated as *fernico*.

Figure 2 shows the thermal contraction of

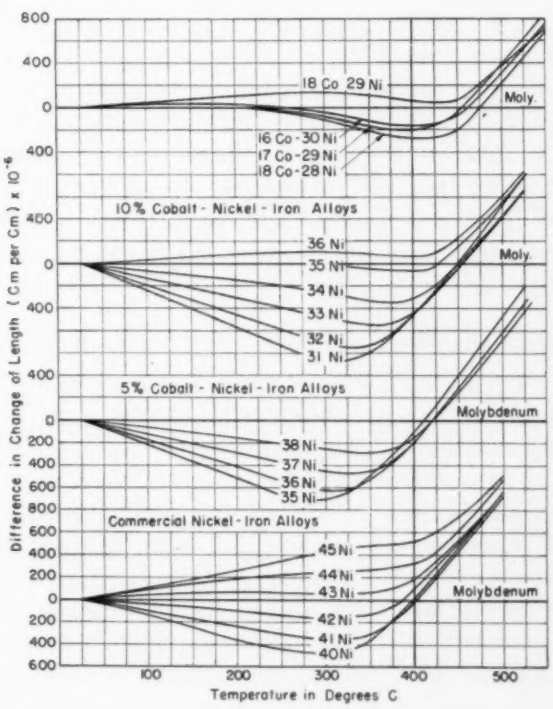

Fig. 1. Thermal expansion of iron-nickel-cobalt alloys, compared to molybdenum.

TABLE I. *Physical properties of fernico:* Fe 54, Ni 31, Co 15

Tensile strength	—72,000 to 80,000 lb. per sq. in.
Percent elongation	—25 to 33
Percent reduction in area	—62 to 63
Elastic modulus	—18×10^6
Density	—8.24 grams per cc
Electrical resistivity	—43.8 microhms per cm cube
Temperature coefficient of expansion	—4.95×10^{-6} from 25° to 300°C
Melting point	—1460°C
Hardness	—75 "Rockwell B"
Yield point	—55,000 lb. per sq. in.

fernico and of 705-AO glass. These curves were taken during cooling at the rate of 1 degree/min. from above the annealing temperature of the glass. Hence the close agreement of the curves from the annealing temperature down to room temperature means that glass and metal, if joined together at the annealing temperature, will contract at the same rate as they cool, and be free from strain both during cooling and after reaching room temperature.

The confirmation of this prediction is shown by the insert in Fig. 2, which gives the photoelastic stress pattern[2] of a test seal made with these materials and cooled at the rate of 1 degree/min. In this pattern, stress in the glass is indicated quantitatively by bending of the interference lines where they cross the samples. For the seal here shown, *viz.*, 705-AO glass of diameter 7.5 mm on a fernico wire of 2.5 mm diameter, a deviation of one-tenth the distance between fringes would represent an axial stress of 0.20 kg/mm². The lines in Fig. 2 are straight within one one-hundredth of a fringe, showing that the stress is less than 0.02 kg/mm².

Dependence of stress on composition of alloy

The chief criterion for freedom from stress in seals is close agreement of both the expansion coefficients and the transition temperatures of metal and glass. This agreement depends principally upon composition of glass and alloy. The sensitiveness of this agreement to composition of the alloy, and hence the maximum allowable variations in composition, can be calculated easily, if expansion and transition temperature are expressed as functions of composition.[3] Instead of transition temperature, it is more useful to calculate the "sealing temperature," defined as the temperature of intersection with the expansion curve of a line 15 percent greater in slope than the average expansion coefficient between 0° and 300°C (see Fig. 2). A point so determined on glass curves represents quite accurately the sealing temperature of borosilicate glasses used with these alloys; hence it also represents the sealing temperature of a metal which matches the glass.

Values of sealing temperature of iron-nickel-cobalt alloys as defined above were obtained from thermal expansion curves like those in Figs. 1 and 10, and are plotted in Fig. 3 as a

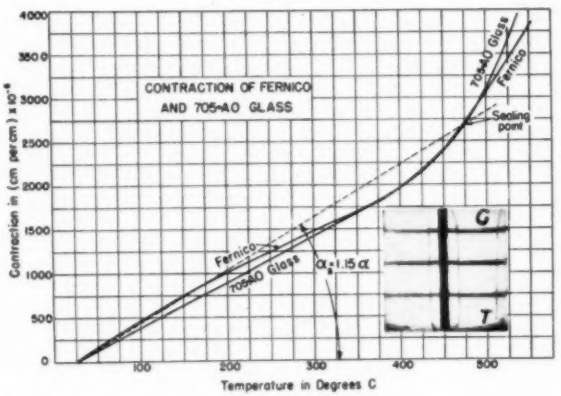

FIG. 2. Thermal contraction of fernico and 705-AO glass. The insert shows the stress pattern of a test seal between these materials.

function of nickel and cobalt content. These data are represented satisfactorily over the complete range of low expansion alloys by a linear relation between sealing temperature and percentage composition:

$$T_s = 36.0\ (\mathrm{Ni} + 0.875\ \mathrm{Co} - 31.0)\ \text{deg. C} \quad (1)$$

when Ni, Co represent percent weights of Ni, Co.

Similarly, the average expansion coefficient *between 25°C and the sealing temperature* is given by

$$\alpha_s = 0.805\ (\mathrm{Ni} + 0.75\ \mathrm{Co} - 34.9) \times 10^{-6}. \quad (2)$$

These equations can be used to calculate the

[2] A. W. Hull and E. E. Burger, Rev. Sci. Inst. **7**, 98 (1936).

[3] H. Scott (Trans. A.I.M.E., Inst. of Metals Div., 1930, p. 506) has given approximate equations for these quantities.

changes in length at sealing caused by variations δT_s and $\delta\alpha_s$ in sealing temperature and expansion coefficient, respectively, of the metal. It can be shown easily (see Fig. 4) that the differences in length at the sealing temperature of the glass between metal and glass (assumed equal in length at room temperature) due to variations δT_s and $\delta\alpha_s$ are:

$$\delta l_T = -(\tan\alpha' + \tan\alpha_s)\delta T_s, \tag{3}$$

$$\delta l_\alpha = (T_s/\cos^2\alpha_s)\delta\alpha_s, \tag{4}$$

where T_s is the sealing temperature, α_s the average expansion coefficient between room temperature and sealing temperature, and α' the coefficient (slope) at the sealing temperature.

Since the angles are small, Eqs. (3) and (4) may be written:

$$\delta l_T = -(\alpha' - \alpha_s)\delta T_s, \tag{3'}$$

$$\delta l_\alpha = T_s\delta\alpha_s. \tag{4'}$$

Insertion of δT_s and $\delta\alpha_s$ from (1) and (2) in Eqs. (3') and (4') gives:

$$\delta l_T = 36\alpha_s(\delta\ \text{Ni} + 0.875\delta\ \text{Co}), \tag{5}$$

$$\delta l_\alpha = 0.805\times10^{-6}T_s(\delta\ \text{Ni} + 0.75\delta\ \text{Co}). \tag{6}$$

For fernico,

$$\alpha' = 12.3\times10^{-6}$$
$$\alpha_s = 5.92\times10^{-6}$$
$$T_s = 472°\text{C}.$$

Hence,

$$\delta l_T = -230\times10^{-6}(\delta\ \text{Ni} + 0.875\delta\ \text{Co})$$
$$\delta l_\alpha = 380\times10^{-6}(\delta\ \text{Ni} + 0.75\delta\ \text{Co}).$$

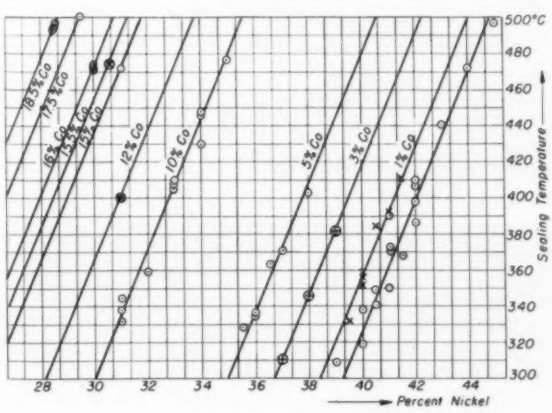

FIG. 3. Sealing temperature of iron-nickel-cobalt alloys as function of nickel and cobalt content.

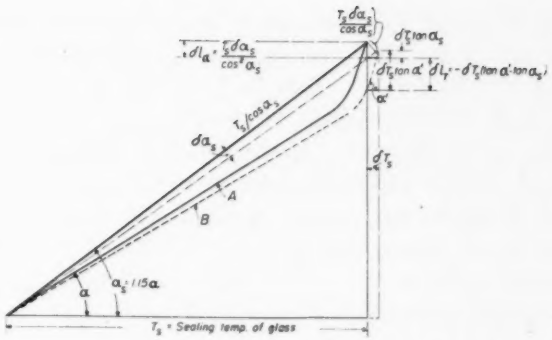

FIG. 4. Plot showing changes in the length of the metal at sealing caused by variations δT_s and $\delta\alpha_s$ in sealing temperature and average expansion, respectively. Curve A is the thermal expansion curve of a correctly matched metal; Curve B, a mismatched one.

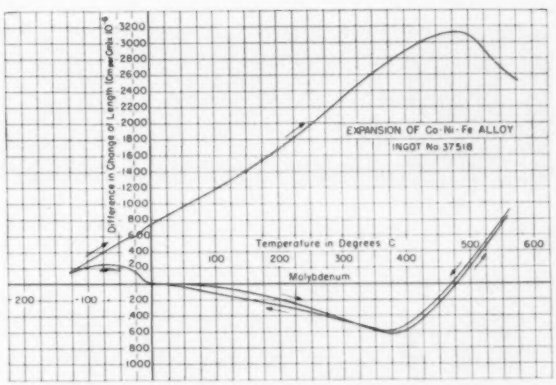

FIG. 5. Thermal expansion cycle of iron-nickel-cobalt alloy with $\gamma-\alpha$ transformation at 0°C, compared to molybdenum. Note the difference in expansion of the α and γ phases.

The total variation in length at sealing is

$$\delta l = \delta l_T + \delta l_\alpha$$
$$= 10^{-6}(150\delta\ \text{Ni} + 84\delta\ \text{Co}). \tag{7}$$

This difference δl in length at sealing is equal to the difference in contraction during cooling, and is a measure of the resulting stress. It was shown in our former paper,[4] that, for thick glass, a difference in contraction of 10^{-6} cm/cm will cause a tensile stress of 0.55 kg/cm². Hence the limiting stress of 100 kg/cm², which was given in our former paper as the "breaking stress," and which represents well our experience with the breakage of seals during the last five years, corresponds to a difference in contraction of $100/0.55\times10^{-6} = 180\times10^{-6}$ cm/cm. Equation (7)

[4] See reference 1, Table I.

shows that this difference in contraction, and hence a breaking stress, can be caused by a variation of 1.2 percent in Ni or 2.1 percent in Co. A seal stressed to the breaking point would not be satisfactory. If we define a satisfactory seal as one which has *not more than one-fourth the breaking stress*, then a total variation in Ni of ±0.3 percent, or a total variation in Co of ±0.5 percent (assuming no variation in Ni), could be tolerated. This is probably within the reach of good metallurgical practice.

The situation is very different with regard to impurities. Only "desirable" impurities will be considered, *viz.*, Mn, Si, and Al, the first being useful as a de-sulphurizer, the latter two as de-oxidizers. The equations for sealing temperature and average expansion at the sealing temperature of alloys containing these impurities are:

$$T_s = 36.0(\text{Ni} + 0.875\ \text{Co} - 0.5\ \text{Mn} - 1.4\ \text{Si} - 1.0\ \text{Al} - 31.0), \quad (1')$$

$$\alpha_s = 0.805(\text{Ni} + 0.75\ \text{Co} + 0.5\ \text{Mn} + 0.6\ \text{Si} + 0.8\ \text{Al} - 34.9) \times 10^{-6} \quad (2')$$

and the changes in length caused by variations are:

$$\delta l_T = -230 \times 10^{-6}(\delta\ \text{Ni} + 0.875\delta\ \text{Co} - 0.5\delta\ \text{Mn} - 1.4\delta\ \text{Si} - 1.0\delta\ \text{Al})$$

$$\delta l_\alpha = 380 \times 10^{-6}(\delta\ \text{Ni} + 0.75\delta\ \text{Co} + 0.5\delta\ \text{Mn} + 0.6\delta\ \text{Si} + 0.8\delta\ \text{Al}).$$

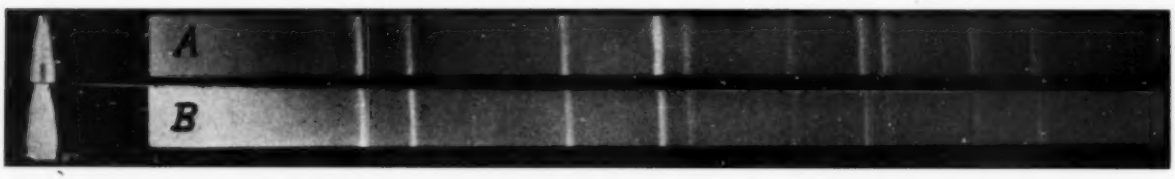

FIG. 6. X-ray diffraction patterns of annealed fernico: (A) before and (B) after 4 hours in liquid air. Both show the face-centered lattice of the γ phase, with no sign of transformation.

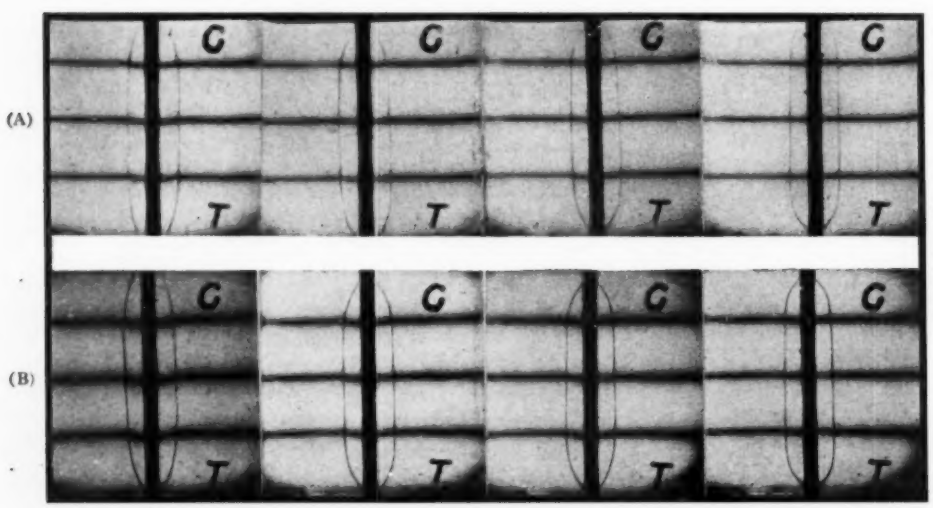

FIG. 7. Photoelastic stress patterns of fernico-705-AO seals: (A) before and (B) after 15 hours in liquid air. No strain has been produced by the low temperature treatment.

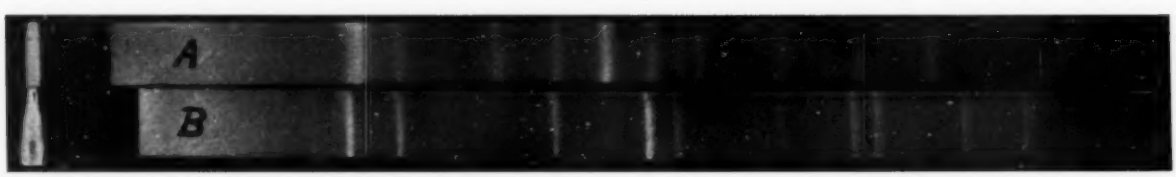

FIG. 8. (A) X-ray diffraction of filings from annealed fernico rod. The body-centered lattice proves transformation to α phase caused by plastic deformation. (B) Pattern of same filings after 5 min. anneal in H_2 at 900°C, showing restoration of γ phase.

The total change, $\delta l = \delta l_T + \delta l_\alpha$ is:

$$\delta l = 10^{-6}(150\delta\ \text{Ni} + 84\delta\ \text{Co} + 305\delta\ \text{Mn} + 550\delta\ \text{Si} + 534\delta\ \text{Al}). \quad (7')$$

Since breaking stress will result when $\delta l = 180 \times 10^{-6}$, the equation for breaking stress is

$$180 = 150\delta\ \text{Ni} + 84\delta\ \text{Co} + 305\delta\ \text{Mn} + 550\delta\ \text{Si} + 534\ \text{Al}. \quad (8)$$

This shows that a breaking stress will result if the alloy contains 0.21 percent more or less of Mn and of [Si+Al] than the prescribed amount; while for a "satisfactory" seal ($<\frac{1}{4}$ breaking stress) the content of Mn and Si must each be accurate to 0.05 percent.

The uncertainty in Mn and Si concentration in commercial alloys is generally much larger than this.

Polymorphism of fernico

The low thermal expansion of fernico is characteristic of its γ (face-centered cubic) phase. This phase is metastable below about 400°C, the stable form being the α (body-centered) phase. The α phase has a much higher thermal expansion than the γ, as can be seen in Fig. 5, which shows the contraction and expansion, as the temperature is changed from +500°C to −100°C and back again, of an alloy whose $\gamma - \alpha$ transformation temperature is 0°C. The composition of this alloy, by analysis, is:

Composition of Fe-Ni-Co Alloy No. 37518
Fe—55.04 (by difference) percent
Ni—27.86
Co—16.59
Si— 0.23
Mn— 0.18
C— .05
P—<.02
S—<.03.

It is evident from Fig. 5 that the presence of even a small amount of the α phase would cause large stresses, and must be avoided.

In the case of 54 percent Fe, 31 Ni, 15 Co fernico, the stability of the γ phase is so great that the $\gamma - \alpha$ transformation point, if it exists, is below the temperature of liquid air; i.e., the transformation to the body-centered form cannot be induced by temperature at any temperature down to and including that of liquid air. This is

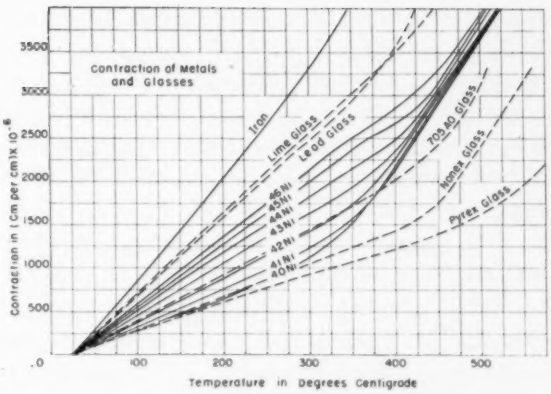

FIG. 9. Thermal expansion of iron-nickel alloys. The expansion curves of the common commercial glasses are shown for comparison.

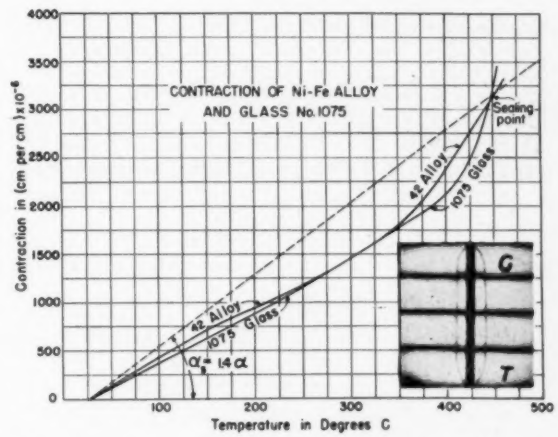

FIG. 10. Thermal expansion curves of 42 alloy and 1075 glass, and photoelastic stress pattern of a seal between them. Absence of stress in the seal is shown by the straightness of the interference lines crossing it.

shown in Fig. 6, in which (A) is the x-ray diffraction pattern of a thin strip of fernico annealed at 1100°C in hydrogen for one hour, and (B) that of the same strip after four hours at liquid-air temperature. Both show the perfect face-centered lattice of the γ phase.

The immunity to transformation at low temperature is also demonstrated by the strain patterns of a group of fernico-705-AO seals, shown in Fig. 7, (A) before, and (B) after 15 hours in liquid air. Not only are the seals uninjured, but no strains can be detected as a result of the prolonged exposure to liquid air.

While these tests prove that the $\gamma \rightarrow \alpha$ transformation of fernico (Fe 54, Ni 31, Co 15) cannot be induced by temperature, it may be produced

by plastic deformation, for example, by rolling, drawing, or filing. Fig. 8(A) shows the x-ray diffraction pattern of filings from a fernico rod which had previously been annealed. The filings show a mixture of the face-centered pattern and the body-centered cubic pattern of the α phase, caused by the plastic deformation of filing. After annealing 5 min. at 900°C, these filings gave the face-centered cubic pattern shown in Fig. 8(B), proving complete restoration of the γ phase. The γ phase can be restored by a brief anneal, e.g., 5 minutes, at any temperature between 900° and 1200°C. But a longer anneal, *viz.*, 4 hours at 900°C or 1 hour at 1100°C in hydrogen, is recommended in order to remove carbon, which causes bubbles in seals by reducing the oxides of the glass.

3. Nickel-Iron Alloys

We have made a careful study of the nickel-iron system, in the hope of finding a combination of glass and nickel-iron alloy whose thermal expansions are "matched" in the sense defined in the last section. Figure 9, which gives the thermal expansions of the iron-nickel alloys in the low expansion range that is of interest, shows that

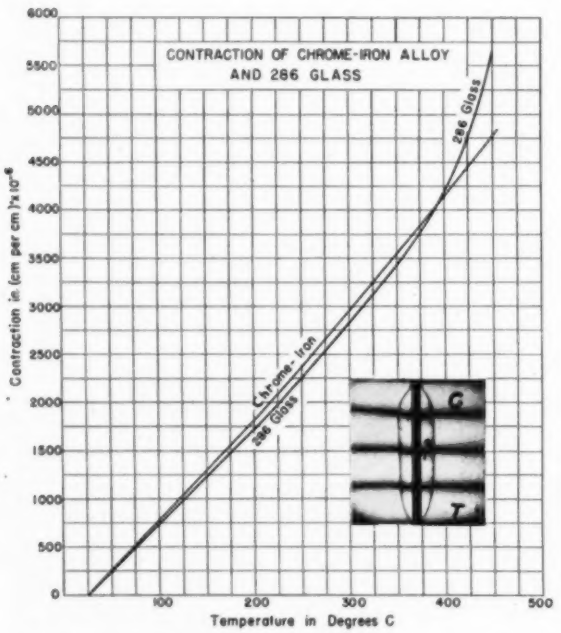

Fig. 11. Thermal expansions of 286 glass and 26 chrome-iron, and photoelastic stress pattern of a seal between them. Absence of stress is shown by the straightness of the dark lines crossing the seal.

the transition temperatures of these alloys are all much lower than those of commercial glasses. Hence a new glass had to be found to meet these conditions. This glass, whose General Electric designation is "1075 glass," is a lead-borosilicate, of the following composition (see Table II):

Table II. *Composition of 1075 glass.*

SiO_2—	34 percent
B_2O_3—	28 "
PbO—	29 "
Al_2O_3—	7 "
Na_2O—	2 "

1075 glass has satisfactory chemical and electrical properties.

The alloy, referred to as *42 alloy*, which matches this glass, has the composition:

Iron—	57.8 percent
Nickel—	41.5
Manganese—	0.5
Silicon—	0.2
Carbon—	<0.06.

The thermal expansions of 42 alloy and 1075 glass are shown in Fig. 10. It will be noted that the expansion in the range 0–300°C is essentially the same as that of fernico and 705-AO glass; but that the sealing point occurs at a lower temperature and much higher up on the curve, i.e., the expansion at the sealing temperature departs more from the low temperature expansion than in the case of 705-AO; the average expansion from room temperature to the sealing temperature being 1.4 times the 0–300°C value, as compared to 1.15 for the fernico—705-AO combination. This difference is characteristic of the two types of glass. As a result of this, the curves of glass and metal depart slightly in the range just below the sealing temperature, to join again at about 350°C. The stresses caused by this departure are not sufficient to cause breakage during cooling, and the seal is free from stress at all temperatures below 350°C. The photoelastic stress pattern of a seal between 1075 glass and 42 alloy, at room temperature, is shown in the insert in Fig. 10.

A special problem encountered in making seals with 1075 glass is the appearance of lead at the interface between glass and metal, lead

oxide being reducible by ferrous metals. This can be avoided by coating the iron-nickel alloy with copper or platinum, which do not reduce lead oxide; or with a lead-free glass, for example, a pure borosilicate. We have obtained excellent results by "precoating" the metal with a thin layer of 705-AO glass.

4. Chrome-Iron Seals

Seals between 26 percent chromium-iron alloy and Corning B-12 glass are highly strained. We have obtained satisfactory seals with this alloy and a glass of the following composition:

Composition of Laboratory Glass No. 286
SiO_2—54 percent
PbO—29
K_2O— 8
Na_2O— 5
BaO— 4

Figure 11 shows the relative thermal expansion of 26 chrome-iron and 286 glass. The insert shows the stress pattern of a seal between them.

5. Iron Seals

Although the art of enameling is old, the glasses used as enamels are generally of lower expansion than the metal. This is desirable for an enamel, since it gives tangential compression of the glass, which prevents cracking, while the radial stress, which is tension, is small so long as the thickness of the enamel is small compared to the radius of curvature. But it is not desirable for a thick glass seal. The standard commercial glasses, also, are all much lower in expansion than iron, as can be seen from Fig. 9.

For thick seals, as contrasted with thin enamels, a glass is needed whose average expansion between room temperature and the sealing point matches iron as closely as possible. A perfect match, such as that between fernico and 705-AO glass, cannot be had, since the expansion of iron is nearly linear. In addition to having the correct expansion, the glass must satisfy the usual requirements, for electrical applications, of high electric resistance and of chemical stability, especially with respect to water and acids. These requirements, as well as the expansion match, have been found to be satisfied by a glass of the following composition:

Composition of 542 Glass
SiO_2—45 percent
K_2O—14
Na_2O— 6
PbO—30
CaF_2— 5

Figure 12 shows the thermal expansion of this glass compared to iron; and the insert shows the stress pattern of a seal, annealed to 1°/min. It is seen that the seal is practically stress-free.

Direct application of 542 glass to iron results in a layer of lead at the interface, as already noted in the case of 1075 glass and 42 alloy. This can be avoided by copper plating, or by

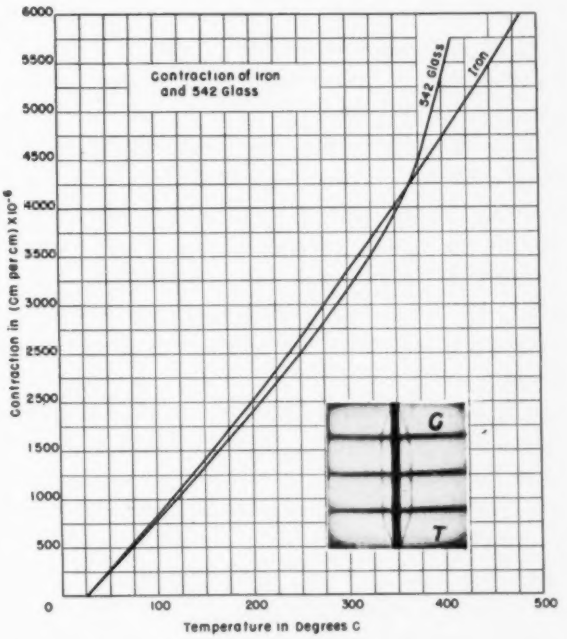

Fig. 12. Thermal expansions of 542 glass and iron, and photoelastic stress pattern of a seal between them.

precoating with a leadless glass. We have had good results from precoating with standard soda-lime lamp glass.

6. The Strength of Seals

It is obvious that a seal which is entirely free from stress may be worthless, unless the glass adheres to the metal. This second half of the problem of sealing, *viz.*, the question of adhesion, must be dismissed with only a brief discussion;

not because it is less important, but because it has not yet been studied. A few rough measurements and some general observations are all that can be given at present.

For the purpose of discussion, several techniques will be described:

(1) Thin oxide bond

The thickness of the oxide formed by heating the metal is carefully controlled: if too thin, it is dissolved by the glass; if too thick, it flakes off.

An example is a combination of tungsten with Corning Nonex Glass. The tungsten wire is carefully oxidized in the flame. A thin tube of "wetting glass" is then slipped over it and quickly sealed, thus preventing further oxidation. The coated wire may now be incorporated in any desired seal, care being taken not to injure the oxide layer by overheating. A certain "straw" color is a reliable index of correct oxide thickness.

This may be termed the Ideal Sealing Technique, since tungsten oxide dissolves in glass sufficiently to form a firm bond, but not so rapidly as to be completely absorbed; and the thin oxide layer may be expected to adhere firmly to the metal. The strength of the bond is not easily measured directly, since this sealing technique has been applied only to wires. But two indirect observations place upper and lower limits to the strength: (a) The bond is weaker than the glass, since tungsten-Nonex seals which are crushed in a vice break at the oxide-metal interface. (b) Tungsten-Pyrex seals, in which the radial tensile stress at the glass-metal surface is 4.8 kg/mm²,[5] frequently do not break during the first few hours, but invariably break in less than a week. Hence the bond initially is stronger than 4.8 kg/mm².

(2) Thick oxide bond

The thick oxide layer behaves like a mismatched enamel coat, which breaks loose from the metal during heating and cooling, because of the difference between its thermal expansion and that of the metal. Typical examples are seals to iron and copper, which over-oxidize easily. The danger may be minimized by careful sealing technique, such as is employed in machine-made Dumet seals. Here two necessary conditions are fulfilled: (a) The wire is kept hot until covered with glass, so that cracking of the oxide layer, which is irreparable, does not occur before sealing. (b) The glass contracts more than the metal during cooling, and thus holds the oxide layer tightly to the metal, both during and after cooling. The strength of the bond is unimportant in this case, since the radial stress is compression.

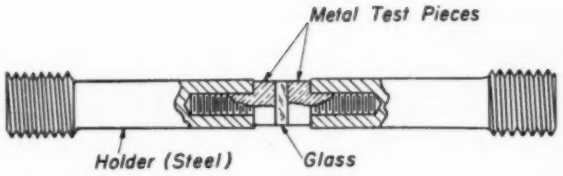

FIG. 13. Form of seal used for testing the strength of bond between metal and glass. The studs, with the glass between them, are screwed into the jaws of a steel-testing machine.

(3) Anchored oxide

An example is 26 percent chromium-iron alloy, deeply etched by chemical pickling or by heating in wet hydrogen. The pores of the honeycomb-like surface support the oxide, which bonds firmly to the glass. Both lead glasses and lime glasses seal strongly to such a surface, and break in the glass rather than at the interface when crushed in a vice. Two direct measurements of the strength of bond between flat surfaces of 26 chrome-iron and 286 glass gave tensile strengths of 4.4 and 6.8 kg/mm². In contrast to this, unetched 26 chrome-iron gives a very weak bond.

(4) Oxide-free seals

Large seals usually require such a long heating time that the oxide layer is completely dissolved in the glass when the seal is finished. This is usually true of fernico-705-AO seals. Measurement of the strength of such seals will therefore be a test of the bond between glass and clean metal.

We have made rough tests of the strength of bond in this and a few other sealing combinations by joining the heads of two tension bolts with a layer of glass, as shown in Fig. 13. The glass was kept smaller in diameter than the studs, or was

[5] Reference 1, p. 407, Table VII.

ground off flush with the metal if it protruded, so that the tension was purely normal. All seals were annealed and were essentially free from strain when tested.

The strength was measured in a standard steel-testing machine. Tests of 28 seals between fernico and 705-AO glass, of ½-inch diameter, gave values ranging from 1.14 to 3.36 kg/mm², the average being 1.48 kg/mm². All but 7 of these broke in the glass at the center, midway between the seals; in these cases the values obtained are those of the strength of the glass; they are not the bond strength, but only lower limits. For the 7 which broke, wholly or partially, at the glass-metal interface, the average strength was 2.23 kg/mm².

A few seals of this same type were made between 42 alloy, which had been precoated with 705-AO glass, and 1075 glass. Tensile tests of 8 of these seals gave strengths varying from 1.56 to 3.05, the average being 2.27 kg/mm². This is somewhat higher than the value found for the fernico-705-AO seals, and may indicate a certain advantage in precoating.

Diffusion Calculations

Interrelation Between Two Solutions of the Fourier Equation

HERMAN A. LIEBHAFSKY
Research Laboratory, General Electric Company, Schenectady, New York
(Received May 1, 1941)

An examination of the interrelation between the sine series solution (for a slab with sealed periphery) and the error function solution (for a semi-infinite body) of the fundamental Fourier equation has yielded the following results: (1) Distribution functions according to the two solutions begin to diverge soon after diffusion has begun. (2) The error function yields an excellent simple approximation, valid until half the material initially present has been lost, for the loss of material from a slab with sealed periphery. (3) A simple, but extremely good, approximation is given for an infinite exponential series in the region of slow convergence. (4) Two simplifications in the calculation of diffusion constants have been given. (5) While the discussion has been restricted to diffusion it is applicable, with obvious modifications, to other cases of flow governed by the fundamental Fourier equation.

IN the evaluation of measured losses of plasticizers from polyvinyl chloride plastics[1] it proved expedient to investigate the interrelation of two solutions for the fundamental Fourier equation

$$\partial c/\partial t = D\partial^2 c/\partial x^2 \qquad (1)$$

(D is the diffusion constant, whose dimensions are l^2t^{-1}; units need not be specified) for the linear diffusion in the x direction of a substance at volume concentration c. As a result, several matters of more general application were discovered, and these will be presented here.

The two solutions are well known.[2] The first,

$$c/c_0 = 2/\pi^{\frac{1}{2}} \int_0^{x/2(Dt)^{\frac{1}{2}}} \exp(-\beta^2)d\beta = \operatorname{erf}(x/2(Dt)^{\frac{1}{2}}), \qquad (2)$$

the "error function" solution, applies to a semi-infinite solid initially of uniform concentration c_0, whose one plane face (situated at $x=0$) is brought at $t=0$ to $c=0$, and maintained in this

[1] An account of this investigation by H. A. Liebhafsky, A. L. Marshall and F. H. Verhoek will appear in the *Journal of the American Chemical Society*.

[2] Cf. W. E. Byerly, *An Elementary Treatise on Fourier's Series, etc.* (Ginn and Company, 1893), where Eq. (2) is given on p. 85 as the solution of example 1; and Eq. (3) as the solution of example 1, p. 106. For values of the "error function," or probability integral (Eq. (2)), see B. O. Peirce, *A Short Table of Integrals* (Ginn and Company, 1910), second edition, p. 116.

condition thereafter. The second solution,

$$c/c_0=4/\pi[e^{-y}\sin\pi x/a+\tfrac{1}{3}e^{-9y}\sin 3\pi x/a+\tfrac{1}{5}e^{-25y}\sin 5\pi x/a+\cdots] \quad (3)$$

where

$$y=D\pi^2t/a^2=\tau\pi^2/4 \quad (3a)$$

applies to a slab with sealed periphery, a units thick, initially of uniform concentration c_0, whose two faces are brought at $t=0$ to $c=0$, and maintained in this condition thereafter.

Comparison of Distribution Functions

The distribution functions (variations of c with x) are easily obtained from Eqs. (2) and (3), provided D, t, and a are known. Assuming $D=1$ and $a=2$ makes t equal to τ (a variable introduced for convenience), and simplifies the comparison. Before $t=0$, $c=c_0$ whatever the value of x, so that the initial distributions are identical. They will remain sensibly identical thereafter so long as c remains sensibly equal to c_0 at $x=1$, the midpoint of the slab. At $t=0.2=\tau$, they diverge appreciably, as Fig. 1 shows. (Here the portion from $x=0$ to $x=1$ of the semi-infinite body represents also an outer half of the slab; the distribution function for the slab is, of course, symmetrical about the center.) The semi-infinite body has the higher c/c_0 (0.886 against 0.772 at $x=1$) because of material that has flowed in from the semi-infinite reservoir beyond $x=1$. The error function solution (Eq. (2)) cannot be used to calculate accurately the distribution within a slab very long after diffusion has begun.

Comparison of Amounts of Material Lost

The amount of material ΔQ lost from *unit area* in the interval $t=0$ to $t=t$ can be calculated from Eqs. (2) or (3) after integrating with respect to t or x. For the semi-infinite body, the former integration is more convenient:

$$Q_0-Q_t=\Delta Q=\int_0^t D(\partial c/\partial x)_{x=0}dt=c_0 2\pi^{-\frac{1}{2}}(Dt)^{\frac{1}{2}}. \quad (4)$$

For the slab, integration with respect to x defines an average concentration $\bar{c}$ (the ratio R is

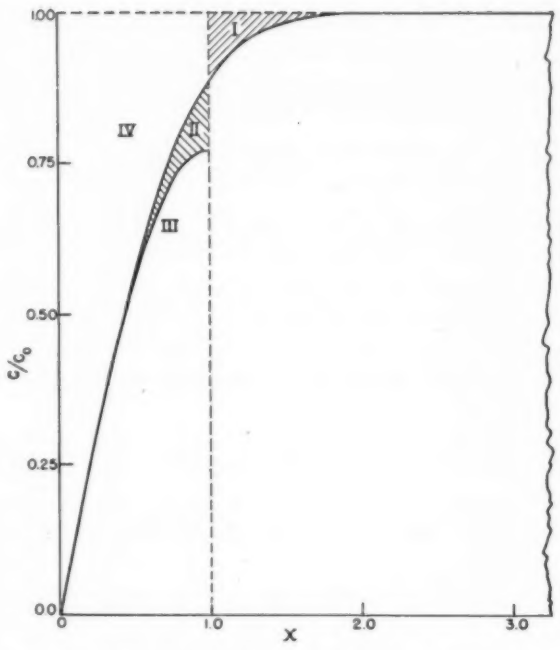

FIG. 1. Distribution function at $\tau=0.2$ according to Eq. (2) (upper curve) and Eq. (3) (lower curve).

introduced for convenience):

$$\bar{c}/c_0=R=1/a\int_0^a(c/c_0)dx$$
$$=8/\pi^2[e^{-y}+\tfrac{1}{9}e^{-9y}+\tfrac{1}{25}e^{-25y}+\cdots]. \quad (5)$$

Since, for a slab of volume V,

$$Q_0=c_0V;\quad Q_t=\bar{c}V;$$
$$R=Q_t/Q_0=1-(\Delta Q/Q_0), \quad (6)$$

R values can be calculated also from Eq. (4). This calculation is illogical to the extent that $\bar{c}$ for the entire semi-infinite body will never be appreciably less than c_0; what the calculation gives (approximately) is R for a unit cube that is part of the semi-infinite body, with one face at $x=0$ (Fig. 1). We shall call this calculation of R the "error function approximation" for the slab. For this unit volume,

$$R=1-\Delta Q/c_0$$
$$=1-(2/\pi^{\frac{1}{2}}(Dt)^{\frac{1}{2}})(\text{approximately}). \quad (7)$$

Values of R from Eq. (5), tediously computed by taking enough terms for five significant figures, and from the much simpler Eq. (7), are given in Table I.

Calculational errors are obviously responsible for the unsystematic difference of 1 in the fifth significant figures of columns 2 and 3, Table I, for $\tau = 0.12$ and less. (Column 4 will be explained later.) This remarkable agreement is the more surprising in view of the divergence of the distribution functions for the two solutions. Even for $\tau = 0.2$, where Fig. 1 shows this divergence to be marked near $x = 1$, the R values differ only by 1 part in a thousand, which suffices for most diffusion measurements. (In the work on plastics, weight changes to 1 part in 500 of the plasticizer could be detected.) In other words, the simple Eq. (7) can replace the cumbersome Eq. (5) for all ordinary diffusion measurements on a slab with sealed periphery so long as not more than half the material originally present is lost.

Equation (7) is thus an excellent approximation for the exponential series, Eq. (5), at values of y below 0.3, where evaluation of the series is relatively tedious. Furthermore, this mathematically interesting approximation is somewhat unlikely of discovery by mathematical methods alone.

TABLE I. *Calculated values of R for the slab.*

τ	Exact Solution (Eq. (5))	Error Function Approximation (Eq. (7))	Error Function Solution
0.01	0.88717	0.88716	0.8872
.02	.84041	.84042	.8404
.04	.77432	.77432	.7744
.06	.72360	.72361	.7240
.08	.68084	.68085	.6824
.10	.64318	.64318	.6470
.12	.60913	.60912	—
.16	.54876	.54865	.5814
.20	.49591	.49537	.5554

The reason for this astonishing agreement is clear from Fig. 1. The area I represents material that has flowed from the semi-infinite reservoir into the unit cube under consideration; the area II represents the excess of material resulting from the divergence of the two distribution functions (Eqs. (2) and (3)). So long as these two areas are sensibly equal, the concentration gradients for the two solutions will also be sensibly equal near $x = 0$. The amount of material that has left the cube through the face at $x = 0$ will consequently be identical for the semi-infinite body and for the

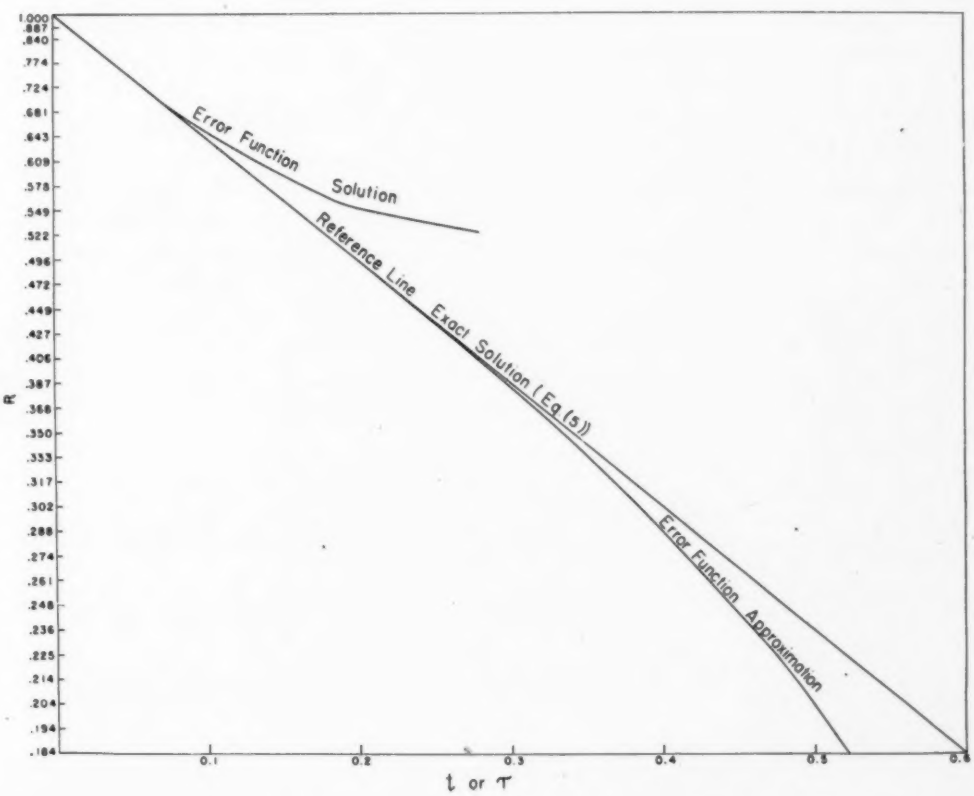

FIG. 2. Three methods of obtaining R for a slab with sealed periphery.

slab; hence the agreement of columns 2 and 3, Table I.

Under the conditions of Fig. 1, the true R for the slab (Eq. (5)) is 1 − (area IV + area II); R from Eq. (7) is 1 − (area IV + area I); the R actually realized for the unit cube attached to the semi-infinite body is 1 − (area IV), and it can be obtained by adding values of area I to the proper values of R from Eq. (7). Area I has been graphically evaluated for a number of τ values; column 4, Table I, and the upper curve, Fig. 2, give the corresponding exact values of R for a unit cube attached to the semi-infinite body. These R values are of interest mainly because they show that an exact calculation of R from the error function is useless as an approximation for the case of the slab.

The Calculation of Diffusion Constants

The use of the error function approximation facilitates the calculation of diffusion constants for the slab series (Eq. (5)) and, by way of reciprocation, this series can be used to simplify the calculation of diffusion constants from the error function solution.

To evaluate D from R values in agreement with Eq. (5), Sherwood[3] has used a special ordinate scale that gives a straight line when such values are plotted against t or τ as abscissa. Our experimental results required the computation of a scale considerably more detailed than Sherwood's.[4] Equation (5) converges very slowly at small τ; at $\tau=0.01$, six terms must be calculated to establish R to three significant figures. The use of Eq. (7) resolves this difficulty for R values above 0.5; between 0.5 and 0.45, only two terms of Eq. (5) are required for three significant figures in R; thereafter, only one term is necessary. For most measurements, therefore, it suffices to use Eq. (7) until half the material initially present in the slab has been lost, and the first term of Eq. (5) thenceforward. A comparison of the three types of R values in Table I is given at the higher τ's by Fig. 2; the error function solution curve tends to be horizontal when the rates of flow across the boundaries $x=0$ and $x=1$ are roughly equal.

A simplification follows of the calculation of D from measurements that fit the error function solution, or from R values near unity for the slab. The usual plot of weight losses (ΔQ's) against $t^{\frac{1}{2}}$ is made. The slope of the resulting straight line (Eq. (4)) divided by Q_0 defines $k=(1-R)/t^{\frac{1}{2}}$. But Fig. 2 relates R to τ; at $\tau=0.5$, for example, $1-R=0.764$. Now, by Eq. (3a),

$$(0.764/k)^2=t=a^2/4\times\tfrac{1}{2}\times 1/D,$$

or

$$D=(ak)^2/4.670. \qquad (8)$$

This combination of the sine series and error function solutions of the Fourier equation has at least two advantages: R is dimensionless so that concentration units disappear from the calculation of D; and the areas of the specimens need not be known, provided no appreciable dimension changes occur during the experiments.

I am indebted to my colleagues in the General Electric Company, especially to Drs. Hillel Poritsky, R. P. Johnson, and Lewi Tonks, for valuable discussions bearing on the foregoing material.

[3] (a) T. K. Sherwood, Ind. Eng. Chem. **21**, 12 (1929). (b) Cf. A. B. Newman, Trans. Am. Inst. Chem. Eng. **27**, 310 (1931).

[4] Figure 2 was prepared as follows. $\tau=0.6$, the highest abscissa of practical interest, was laid off 30 cm from the origin on millimeter graph paper. $R=1.000$, the ordinate for $t=0=\tau$, was laid off 24 cm from the origin, and a straight line, the reference line, was drawn through the two points thus plotted. The ordinate scale that will make this reference line satisfy Eq. (5) for $D=1$, $a=2$, is now required. It was obtained by solving Eq. (5) for values of τ from 0.60 to 0.02 in steps of 0.02, and for the value $\tau=0.01$. The resulting R values are given in Fig. 2, in which a change of 0.02 in τ is a change of 10 mm on the original abscissa scale, and corresponds to a change of 8 mm on the original ordinate.

If experimental R values when plotted against t lie on a straight line different in slope from the reference line, Eq. (5) is obeyed; but the conditions $D=1$, $a=2$, are not both satisfied. D at any such R can be calculated by Eq. (3a), t being the experimental abscissa for this value of R; τ, that from the reference line.